UNIVERSITY OF BELGRADE
FACULTY OF MATHEMATICS

UNIVERSITY OF PADOVA
DEPARTMENT OF ASTRONOMY

- PhD THESIS -

Plasma Diagnostics in the Broad Line Region of Active Galaxies using Emission Lines

Dragana Ilić

Belgrade 2008.

* * *

This PhD Thesis is made as a part of the research project 146002: "Astrophysical spectroscopy of extragalactic objects" supported by the Ministry of Science of Republic of Serbia, under co-supervision of dr Luka Č. Popović. I would like to use this opportunity to thank him for his unselfish help, support and guidance during my work on this PhD thesis.

Part of the research presented here is done during my 6-months stay at the Department of Astronomy, University of Padova, under co-supervision of dr Stefano Ciroi, to whom I would like to particulary thank for his help and support. Moreover, I would like to thank the whole Department of Astronomy for their support and hospitality, especially to professor Piero Rafanelli, dr Francesco di Mille and Giovanni La Mura for useful discussions and advices.

I thank dr Peter van Hoof from the Observatory of Brussels for the help on the work with the numerical code CLOUDY. I have used a lot of data in my work that has been collected for many years at the Special Astrophysical Observatory in Russia. I would like to especially thank dr Alla Shapovalova for providing data and for the help during data analysis. Also, part of the research was done at the Max-Planck Institute for Radio Astronomy in Bonn, thus I thank dr Andrei Lobanov and Jonathan León-Tavares for help and hospitality.

Finally, I would like to thank my family, friends and colleagues, especially to my Department of Astronomy, on great support and help during the work on this PhD Thesis.

Belgrade, 10.09.2008.

Dragana Ilić

Abstract

The electromagnetic spectrum of active galactic nuclei (AGN) has two specific features: an intensive broad-band continuum that comes from γ to radio wavelengths, and broad and intensive emission lines. In this emission line spectrum there are broad emission lines (BELs) that come from the so-called Broad Line Region (BLR). Even today, kinematics and physics of the BLR are not fully understood, and there is no unique geometry of the BLR that can be applied to all AGN. So far it has been assumed and accepted that the BLR is ionized by the intensive continuum coming from the accretion disk around a supermassive black hole that is in the center of an AGN. Thus, it is assumed that the major ionization mechanism of this region is photoionization and that the BELs are the result of recombination.

In this PhD Thesis we study the physical properties of the BLR using broad hydrogen and helium lines. In previous investigations, physical properties, i.e. the temperature and electron density, have been estimated according to the similarity of this region to the emission nebulae (e.g. H II regions) where ratios of some forbidden lines (e.g. [O III] and [N II] lines) have been used. Another way to estimate these parameters is to use complex numerical codes to reproduce the observed emission line spectrum. In this work we propose a direct method for estimation of the physical properties of the BLR using the flux ratios of hydrogen Balmer and helium (He I 5876 Å i He II 4687 Å) emission lines. The method is performed using Boltzmann-plot method (widely used for the laboratory plasma diagnostics) and numerical simulations of the plasma conditions in the BLR, that are done with the spectral synthesis code CLOUDY. The method is applied to a sample of AGN spectra were taken from the SDSS (Sloan Digital Sky Survey) database. We found that in this sample the BLR temperature is in the range $T_{\rm BLR} = 4000 - 18000$ K while the hydrogen density is $n_{\rm H} = 10^{8.6} - 10^{11.5}$ cm^{-3}. The obtained results are in good agreement with previous rough estimates of these BLR physical parameters. Moreover, we study here the variation of the BLR temperature and density in two well known AGN (NGC 5548 and NGC 4151), that were observed in a large period (8 years for NGC 5548 and 11 years for NGC 4151) with 6m SAO telescope from Russia and 2.1 INAOE telescope from Mexico.

At the end, let us say that the work in this PhD Thesis is an attempt to clarify and better understand the nature of the BLR in AGN.

Keywords: *galaxies: active – (galaxies:) quasars: emission lines – lines: formation – plasma*

Sažetak

Elektromagnetni spektar aktivnih galaktičkih jezgara (AGJ) karakteriše intenzivno zračenje u kontinuumu na svim talasnim dužinama (od γ do radio), ali i vrlo intenzivne emisione linije. Tu se izdvajaju široke emisione linije, najšire linije u svemiru, koje nastaju u oblasti koja se po njima naziva širokolinijska oblast. I danas, fizičke i kinematičke osobine ove oblasti nisu do kraja objašnjene, pa i sama geometrija nije jedinstvena za sva AGJ. Za sada se pretpostavlja da je širokolinijska oblast jonizovana od strane intenzivnog zračenja u kontinuumu koje dolazi iz akrecionog diska oko supermasivne crne rupe koja se nalazi u centru AGJ. Dakle, pretpostavlja se da je glavni oblik jonizacije ove sredine fotojonizacija, a da su široke emisione linije rezultat rekombinacije.

U ovoj doktorskoj disertaciji istražuju se fizičke osobine (temperatura i koncentracija) širokolinijske oblasi koristeći emisione linije vodonika i helijuma. U dosadašnjim istraživanjima, temperatura i koncentracija su procenjivane na osnovu sličnosti ove oblasti sa emisionim maglinama (npr. H II regionima), gde se koriste odnosi flukseva zabranjenih linija za dijagnostiku plazme. Takođe, moguće je proceniti ove veličine i pomoću kompleksnih numeričkih simulacija, gde se pokušava reprodukovati posmatrani emisioni spektar. U ovoj disertaciji prikazan je direktan metod procene fizičkih karakteristika širokolinijske oblasti koristeći samo odnose flukseva emisionih linija Balmerove serije vodonika i linija helijuma (He I 5876 Å i He II 4687 Å). Metod se bazira na Bolcman-plot metodu (koji se primenjuje u dijagnostici laboratorijske plazme) i razvijen je uz pomoć numeričkih simulacija uslova plazme u širokolinijskoj oblasti, koje su rađene u programu CLOUDY. Metod je primenjen na uzorak AGJ spektara preuzetih iz SDSS (*Sloan Digital Sky Survey*) spektralne baze. Za razmatrani uzorak je pokazano da su temperatura i koncentracija u širokolinijskoj oblasti u opsegu $T_{\rm BLR} = 4000 - 18000$ K i $n_{\rm H} = 10^{8.6} - 10^{11.5}$ cm^{-3}. Ovi rezultati su u saglasnosti sa prethodnim grubim procenama ovih parametara. Takođe, u ovoj disertaciji se proučava i vremenska zavisnost fizičkih karakteristika u slučaju promenjivih aktivnih galaksija NGC 5548 i NGC 4151, koje su posmatrane u dugačkom vremenskom intervalu (8 odnosno 11 godina, respektivno) sa 6 m teleskopom SAO-a u Rusiji i 2.1 m INAOE teleskopom u Meksiku

Na kraju, naglasimo da je rad u ovoj doktorskoj disertaciji pokušaj da se razjasni i bolje razume priroda širokolinijske oblasti aktivnih galaktičkih jezgara.

Abstract

Lo spettro elettromagnetico dei nuclei galattici attivi (AGN) ha due caratteristiche specifiche: un intenso ed esteso continuo che va dalle lunghezze d'onda gamma al radio, e larghe ed intense righe di emissione (BEL) che provengono dalla cosidetta Broad Line Region (BLR). Ad oggi la cinematica e la fisica della BLR non sono pienamente comprese e non esiste un'unica geometria per la BLR che possa essere applicata agli AGN. Finora è stato assunto e accettato che la BLR sia ionizzata dall'intenso continuo proveniente dal disco di accrescimento attorno a un buco nero supermassiccio che sta al centro dell'AGN. Perciò si è assunto che il principale meccanismo di ionizzazione di questa regione sia la fotoionizzazione e che le BEL siano il risultato della ricombinazione.

In questa tesi di dottorato studiamo le proprietà fisiche della BLR utilizzando le righe larghe di idrogeno ed elio. In precedenti ricerche le proprietà fisiche, cioè temperatura e densità elettronica, sono state stimate in analogia alle nebulose in emissione (per esempio le regioni H II), per le quali sono state usati i rapporti di alcune righe in emissione (ad esempio le righe di [O III] e [N II]). Un altro modo di stimare questi parametri consiste nell'usare codici numerici complessi al fine di riprodurre lo spettro delle righe di emissione osservate. In questo lavoro proponiamo un metodo diretto per la stima delle proprietà fisiche della BLR usando i rapporti di flusso delle righe in emissione della serie di Balmer dell'idrogeno e dell'elio (He I 5876 Å e He II 4687 Å). Questo metodo è realizzato combinando il metodo del Boltzmann-plot (ampiamente usato per analizzare il plasma di laboratorio) e le simulazioni numeriche delle condizioni del plasma nella BLR, che sono realizzate con il codice di sintesi spettrale CLOUDY. Il metodo è applicato ad un campione di spettri di AGN estratti dal database della SDSS (Sloan Digital Sky Survey). Abbiamo trovato che in questo campione la temperatura della BLR cade nell'intervallo $T_{\rm BLR} = 4000 - 18000$ K, mentre la densità di idrogeno vale $n_{\rm H} = 10^{8.6} - 10^{11.5}$ cm^{-3}. I risultati ottenuti sono in buon accordo con precedenti stime approssimative di questi parametri fisici della BLR. Inoltre, studiamo qui la variazione della temperatura e della densità della BLR in due AGN molto noti (NGC 5548 e NGC 4151), che sono stati osservati in un lungo periodo (8 anni per NGC 5548 e 11 anni per NGC 4151) con il telescopio russo di 6 m del SAO e il telescopio messicano di 2.1 m del INAOE.

In conclusione, possiamo dire che il lavoro condotto in questa tesi di dottorato è un tentativo di chiarire e comprendere meglio la natura della BLR negli AGN.

Contents

1 Introduction

Active galaxies (AG) have been the subject of an intensive astrophysical research for the last 3-4 decades. The class of AG contains many different objects, such as quasars, gigantic elliptic radio galaxies, luminous spiral Seyfert galaxies, blazars, etc. They are the most luminous and the most distant observed objects in the Universe. A huge amount of energy is coming from their nuclei, therefore they are called active galactic nuclei (AGN). AGN can have luminosities in the range from $\approx 10^{42}$ to $\approx 10^{48}$ erg s^{-1}, that can be $\approx 10^4$ greater than in the case of a typical galaxy. Apart from great luminosities, AGN are emitting in the broad band of electromagnetic spectrum. The observed emission of AGN is in the continuum and in lines, from the γ and X domain to the far infrared and radio bands. AGN are for sure the most powerful radio sources (Figure 1). In the optical and UV band, they display emission (and occasionally absorbtion) lines whose total flux is several percent to tens of percent of the continuum flux, and whose widths suggest velocities ranging up to $\approx 10^4$km s^{-1}.

Today, it is widely accepted that the mechanism which powers AGN is accretion onto supermassive black hole, i.e. the greatest part of the continuum emission comes from an accretion disk and its corona. Thus, in the center of an AGN there is a super-massive black hole (SBH) with accretion disk surrounded by gas and dust in the shape of a torus. There are also other regions present in the vicinity of the SBH, such as ionized gas clouds that produce intensive emission lines or jets of matter that are mostly visible in the radio band (Figure 1), but sometimes also can be seen in the optical band. The kinematics of these regions is very complex as well as the physical processes that produce such specific spectra of these objects.

Since AGN (i.e. quasars) are the brightest objects in the Universe and thus the furthermost, these objects are important for the studies of the early Universe and cosmology in general. For instance, studies of their luminosity functions or quasar host galaxies are crucial for understanding the formation and evolution of galaxies in general.

AGN have very small dimensions. This comes from the fact that fast changes are observed in the AGN brightness (sometimes just a couple of days, e.g. the case of galaxy NGC 4151). This leads to the conclusion that the emission regions in the AGN are of relatively small dimensions (from only couple of light days up to couple of light months). Also, the brightness of AGN can be so hight that the brightness of the host galaxy can be neglected in the total brightness (as e.g. in the case of quasars). Consequently, they are compact regions which could not be directly observed in the most bands of

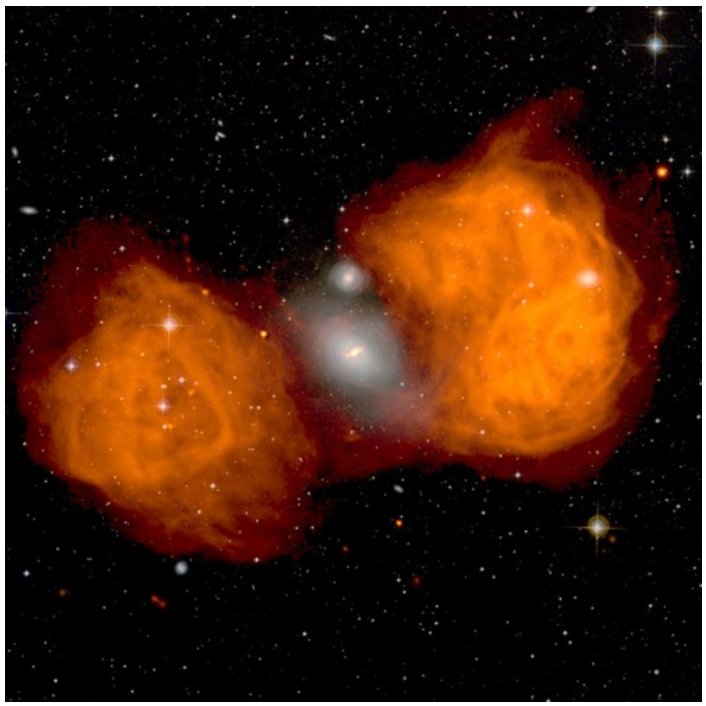

Figure 1: The giant elliptical galaxy, NGC1316 (center of the image), began devouring its small northern neighbor. This image shows the radio emission superimposed on an optical image. The complex radio emission (called Fornax A, shown in orange) and the activity in this galaxy is due to the merger of these two galaxies. As NGC 1316 cannibalizes the smaller galaxy, it strips away material that spirals toward a black hole at the center of the giant elliptical (Image courtesy of NRAO/AUI and J. M. Uson, *http://www.nrao.edu/*).

electromagnetic spectrum[1]. Therefore, AGN and their physical/kinematical properties are indirectly studied through the analysis of their spectrum. The method that is mostly used in the research of these objects is spectroscopy. The spectral analysis is very important tool for the studies of AGN properties, as AGN have very characteristic spectra with prominent emission lines which can give a lot of information about their complex kinematical and physical structure. An AGN has more than one emission region with different kinematical and physical properties. With the reduction, analysis and modeling of the total AGN spectrum one could separate the contributions of each different emission region, and in that way determine their characteristics and position with respect to the SMBH.

In this PhD thesis we present the investigation of the properties of one of the emission regions of active galactic nuclei, so-called the broad line region (BLR).

[1]So far only in the radio band the parsec scale structures have been observed.

In this region very broad emission lines are formed (BELs) whose widths at the half maximum are in the range from 1000 km s^{-1}up to 10000 km s^{-1}. More precisely, we study here the BLR's physical properties (temperature and density) as well as the methods that could be used for their estimates. Even though more than 40 years have passed since AGN were discovered, there are still many open questions about their structure and physical processes. One of which is what are the temperature and density of the BLR. So far there are no simple and direct methods (that would use only the observed BELs) to determine the physical characteristics of this region, instead we use complex numerical codes for simulations of spectra (as is e.g. CLOUDY), from which we conclude about these properties, e.g. temperature, ionization level or chemical composition.

The aim of this PhD thesis is to, combining the results of the numerical simulations (made with the help of the numerical code for spectral simulations - CLOUDY) and the observed AGN spectra, give a direct and simple method, that would use the observed broad emission lines, to estimate the physical properties (primarily the temperature and density) of the BLR. Also, we give various tests that estimate the validity of this method. The method is based on the Boltzmann-plot (BP), the method that is widely used in the laboratory plasma diagnostics. Using the BP method, one can estimate the plasma temperature from the line fluxes of one spectral series, e.g. from the Balmer line series. Apart from the numerical simulation results, in this research we also use the observations of: (a) the active galaxy NGC 5548 that was observed in the period of 8 years with the 6m SAO telescope from Russia and 2.1 INAOE telescope from Mexico, (b) the active galaxy NGC 4151 for which data were obtained in the period of 11 years using the same telescopes, and (c) the sample of 50 galaxies taken from the Sloan Digital Sky Survey (SDSS) database. Galaxies NGC 5548 and NGC 4151 are quite specific cases as their flux in the continuum and in emission lines is changing in time, with a consequence that these galaxies even change their type from Seyfert 1 (that have broad lines with superposed narrow lines) up to Seyfert 2 galaxies (with just narrow lines). This fact makes these galaxies very interesting for investigations of the change of the BLR physical properties. On the other hand, a study of the sample of the SDSS galaxies gives some statistical points to the analysis of the BLR physical properties.

In the first part of this thesis we give a general introduction on AGN, a detail review of the BLR properties and previous results, as well as the physical basis of the research proposed here. Further in the text, we describe in details the method to generate grids of numerical simulations of the BLR physical conditions using the CLOUDY code. The obtained grids of models are compared to the observed spectra, where the special attention is given to the comparison of the flux ratios of the observed emission lines and those

obtained with the numerical simulations, as well as to the connection between the flux ratios of hydrogen Balmer lines and the flux ratio of helium lines He I 5876 Å and He II 4687 Å. In the last part of the thesis we present a study of the time dependance of the physical properties for the case of the variable active galaxies NGC 5548 and NGC 4151. Finally, we give conclusions of this research and the list of references mentioned in the text. In the Appendix we give detail description of the numerical code CLOUDY, its installation, usage and application, and we explain some basic atomic processes which are relevant in the ionized gas.

2 Active galactic nuclei (AGN)

Active galaxies differ from the so-called "normal" galaxies in the amount of energy emitted from their nucleus that does not come from stars. But even among AGN there are differences. The first group of stellar systems with active nucleus consists of Seyfert galaxies[2]. These are spiral galaxies with very bright nucleus which spectrum has strong emission lines of neutral and multi-ionized emitters. The presence of highly ionized emission lines indicates the existence of a non-stellar ionization continuum. We distinguish the basic types of Spiral galaxies: Seyfert 1, which spectrum contains broad lines from permitted transitions and narrow lines from forbidden transitions, and Seyfert 2 galaxies that show only narrow emission lines (from both permitted and forbidden transitions). Many low luminosity galaxies have a nucleus that resembles the Seyfert 2 nucleus, but with the spectrum that shows the forbidden lines from lower ionization states. Therefore, these galaxies are called Low-Ionization Nuclear Emission-line Regions, i.e LINERs.

Active galaxies that emit intensively in the radio band are called radio galaxies. These are dominantly elliptic galaxies that are divided into two morphologically different types: FR I and FR II[3]. The classification is done according to the relative position of the surface brightness maximum (called the hot spot) in the radio lobes. For example, in the FR I radio galaxy the distance between the hot spot in the radio lobes is less than half of the maximum diameter of the radio source, while in the FR II type this distance is larger (Binney & Merrifield 1998). Like Seyfert galaxies, radio galaxies can be divided into subgroups according to the widths of their emission lines, i.e. Narrow Line Radio Galaxies (NLRG) that emit narrow emission lines characteristic for Seyfert 2 galaxies, and Broad Line Radio Galaxies (BLRG) that emit broad lines as Seyfert 1 galaxies.

Being the most powerful sources in the Universe, quasars belongs to the group of active galaxies with the absolute magnitude $M_B < -23$ (Osterborck 1989). These quasi stellar (quasars) objects emit intensively in the radio domain and their spectrum shows broad emission lines significantly redshifted. In this group of AGN are also Quasi-Stellar Objects (QSOs) which have the same observed properties as quasars, but they are weak radio sources.

Finally, the separate class of AGN are so called BL Lacerte (Lacs) objects. BL Lacs are the nuclei of elliptical galaxies that emit highly variable and polarized radiation, and have a non thermal optical continuum and a strong radio

[2]These galaxies were named by Carl Seyfert. In 1943 he discovered the first class of stellar systems with active nucleus (Seyfert 1943).

[3]The acronym FR is based on the names of the authors Fanaroff and Riley who made this classification in 1974 (Fanaroff & Riley 1974).

emission. With this group of galaxies, we often connect another type of AGN, Optically Violently Variable (OVVs) quasars that. The OVVs, in contrast to BL Lacs who have featureless continuum, emit broad optical emission lines characteristic for quasars. Both these groups of objects are often referred to as one class called as blazars.

2.1 Properties of AGN

First of all, active galactic nuclei have very small angular size[4]. Their angular size depends on the observed flux as $\propto F_{\rm obs}^{1/2}$, so that apparently brightest AGN are also the largest (in angular terms), but even they are still very small for the nucleus to be directly observed. However, some emission regions of the nearby AGN can be directly observed. AGN have enormously big luminosities ranging from $\sim 10^{42}$ to $\sim 10^{48}$ erg s^{-1}, i.e. we have AGN with luminosity $\sim 10^4$ times greater than a typical galaxy. However, one must consider these limits with caution as there could be a large population of mini AGN that we cannot easily detect due to the bright host galaxy. On the other hand, there is a possibility that there exist many active galaxies which nucleus is obscured by extremely thick dust extinction. Therefore, one could be misled to its true luminosity if observations are in the optical or ultraviolet band. The AGN have the broad-band continuum emission. In contrast to the spectral energy distribution (SED) of an ordinary galaxy (that represents a sum of stellar spectra, thus the great majority of its luminosity comes within no more than one decade of frequency), AGN emit across the broad range of frequencies (of order 10^5 Hz). The SED can be approximated with the power law function $F_\nu = k\nu^{-\alpha}$ where α is the spectral index (e.g. Krolik 1999, Peterson 2004). Some AGN have the SED almost flat from the infrared to X-ray part of the spectrum, so that the spectra index is $\alpha \approx 1$, although it is usually steeper. In the radio band, the brightness of active galaxies is usually an order of magnitude higher than of normal galaxies. But still, even if it so intensive, the radio luminosity is never more than $\sim$1% of the bolometric luminosity. The fraction of the power emitted in the X-ray is three or four times larger in AGN than in normal galaxies, while for some AGN subsets, the γ flux was registered to be of the same order of magnitude as the flux on significantly lower frequencies (Krolik 1999, Peterson 2004).

Variability is another remarkable property of AGN, but it depends on the wavelength and time scales in which the studied object is observed. In most

[4]This of course depends strongly on the observed wavelength, as e.g. the radio emission of an AGN more often extends over a sizable region, frequently much larger than a galaxy, while in the X-ray they appear as a point-like source.

cases, AGN vary with no special period or easily measured amplitude. There is a small subset of AGN that vary strongly in all spectral domains, and for which, this strong variability is correlated with strong polarization, compact radio structure and strong high-energy γ-ray emission. These AGN are called blazars and they contains BL Lac and OVV objects. Most AGN emit linearly polarized radiation, with fractional polarization $\simeq 0.5-2\%$. However, the level of polarization depends on the observed wavelength, e.g. radio emission can be linearly polarized up to few tens of percents.

Even though it is possible that every different type of AGN is an object where essentially different physical mechanisms dominate, today it is widely accepted that all types of AGN are very similar objects. Their observed differences can be explained with different luminosities and different viewing angles. These are the basics of the so called unification model of AGN that assumes that in every AGN there is a super-massive black hole with an accretion disk, surrounded by an opaque dusty tours. Besides the torus, in the vicinity of the black hole there are two other emission regions, the broad and narrow line regions, which are ionized with the continuum coming from the accretion disk and its corona. Also, from the vicinity of the SMBH, arouse two opposite outflows of relativistic particles - so called jets that emit predominantly in radio band, but are also visible in other wavelengths.

2.2 Emission lines of AGN

One of the characteristics of AGN are their emission line spectrum. As already mentioned, in the AGN spectrum, the electromagnetic radiation of all wavelengths is present: γ and X-ray, ultraviolet, optical, infrared and radio emission come from different radiation mechanisms (Bremsstrahlung radiation, inverse-Compton scattering, synchrotron radiation and creation/anhilation of electron-positron pairs). The continuum emission predominantly comes from the center of an AGN, more precisely from the accretion disk, and it ionize the surrounding regions of gas and clouds. It is obvious that the emission regions of such compact objects cannot be separately observed, therefore the observed spectrum is actually the superposition of the emissions coming from the center itself and from the surrounding gas, where the emission and absorption lines are formed.

The emission lines are interesting because of two reasons. First of all, they are often very broad with Full Width at Half Maximum (FWHM) up to 10^4 km s^{-1}, thus, they are surely the broadest lines in the known Universe. Second, according to the current knowledge in the field of atomic physics, the lines are quite suitable to study the physical properties of the emitting gas. The

most intensive lines in AGN spectrum are hydrogen Lyα line, hydrogen Balmer line series, doublet C IV $\lambda\lambda$1548, 1550, [O III] $\lambda\lambda$4959, 5007 lines and many others that are weaker. Also, very often the iron Fe Kα line (energy of 6.4 keV) is detected in the X-ray domain. The peculiarity of these lines is that there is a great difference in their width at half maximum of intensity, i.e. the FWHM varies from 10^2 up to 10^4 km s^{-1}. Some objects have lines with very broad wings that spread up to several thousands km s^{-1} from the center of the line, while other have lines that are not more than couple of hundreds wide. It is interesting that most of the objects show both lines from permitted and forbidden transitions, where these forbidden lines are always narrow.

The physical explanations to the existence of the broad and narrow emission lines comes from the fact that an AGN contains two distinguished emission line regions with different kinematics, density, ionization, optical thickness and radiation transfer. These emission line regions are named according to the type of the emission lines that they are producing, therefore there are:

- **The broad line region**, further in the text the BLR, is a compact region, with dimensions from only couple of light days up to couple of light weeks (see e.g. Kaspi et al. 2000, Peterson et al. 2004, 2005), that is located in the vicinity of the black hole ($<$ 1 pc). The structure of this region is very complex and most likely it consists from at least two separated subregion (see e.g. Marziani et al. 1996, Popović et al. 2004, Sulentić et al. 2000). The ionized gas in this region is of relatively high density ($n \sim 10^9 - 10^{10}$ cm^{-3}) and temperature $T \sim 10^4$K. Emitters are moving with high velocities, up to several thousands of km/s. In this region the broad emission lines (BELs) are formed.

- **The narrow line region**, further in the text the NLR, extends even up to 1 kpc far from the central source (Peterson 2004). The density in this region is pretty smaller ($n \sim 10^3$ cm^{-3}) than in the BLR, as well as the velocity of the emitters (up to 1000 km/s), while the temperature is little less, but still of the same order of magnitude. From this region arouse the narrow emission lines (NELs) that are often coming from the forbidden transitions. The physical properties of this region are much closer to the properties of emission nebulae. Therefore for their diagnostic one can use the standard methods based on the forbidden line ratios (Osterbrock 1989, Osterbrock & Ferland 2006).

In this thesis, the research is devoted to the broad line region and its physical properties, therefore, in the next sections the BLR properties and structure will be described in details. For detail review of observed properties of AGN, their classification, structure and description of every emission region see Ilić (2006).

3 The physics of the broad line region

The physics and kinematics od the BLR of active galactic nuclei are very complex, surely more complex than in the case of the NLR or emission nebula (Osterbrock 1989, Krolik 1999, Sulentic et al. 2000). That is the region of ionized gas relatively close to the SMBH which dimensions can be of order of only a couple of light days. The name of this region comes from the broad emission lines that are arising there, such as Lyα, Balmer lines, C IV, C III], He II, He I, Fe II. Their widths are in the range from couple of thousands up to 10 000 km s^{-1}. Such large widths are probably a consequence of Doppler motion in the strong gravitational field. Having the velocities even high as 10% of speed of light, the distance from the black hole can be quite small, i.e around 100 R_g ($v \propto r^{-1/2}$). The structure of this region is still not fully understand, but most likely this regions is stratified and consists of more subregions with different kinematical properties. The estimates are that its gas temperatures are of the order of 10^4 K, and densities of $n \sim 10^9 - 10^{10}$ cm^{-3}, that is concluded based on the presence or absence of some broad lines in AGN spectra. In contrast to the NLR, H II regions or planetary nebula, where some ratios of the forbidden lines (e.g. [O III], [N II] or [S II] lines) can be used for relatively simple and straightforward temperature and density diagnostics (Osterbrock 1989), in the case of the BLR the physical properties cannot be determined directly from the measured line ratios. An exception is the method for the electron temperature estimates proposed by Laor (2006), but it can be applied only for some specific AGN[5].

3.1 The structure of the BLR

The BEL profiles are substantially different from one object to another. Even the line profiles of one object can sometimes be quite different when observed in different epochs. For instance, it is shown that there are significant differences between the line profiles of radio loud (RL) and radio quiet (RQ) active galaxies (Sulentic et al. 2000). Also, it is believed that high ionization lines (HIL), such as Lyα, C IV λ1550 or He II λ4686, and low ionization lines (LIL)[6], such as Balmer lines or Fe II lines, are formed within kinematically and physically different components of the BLR (Sulentic et al. 2000, Marziani et al. 1996). The difference between the HIL and LIL is particulary seen in the case of radio quiet AGN. Also, the asymmetry is often present in the line profiles. It can

[5]More about this method is given in section 3.2

[6]The HIL are the lines that are produced by the emitters with ionization potential $\geq$ 50 eV, while the lines of the emitters with ionization potential $\leq$ 20 eV are the LIL.

be in both blue and red part of a line, where the blue asymmetry is usually associated with the idea of the outflow towards the observer. The investigations of the emission line wings are especially interesting. The emphasized shape, large widths, asymmetry or rounded shape indicate that the line wings are coming from the region with different characteristics than the region where the line core is formed. One is evident, the broad line region is a complex region that consists of different subregion. These subregions are located on different distances from the central continuum source and they probably have different geometry, kinematical and thermodynamical parameters (Krolik 1999, Wandel et al. 1999, Sulentic et al. 2000).

One reliable method to study the geometry and kinematics of the broad line region is the "reverberation mapping" technique (Blandford & McKee 1982, Netzer & Peterson 1997). The method is based on the response of the ambient gas to changes in the central continuum source. It uses the time lag between the line light curve and the continuum light curve, to estimate the size of the emission line region and to deduce the mass of the central black hole, where this time delay is due to the fact that a photon needs a certain amount of time to travel from the source of the ionizing continuum to the line emission region. The technique is possible to apply to a limited number of AGN, as it requires a variable source that has been monitored frequently over a period of time (from days to weeks depending on the AGN luminosity and variability characteristics). These kind of data is difficult to provide and these monitoring campaigns were carried out in about three dozen AGN, usually Seyfert galaxies of moderate luminosity. The reverberation method has been applied to approximately forty active galaxies that were possible to observe during the long period of time (Kaspi et al. 2000, Peterson et al. 2004). The results of that studied AGN sample show that the size of the BLR is in the range from 1 to 387 light days, and that the mass of their black holes are in the range $(0.13 - 55) \times 10^7 M_\odot$.

As mentioned, the results of the reverberation techniques can be used to estimate the mass of the black hole in the center of an AGN, using the virial assumption, i.e. the BLR gas is gravitationally bounded, than

$$M \approx G^{-1} v^2 r, \tag{3.1.1}$$

where r is the radius determined from the time lags and v is the velocity that is estimated from the FWHM (Gaskell 1988, Wandel et al. 1999). These studies show that the BLR size scales approximately with the square root of the luminosity, which is following the theoretical expected slope obtained with photoionization models with the simple assumption of all AGN having on average the same ionization parameter, BLR density, column density, and ionizing spectral energy distribution (Kaspi et al. 2000, 2005). The experiments give the following power-low dependance between BLR radius and the luminosity

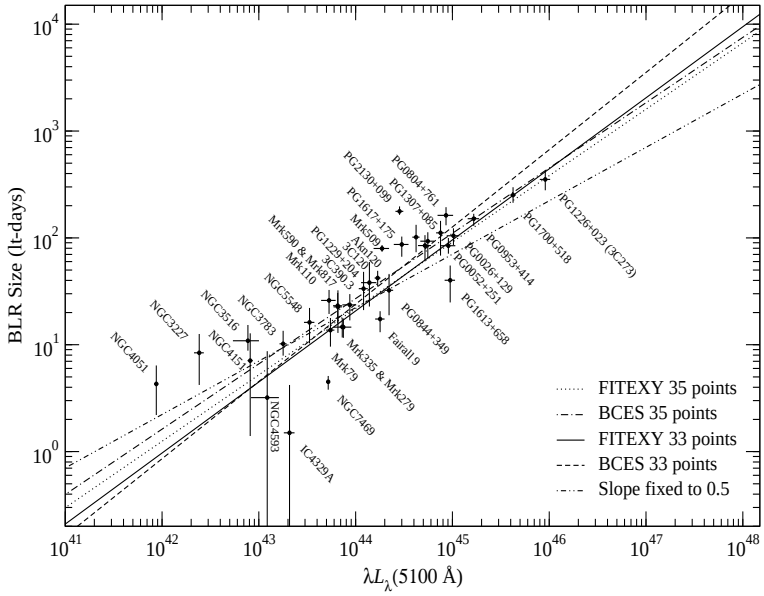

Figure 2: Balmer-line BLR size plotted versus the $\lambda L_\lambda(5100\,\text{Å})$ luminosity (in units of erg s^{-1}). The BLR size of each data set is determined from the averaged Balmer-line time lags. Objects with multiple data sets have been averaged to one point per object. Four fits are shown: using all 35 points, excluding the two low luminosity AGN (which are heavily influenced by intrinsic reddening), and with the two fitting methods, as well as the theoretical expected slope of with $\alpha = 0.5$ (dot-dot-dashed line) (Kaspi et al. 2005, Kaspi 2007).

(Kaspi et al. 2000, 2005, Bentz et al. 2006, 2007b):

$$\log(R_{\text{BLR}}) = K + \alpha \log[\lambda L_\nu], \tag{3.1.2}$$

where α is the slope of the power-low function between the BLR radius and the monochromatic luminosity, while K is the scaling coefficient. The value of the best-fitting slope α is still not precisely determined (it varies in the range from 0.47 to 0.88) due to relatively small number of objects for which the reverberation analysis has been performed, as well due to studying the light curves of different emission lines and continuum wavelengths (see McGill et al. 2008 for review of all latest results). It is interesting to mention the slope value of $\alpha \approx 0.50$ obtained by Bentz et al. (Bentz et al. 2006, 2007b), that is in an agreement with the simple predictions of the photoionization theory where $\alpha = 0.50$ with the assumption that all AGN are having on average the same ionization parameter, BLR density, column density and ionizing spectral energy distribution.

In Figure 2 the mean Balmer-line BLR size (in light days) versus the luminosity $\lambda L_\lambda(5100\,\text{Å})$ is plotted, with one averaged point per object. The figure

shows four fits: using all 35 points, excluding the two low luminosity AGN (which are heavily influenced by the intrinsic reddening), and with the two fitting methods. Within the luminosity range of the measurements (10^{42}–10^{46} erg s^{-1}) all 4 fits are consistent with each other and all are well within the scatter of the points in the plot. The disagreement of these results with the theoretical expected slope of 0.5 indicates that the above simple assumptions are not valid and there is likely some evolution of a few of these characteristics along the luminosity scale (Kaspi et al. 2005, Kaspi 2007).

The kinematics and geometry of the BLR is still not fully understood. One of the main obstacle in its research is that even for the closest AGN the angular size of the nucleus is of order 10^{-6} arcsec. Therefore, up to now spectroscopy is the only method to probe gas motions in the BLR, i.e. the BLR geometry. From the studies of the BEL profiles one can extract some basic facts of the BLR nature. First of all, there is a strong evidence of the existence of the disk-like component at least in the case of some AGN. In particular, there is a relatively small sample of AGN (2% - 5%), whose spectra have double peaked Balmer lines, only about 4% at distances of $z < 0.33$ (Eracleous & Halpern 2004). These lines are usually connected to the rotating keplerian accretion disk. Moreover, there is a strong evidence of the presence of outflows in many AGN. In particular, some emission lines have strong blue asymmetry which indicates that the matter is ejected towards the observer. In the spectra of AGN we also detect the absorption lines that are blueshifted with the respect to the cosmological redshift of the galaxy. There are many indications that this absorbtion, mainly detected in the X and UV part of the spectra, is coming from the same regions as the broad emission lines. Finally, it is shown that the gas in the BLR is under significant gravitational influence of the SMBH. As we already described, the size of the BLR could be estimated using the reverberation mapping techniques, but the obtained dimensions are different for different BELs (e.g. the emission region of the Hα line can have significantly different dimension than He II λ4686 line region (see e.g. Kollatschny 2003)). When applied to HIL, the results indicate that the HIL are formed in the regions closer to the central source than the LIL, thus we can conclude that there is ionization stratification in the BLR. Besides, the HIL are often broader and the relation between the radius and the velocity dispersion of the BLR really resemble the relation obtained from the virial theorem $r \propto \Delta V^{-2}$, where r is the radius and ΔV is the velocity dispersion.

Investigation of the BLR structure is necessary for understanding the nature of the AGN phenomenon. Primarily in order to estimate (as precisely as possible) the mass of the SMBH, but also to understand the process of matter infalls and outflows in AGN. So far many dynamical models of the BLR region were proposed, that are based on the certain emitting gas motion (biconical ejections, rotation, etc.). In principal, all proposed models can fit well

the observed emission profiles of some objects or lines, but so far there is no unique model that can satisfactory describe all observed BEL profiles. Here we mention some of the currently used models:

1. *The binary black hole.* The main assumption in this model is that in the center of an AGN exists two black holes, and thus two BLR with different properties that are determined by the properties of the black holes. This explains the two peaks visible in some BELs, as well as the presence of two different components in the wings of some lines (Gaskell 1988, 1996). One of the disadvantage of this model is that in a such system the two broad line region would hardly remain stable (Eracleous & Halpern 1994).

2. *The clouds of gas.* The stratification of the BLR is explained with the great number of clouds with different physical properties, spherically distributed around the SMBH. The line asymmetry is explained with the mobility of the gas clouds, as well as with the radiation scattering. The great disadvantage of this model is that for such observed smooth line profiles it is necessary to have extremely large number of clouds (10^7-10^8), but also the fact that the clouds are thermodynamically unstable if they are in the radiation equilibrium with the surrounding medium (Baldwin et al. 1995, Goad & Wanders 1996). Here we should mention the model of Locally Optimally emitting Clouds (LOCs), that assumes that only the clouds of specific and narrow range of densities and distances from the central source are responsible for formation of each broad emission line, that results with the maximal efficiency of the emission (Baldwin et al. 1995).

3. *The disk.* This model predicts that the broad emission lines are formed in the keplerian relativistic dsik[7] that surrounds the SMBH (Chen et al. 1989, Eracleous & Halpern 1994, 2003, Strateva et al. 2003). The biggest advantage of this model is that it successfully explains the profiles of the double-peaked lines (especially those lines with two significantly separated peaks), but it also explains large electron densities needed for the formation of Fe $\mathrm{II_{opt}}$ and other low ionization lines, such as Ca II. Moreover, the results of the reverberation mapping are in agreement with this model. On the other hand, the existence of the single-peaked lines is explained with the high inclination angle of the disk or with the fact that they could come from the outer regions of the disk. The shortcoming of this model is that it cannot explain the variability of emission lines, as in the case of the disk, both side of the line profiles are changed due to the change of the ionizing continuum flux (Gaskell 1988), as well as the fact that the objects with prominent double peaked lines are usually radio

[7]or some form of the flatten region that surrounds the accretion disk

loud objects that have the weakest $FeII_{opt}$ emission (Chen & Halpern 1989).

4. *The biconical ejection.* One possible solution for the asymmetry seen in the wings of some BELs, as well as to the existence of the peaks, can be the biconical ejection of matter (Zheng et al. 1990, Marziani et al. 1996). The problem of this model is the fact that we often do not detect the asymmetry in the lines, as well as the fact that we usually only see the visible asymmetry in the blue part of the line, while this model assumes that we have the ejection also in another direction, away from the observer, i.e. the red asymmetry that is hardly observed in the BELs.

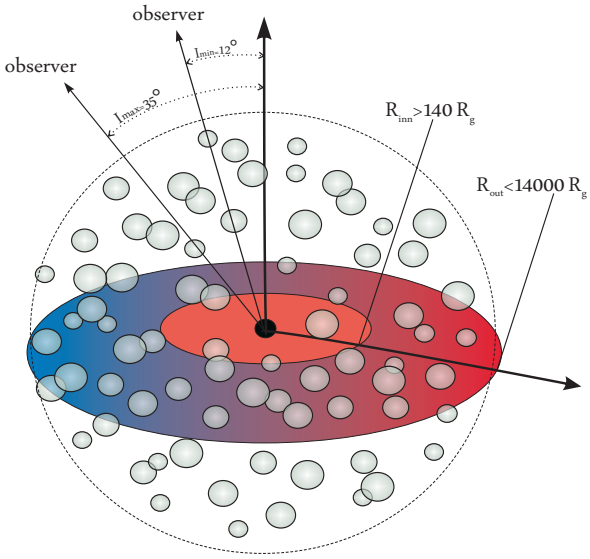

Figure 3: The scheme of the two-component model of the central emission region of active galaxy Mrk 817 (Ilić 2005, Ilić et al. 2006).

5. *The two-component model.* Many authors consider the BLR to consist from two subregions, defined as a very broad line region (VBLR) that contributes to the line wings, and an intermediate line region (ILR), where the line core is formed (Brotherton et al. 1994, Popović et al. 1995, Sulentic et al. 2000, Popović et al. 2001, 2002, 2003, 2004, Ilić 2005, 2006, Ilić et al. 2006b, Bon et al. 2006). The inner part of the BLR form the VBLR, thus the gas in the VBLR has greater velocities and is most likely optically thin (one of the facts that indicates such property is that the FWHM of the rms spectrum of Hβ line is smaller than the mean FWHM) of large density ($n_e \sim 10^{11} - 10^{13}$) and high ionization

level ($U \approx 0.1 - 1$). The ILR is than the transition region between the BLR and NLR, that would form the outer part of the BLR. In the ILR gas velocities are somewhat lower while the ionization level is still high. One of the assumptions is that the VBLR could be a disk while the ILR could be a part of the disk wind (Popović et al. 2004).

A scheme of the two-component model for the case of the BLR of active galaxy Mrk 817 is given in Figure 3. The figure show the accretion disk with spherical emission region that is presented with great number of spherically distributed gas clouds (Ilić 2005, Ilić et al. 2006b).

Finally, statistically significant reverberation studies of the BLR (Kaspi et al. 2000, 2005, Peterson et al. 2004, 2005) show that there is an anti-correlation between ionization state and the time lag between the emission line light curve and the continuum light curve, as well as the anti-correlation between the time lag and the width of the line, that confirms the hypothesis that the FWHM of each line is an indicator of a distance from the central source. From all these facts it is evident that the broad line region is a stratified photoionized region where emission lines are formed under wide range physical conditions and in wide range of distances from the central continuum source.

3.2 The physical properties of the BLR

Investigations of physical and kinematical properties of the BLR of AGN is important for many reasons, out of which the most obvious one is the connection of the BLR to the bright central source of radiation. Understanding the physical processes in the BLR can give us important hints about the processes occurring in the vicinity of the SMBH, the origin of the continuum that is heating the BLR and physical processes that are responsible for the production of the powerful AGN emission in general. Unfortunately, the BLR has not been directly observed[8] and thus, the physical understanding of the BLR requires detail theoretical calculations, numerical simulations and obtaining a great number of high quality spectra. Even today, after many years of research, there are some fundamental issues about the BLR that we still do not understand, and these are the geometry, physical properties and origin of the gas in the BLR.

The BLR consists of the gas photoionized by the thermal continuum emis-

[8]The parsec scale structures have been observed in the radio band with the VLBI measurement, although, due to large errors in the optical observations it is impossible to connect these radio structures with the center of the optical emission that eventually could be taken to be the center of the continuum source. However, scientists today are making a lot of effort to obtain the optical images with the same spatial resolution as present radio observations.

sion coming from the accretion disk and its corona, and it is located in the vicinity of the black hole and accretion disk (< 1 pc). Beiing so close to the massive object, the physical properties of the BLR gas are surely influenced by the strong gravitational field. The comparison of continuum and BLR fluxes indicates that only 10% of the continuum radiation is absorbed by the BLR clouds. Also, the volume filling factor is very low - only a small part of the central region is occupied by the BLR clouds. The mass in the BLR that is necessary to produce the observed luminosity is only a few solar masses. Even in the case of the brightest AGN, the mass of the BLR is negligible compared to the mass of the SMBH.

The classical theory assumes that the main heating source, i.e. the source ionization of the BLR gas is the photoionization by the continuum radiation coming from the center (see e.g. Kwan & Krolik 1981, Osterbrock 1989, Baldwin et al. 1995, 1996, Marziani et al. 1996, Ferland et al. 1998, Krolik 1999, Korista & Goad 2004), although in some cases it is shown that a non-radiately heated region contributes to the total BLR spectrum (Dumont et al. 1998, Shapovalova et al. 2008). Moreover, since the densities in the BLR are high ($n_{\rm H} \sim 10^8 - 10^{12}$ cm^{-3}) and the temperatures are $\sim 10^4$ K, it is more likely that the conditions in the BLR are similar to the stellar atmospheres than to photoionized nebulae, such as planetary nebulae or H II regions (Osterbrock 1989). Therefore, many of the techniques commonly used to derive the physical properties of photoionized nebulae (e.g. the temperature and density diagnostics using the ratio of the forbidden lines) are not applicable in the case of the BLR (Osterbrock 1989, Griem 1997). Particularly, it is hard to find a straightforward method that would use only the observed BELs for the BLR temperature and density estimations.

There is practically no direct information on the temperature in the BLR. There are some indications that the BLR temperature is $T < 35,000$ K according to the observed Fe II emission, as for the higher temperatures Fe II would be almost completely collisionally ionized to Fe III (Osterbrock & Ferland 2006). Furthermore, there are some rough limits to the density obtained from the observed emission lines. For example, the fact that the forbidden [O III] lines are suppressed in the BLR gives the lower limit for the density, i.e. the critical density for the collisional deexcitation of the ^{1}S$_0$ level of O^{++} is $\approx 10^8$cm^{-3}. On the other hand, the upper limit can be estimated from the presence of the broad C III]λ1909 line in the BLR spectrum. The critical density for collisional deexcitation of ^{3}P$_1$ level of C^{++} is 10^{10} cm^{-3}. However, for the upper limit of the BLR density the critical density of around $n_c \approx 10^{14}$cm^{-3} for collisional deexcitation of the broad lines should be taken. Anyhow, some lines can give us some indications of the density values in the BLR, but only in same range of densities. For instance, in the range of densities from 10^9 to 10^{11}cm^{-3} some semi-forbidden lines are sensitive to density changes. The

ratio of Si III]λ1892/C IIIλ1909 lines, which increases with density, becomes a useful diagnostic. Also, the strength of Al IIIλ1860 line should be especially enhanced at $n_{\rm e} \sim 10^{12}{\rm cm}^{-3}$ (Sulentic et al. 2000).

The problem of the direct measurement of the physical properties of the BLR using the observed broad emission lines is still opened. There is always a possibility to estimate the physical conditions in the BLR assuming a theoretical model and then compare it with the observed spectrum (Osterbrock & Ferland 2006), or using the numerical simulations (Ferland et al. 1998, Korista & Goad 2000, 2004), although numerical simulations are not always capable to reproduce some observed properties as well[9]. Recently, Laor (2006) proposed one method that considers electron scattering influence on the line shapes and determines the physical parameters of the BLR by fitting the emission line exponential wings, in the case of the low luminosity AGN (Laor 2006). The method assumes that the exponential wings are produced by the optically thin, isotropic, thermal electron scattering. In that case, by fitting the line wings with an electron-scattering model one can estimate the electron density and optical depth of the region (Laor 2006). However, the problem of this direct method for BLR diagnostics is that it can be applied only for the rare cases of the BEL profiles with exponential wings (e.g. the case of galaxy NGC 4395). Besides, another problem of this method is that kinematics of the emission gas in the BLR can strongly affect the BEL profiles.

Moreover, Popović (2003, 2006ab) showed that in the case of the broad line region of some AGN, fluxes of the hydrogen Balmer lines follow the Boltzmann plot (BP), which indicates that populations of the higher energy level ($n \geq 3$) could be explained with the Saha-Boltzmann equation. In that case, if the Saha-Boltzmann distribution can be used to describe higher energy levels of hydrogen, then the temperature of the region where these lines are formed can be estimated[10]. This method has already been successfully applied on the broad Balmer lines of some AGN (Popović et al. 2002, 2003, Ilić et al. 2006a,b, La Mura et al. 2007a,b, Popović et al. 2008a). This method, as well as the method proposed by Laor (Laor 2006), enables us to directly probe the physical (thermodynamical) properties of the BLR, only from the measured parameters of the BELs. One of the basic goals of this thesis is to propose a simple and straightforward method for diagnostics of the BLR physical properties (the temperature and density) using only the observed hydrogen and helium lines from the optical part of the spectrum.

The emission lines in the BLR are the result of the recombination of the photoionized medium. But, the conditions of the pure recombination cannot be completely applied in the case of the BLR as e.g. observations show that

[9]More details about the shortcomings of the numerical simulations will be given in section 3.6.1

[10]More details about this method will be given in section 3.5.

some observed line ratios are much different from the ratios predicted by the recombination theory. As an example the Lyα/Hβ line ratio is often mentioned in the literature, as in cases of some AGN it is ≈ 10, while the theory predicts much higher values, even over 30 (Netzer et al. 1995, Osterbrock 1989)). Some processes can lead to such observed hydrogen line ratios, first of all the collisional excitation and deexcitation, as well as extinction. In the last 30 years there are many papers dedicated to this problem, see e.g. Netzer (1975), Ferland & Netzer (1979), Ferland et al. 1979, Kwan (1984), Rees et al. (1989), Ferland et al. (1992), Shields & Ferland (1993), Dumont et al. (1998), etc. The dust is also present in the AGN (see e.g. Crenshaw et al. 2002, 2004, Gabel et al. 2005, etc.), but it seems that in same cases the extinction itself cannot explain the measured line ratios. Therefore, the photoionization, recombination and collisions should be considered as relevant processes that occur in the BLR. At larger ionization parameters, the recombination is more important, but at higher temperatures or in the case of low ionization parameters the collisional excitation becomes important as well (Osterbrock 1989). These two effects, as well as radiative-transfer effects in Balmer lines, should be taken into account when explaining the ratios of hydrogen lines. Moreover, the geometry and possible stratification in the BLR may affect the continuum and line spectra of AGN (Goad et al. 1993). Further in the text, we will describe in details the photoionization and methods to determine the temperatures of the ionized gas, such is the Boltzmann plot method.

3.3 Physical processes in plasma

The kinetic theory of gases attempts to explain macroscopic thermodynamic properties of plasma, such as pressure or temperature, by considering the chemical composition and particle's motion, as well as the microscopic characteristics of the particles. Before discussing some basic kinetic models of the plasma, it is necessary to clarify what different temperatures can determine the plasma conditions. First of all we distinguish the *kinetic gas temperature*, $T_{\rm kin}$, that is defined with the Maxwell-Boltzmann velocity distribution

$$f(v)dv = \left(\frac{m}{2\pi k T_{\rm kin}}\right)^{3/2} 4\pi v^2 \exp\left(-\frac{mv^2}{2kT_{\rm kin}}\right) dv, \tag{3.3.1}$$

where m and v are the mass and velocity of particles, and k is the Boltzmann constant. There is also the *excitation temperature*, $T_{\rm exc}$, that follows the Boltzmann distribution which describes the ratio of populations of two energy levels N_1 and N_2

$$\frac{N_1}{N_2} = \frac{g_1}{g_2} \exp\left(-\frac{E_1 - E_2}{kT_{\rm exc}}\right), \tag{3.3.2}$$

where g and E are statistical weight and energy of a particular discrete energy level. The *ionization temperature*, T_{ion}, is defined by the Saha distribution which describes the ratio of populations of two ionization states N_{k+1} and N_k

$$\frac{N_{k+1}}{N_k} = \frac{2}{n_{\mathrm{e}}} \frac{(2\pi m_{\mathrm{e}} k T_{\mathrm{ion}})^{3/2}}{h^3} \frac{g_{k+1}}{g_k} \exp\left(-\frac{E_{k+1} - E_k}{k T_{\mathrm{ion}}}\right), \tag{3.3.3}$$

where n_{e} is the electron density and E_{k+1} are E_k ionization energies of the ionization states $k+1$ and k respectively. Further, the *gas electron temperature*, T_{e}, is obtained from the energy that is carried by the free electrons

$$E_k = k T_{\mathrm{e}}. \tag{3.3.4}$$

And finally, the *radiation temperature*, T_{rad}, defines the Planck radiation distribution

$$B_\nu(T) = \frac{2h\nu^3}{c^2} \frac{1}{\exp(h\nu / k T_{\mathrm{rad}}) - 1}, \tag{3.3.5}$$

where h is the Planck constant and c is the speed of light.

The simplest kinetic model that can be used to describe the ionized gas is the model of **thermodynamical equilibrium** (TE). In that case, the gas properties are constant in space and time and they can be described with the Maxwell, Boltzmann and Saha distribution, and all previously mentioned temperatures are equal:

$$T_{\mathrm{kin}} = T_{\mathrm{exc}} = T_{\mathrm{ion}} = T_{\mathrm{e}} = T_{\mathrm{rad}}.$$

However, it is hard to expect that in nature one could find the gas that would be in the complete TE, yet it is more likely that the gas would be in the **local thermodynamical equilibrium** (LTE), which means that the gas properties change in space and time, but these changes are so slow that for every point one can assume that in its vicinity the thermodynamical equilibrium is valid. In the case of the LTE all temperatures are equal apart from the radiation temperature:

$$T_{\mathrm{kin}} = T_{\mathrm{exc}} = T_{\mathrm{ion}} = T_{\mathrm{e}} \neq T_{\mathrm{rad}}.$$

Anyhow, often plasmas are not even in the case of the complete LTE, but in some cases it is possible to have so called **partial local thermodynamical equilibrium** (PLTE) in the sense that populations of sufficiently highly excited levels are related to the next ion's ground state population by Saha-Boltzmann relations (Griem 1997). In the case of the PLTE we have that only the excitation temperature can be approximated with the electron temperature:

$$T_{\mathrm{kin}} \neq T_{\mathrm{ion}} \neq T_{\mathrm{exc}} \neq T_{\mathrm{exc}} \simeq T_{\mathrm{e}}.$$

Besides these gas kinetic models, there are the model of **coronal plasma** and **collisional-radiative model**. The first one can be applied in the case of low

density gas. The gas is then in the coronal ionization equilibrium which means that there is a balance between the rate of collisional ionization in the charge state $z-1$ and radiative recombination in the charge state z per unit volume. The collisional-radiative model can be applied in the case of higher densities, but also for the case of steady state and spatial homogenous plasma as previous models, and represents the bridge between the coronal model and LTE model. The basic relations that describes the plasma conditions is the **ionization equilibrium equation** that describes the balance between all processes of ionization and recombination.

Coronal equilibrium or collisional ionization equilibrium[11] is a dynamic balance at a given temperature between collisional ionization from the ground states of various atoms and ions present in the plasma and the process of recombination from higher ionization states, where all ions are effectively in the ground state. The main difference between the coronal equilibrium and LTE model is that the LTE is described by the Saha equation, but the excited states are populated according to the Boltzmann equation. The collisional ionization balance involves, in general, three ionization stages of a given element, $i-1$, i and $i+1$, coupled through collisional ionization, the various means of recombination and through charge exchange reactions[12]. If the number density of these ionization stages are n_{i-1}, n_i and n_{i+1} respectively, then the collisional ionization equilibrium condition can be written as

$$n_{\mathrm{e}} n_i \alpha^i_{\mathrm{coll}} + n_i \sum_{x=H^0,He^0} n_x \alpha^i_{\mathrm{ce}} = n_{\mathrm{e}} n_{i+1} \alpha^{i+1}_{\mathrm{rec}} + n_{i+1} \sum_{x=H^0,He^0} n_x \alpha^{i+1}_{\mathrm{ce}}, \qquad (3.3.6)$$

where α_{coll} is the collisional ionization rate, α_{ce} is the charge exchange rate and α_{rec} is the recombination rate (Dopita & Sutherland 2003). The case of the coronal approximation is based on the assumption that the ionization rates on the left-hand side of the above equation refer only to the ground state of the ion. If the charge exchange reactions can be ignored completely (which is the valid assumption for the hydrogen or helium in the plasma with solar abundances), the equation 3.3.6 simplifies to an elegant solution

$$\frac{n_{i+1}}{n_i} = \frac{\alpha^i_{\mathrm{coll}}}{\alpha^{i+1}_{\mathrm{rec}}}. \qquad (3.3.7)$$

3.3.1 Photoionization

What is behind the photoionization process, i.e. the spectrum of a photoionized gas? Let's take that the spectrum is formed within a cloud that is transparent, or nearly so, to the observed radiation. It is exposed to a source of the

[11] The name comes from its application to the hot coronae of stars.

[12] More details on atomic processes in plasma is given in Appendix B.

high-energy radiation (e.g. in the case of AGN it is an energetic continuum from an accretion disk). Energetic photons ionize the gas, and the residual energy of the photoelectrons heats the gas. The photoelectrons collide with ions and cause internal excitations, which decay to produce **collisionally excited emission lines**. The electrons eventually recombine with ions and produce **recombination lines**. If our line of sight to the continuum source passes through the gas, the gas produces **absorption lines**. Analysis of this emitted spectrum can provide information regarding the composition, density, pressure, and temperature of the gas. In turn, this information reveals much about the gas' history and the properties of the central energy source (Ferland 2003).

The line formation depends on the density (or pressure) of the emitting gas, ionization state, temperature, distribution of the population of certain energy states, intensity of the background ionization source and the possibility for the created photons to escape from the region. In order to predict the total line spectrum, each of above parameters should be determine and all processes possibly occurring in the plasma need to be treated consistently. In most cases, the thermal and ionization balance equations are used. Usually it is assumed that all processes are constant in time, although it is not always a valid assumption. The final form of the ionization balance equation depends on the atomic parameters and the whole picture gets even more complicated if atom or ion has more electrons. Also, the atomic parameters differs from one author to another, and the question is which one are most reliable. The thing gets a little bit easier with the use of the Milne relation which says that in the thermodynamical equilibrium all processes and their inverse one should be balanced. When applied to photoionization and its inverse process of recombination, this relation states that the rate of spontaneous and radiatively induced recombinations of an electron in the velocity range $v, v+dv$ is matched by the photoionization rate in the frequency range $\nu, \nu + d\nu$, where $m_{\rm e}v^2/2 + h\nu_{\rm I} = h\nu$ ($\nu_{\rm I}$ is the frequency that corresponds to the energy of the ionization state I). As a consequence of this $m_{\rm e}vdv = hd\nu$. In the case of the LTE, combining the Planck function for the radiation distribution, the Saha equation for the ionization balance and the Maxwell-Boltzmann velocity distribution, we obtain the Milne relation between the photoionization and recombination cross section, $\sigma_{\rm phot}(v)$ and $\sigma_{\rm rec}(v)$ respectively, for electron velocity v and statistical weight of a state g, to be

$$(m_{\rm e}cv)^2\sigma_{\rm rec}(v) = \frac{g_i}{g_{i+1}}(h\nu)^2\sigma_{\rm phot}(v). \tag{3.3.8}$$

The intimate connection between the ionization (collisional ionization and photoionization) and recombination (dielectric and radiative recombination) processes, means that the rate calculations of all these processes should be computed in a fundamentally consistent manner using the same set of atomic

parameters. In the past, these have been usually treated separately and by different methods, but recently Nahar & Pradhan (1997) gave the first such fully self consistent computation of the photoionization and recombination cross sections using the R-matrix method. In the case of hydrogen-like ions with charge Z, the photoionization cross section, $\sigma_{1s}(E)$ and the threshold energy, E_{1s}, for large frequencies can be calculated analytically

$$E_{1s} = Z^2 I_H \text{ and}$$

$$\sigma_{1s}(\nu) = \frac{2^9\pi^2\alpha a_0^2}{3Z^2 e^4}\left(\frac{E_{1s}}{h\nu}\right)^{3.5} = \frac{6.3042\times10^{-18}}{Z^2}\left(\frac{\nu}{\nu_0}\right)^{-3.5}[\text{cm}^2], \qquad (3.3.9)$$

where I_H is the hydrogen ionization potential, ν_0 is the associated frequency, α is the fine structure constant, and a_0 is the Bohr radius (Dopita & Sutherland 2003).

The properties of any photoionized gas are often described with the ionization parameter U (sometimes denoted as Γ). There are several different definitions of ionization parameter in the literature. They are all conceptually the same, but each has its own technical advantages and disadvantages. For the purposes of calculating the ionization equilibrium the most useful definition of ionization parameter is

$$U = \int \frac{J_\nu d\nu}{ch\nu n_H}, \qquad (3.3.10)$$

where J_ν is the mean intensity (given in energy units per unit area, time, solid angle and per unit frequency interval), n_H is the hydrogen number density, c is the speed of light, h is the Planck constant, and integral is over the entire ionization range (Krolik 1999). Defined like this, the ionization parameter is the ratio of the number density of ionizing photons, that leads to photoionization, to hydrogen nuclei, that influence the recombination. The most dominant process of the photon emission from the photoionized species is radiative recombination being the inverse process to photoionization. There are several similar processes that can also be relevant for the line emission in AGN. These are the process of dielectronic recombination, three-body recombination and charge exchange reactions (More details in Appendix B).

The photoionization theory can be checked by comparing the total number of ionizing photons emitted by the central source and the total number of recombinations in the ionized gas. The total number of ionizing photons must be large enough to balance the total number of recombinations, that are of course related directly to the total number of Hβ photons emitted in the gas. The connection between luminosity in the Hβ line, $L_{H\beta}$, and the featureless continuum luminosity per unit wavelength interval, L_λ, is the following (Osterbrock 1989):

$$L_{H\beta} = L_\lambda(\lambda4861)W_0(H\beta) = L_\nu(\lambda4861)\frac{d\nu}{d\lambda}W_0(H\beta), \qquad (3.3.11),$$

where $W_0(\mathrm{H}\beta)$ is the equivalent width of the Hβ line. If we assume the power-law form of the featureless continuum emission

$$L_\nu \sim \nu^{-n} \tag{3.3.12}$$

and that the luminosity in the Hβ line is given with the expression (Osterbrock 1989)

$$L_{\mathrm{H}\beta} = h\nu_{\mathrm{H}\beta}\frac{\alpha^{\mathrm{eff}}_{\mathrm{H}\beta}(\mathrm{H}^0,T)}{\alpha_B(\mathrm{H}^0,T)}\int_{\nu_o}^{\infty}\frac{L_\nu}{h\nu}d\nu, \tag{3.3.13}$$

then the above relation becomes

$$W_0 = \frac{\lambda_{\mathrm{H}\beta}}{n}\frac{\alpha^{\mathrm{eff}}_{\mathrm{H}\beta}(\mathrm{H}^0,T)}{\alpha_B(\mathrm{H}^0,T)}(\frac{\nu_0}{\nu_{\mathrm{H}\beta}})^{-n} = \frac{568}{n}(5.33)^{-n}, \tag{3.3.14}$$

where the numerical value is given in Å and is calculated for the temperature $T = 10^4$ K, though the ratio of recombination coefficients $(\alpha^{\mathrm{eff}}_{\mathrm{H}\beta}(\mathrm{H}^0,T)/\alpha_B(\mathrm{H}^0,T))$ is almost independent of temperature (Osterbrock 1989). $\alpha^{\mathrm{eff}}_{H\beta}$ is the effective recombination coefficient of the Hβ line, while α_{B} is the total recombination coefficient of the neutral hydrogen, which does not include the recombination to the ground level. Measuring the equivalent width of the Hβ line, W_0, and using the above relation, one can calculate the index n, which describe the continuum emission of the central source and see how it coincides with the observed spectrum.

It is evident that in the case of AGN, hot stars can not be the source of ionization of the line emitting regions, as in the case of H II regions which spectra show similar emission lines. First of all, the stellar continuum could not produce such a wide range of ionizations that is seen in NLRG and Seyfert 2 galaxies, with the emission lines of low ionized emitters, such as [O II] and [S II], but also with prominent emission lines of high ionization elements, such as [Ne V] or [Fe VII]. Of course, for such spectra it is necessary to have "harder" continuum radiation in the UV part of spectrum, but also from the higher frequencies (as in X-rays).

Even though there are pretty solid evidences that in most of AGN the emission line spectrum is induced by the continuum emission coming from the accretion disk and its corona, there is still a possibility that in some objects the heating of the emission line regions comes from the mechanic energy of the shock waves. The continuum emission is directly detected and it can be easily estimated how much of the energy is available for the line production, while in the case of the shock waves evidences are still indirect, therefore this explanation is still unsure. One of the way to study these effects is to assume certain type of shock waves and then determine what emission lines could form under such conditions, and then compare how the theoretical results agree with observations, in contrast to the photoionization models (where both shock wave

and photoionization approaches use the same number of free parameters). Also, in some radio galaxies it is observed that the NLR is extended much further away from the center than the radio jets, which excludes the fact that shock waves along the radio jets are the only excitation mechanism of this region.

The great disadvantage of the photoionization model is the fact that the NELs nearly never change. Therefore, the conclusion that there is a connection between the continuum flux and line flux variabilities is simply not valid, which is assumed to be correct in the case of the BELs. Of course, even though the model can successfully describe some observed properties of the line emission spectrum, that does not necessarily mean that it is an unique mechanism for the line production. It could be that some group of lines is produced by shock ionization. For example, there are cases of AGN where the line-emitting gas clouds follow the radio-jet structure, that indicates that shock excitation by passage of the radio jet could be one additional excitation mechanism for the NLR (e.g. the galaxy NGC 4151 (Mundell et al. 2003)).

3.4 Temperature diagnostics in laboratory plasmas

To estimate the gas temperature, it is necessary to distinguish between kinetic temperatures of electrons, ions and atoms (T_e, T_j, T_a). These temperatures may differ from each other even if the individual velocity distributions are close to Maxwellians. However, most laboratory plasmas are sufficiently dense and long-lived, and also have only relatively smooth spatial variations, therefore the electron distributions could be indeed described with the Maxwell distribution. In that case, the concept of a local electron temperature is normally valid and useful (Griem 1997). Most of the spectroscopic temperature measurements primarily yield the electron temperature. They are based on relative line intensities either of the same atom or ion or of neighboring ionization stages of the same element, then based on relative continuum intensities, or on ratios of line and continuum intensities, etc. (Griem 1997). The basic assumption here is that the nonrelativistic Doppler effects dominate over the various other line broadening mechanisms. Here we will describe in details only two methods for temperature diagnostics: one that is based on the relative line intensities of the same atom or ion, and the other based on the relative line intensities of neighboring ionization stages of the same element.

3.4.1 Relative intensities of lines of the same atom or ion

This method assumes that in optically thin and homogeneous plasma of length l along the line of sight, spectrally integrated emission line intensities are given by (Griem 1997):

$$i_{nm} = \frac{\hbar \nu_{mn}}{4\pi} A_{mn} N_m l, \tag{3.4.1}$$

where ν_{mn} is the frequency of the considered transition, A_{mn} is the transition probability, N_m is the population of the energy level m, and $\hbar$ is the reduced Planck constant.

For the plasma in PLTE as discussed in the section 3.3, down to the upper levels m_1 and m_2 of two lines of the same atom or ion, one can use the Saha-Boltzmann equation do describe the ratio of the two populations. Using the equation 3.3.2, one thus obtains for the ratio of the two emission lines whose upper levels are m_1 and m_2 with energies E_{m_1} and E_{m_2}

$$R = \frac{i_{n_1 m_1}}{i_{n_2 m_2}} = \frac{\nu_{m_1 n_1} A_{m_1 n_1} g_{m_1}}{\nu_{m_2 n_2} A_{m_2 n_2} g_{m_2}} \exp\left(-\frac{E_{m_1} - E_{m_2}}{kT}\right). \tag{3.4.2}$$

From this one gets the temperature corresponding to the given line ratio,

$$kT = \frac{E_{m_2} - E_{m_1}}{\ln(\nu_{m_2 n_2} A_{m_2 n_2} g_{m_2} R / \nu_{m_1 n_1} A_{m_1 n_1} g_{m_1})} \tag{3.4.3}$$

that depends only logarithmically on the line ratio R and the other quantities in the argument of the logarithm. If we mark the argument as X, than the relative error in the temperature is related to any error ΔX of this argument through

$$\left|\frac{\Delta T}{T}\right| = \frac{kT}{E_{m_2} - E_{m_1}} \left|\frac{\Delta X}{X}\right|. \tag{3.4.4}$$

Experimental errors in $\Delta X/X$ are rarely below 0.1, so this suggests that the error in electron temperatures from such line ratios is $\sim \pm 10\%$, even under favorable conditions concerning the validity of PLTE conditions and the availability of accurate transition probabilities A. The accuracy of the temperature estimates can be improved by measuring line ratios along some spectral series and then plotting the logarithms of the relative intensities, each previously multiplied with the appropriate factors occurring in equation 3.4.3, as a function of the excitation energies of the upper levels. If the corresponding data on such a Boltzmann plot fall close to a straight line, one may obtain a more accurate value for kT from the reciprocal of the slope of this line. Any significant deviations from such linear fit could signal deviations from PLTE, or errors in transition probabilities, or errors in extracting and measuring line intensities from observed spectra.

For plasmas for which PLTE cannot be assumed for the upper levels of otherwise suitable lines, the above relations should not be used. However, if there are available collisional rate coefficients and sufficiently realistic kinetic model to describe the considered plasma, one may still determine temperatures from measured line ratios, either by fitting synthetic spectra or by considering

limiting, i.e. simple cases. An example for such simple case are resonance lines and higher series members of lithium-like ions for coronal plasmas. In such situations the line ratio R is given with (Griem 1997)

$$R = \frac{i_{n_g m_1}}{i_{n_g m_2}} \approx \frac{\nu_{m_1 n_g} X_{m_1 g}}{\nu_{m_2 n_g} X_{m_2 g}} \approx \frac{(\bar{g} f)_{m_1 g}}{(\bar{g} f)_{m_2 g}} \exp\left(-\frac{E_{m_1} - E_{m_2}}{kT}\right), \tag{3.4.5}$$

where X_{mg} is the excitation rate coefficient (that is basically the collisional excitation coefficient), which approximatively can be represented by the constant Gaunt factor $\bar{g}$ and absorption oscillator strength f. The temperature dependance of line ratios is therefore the same as for line ratios in the PLTE case, although one has the additional uncertainty from the collisional cross sections. Even though this method for the temperature diagnostics is pretty simple and straightforward, due to relatively small differences between excitation energies, experimental errors, and theoretical uncertainties, it does not lead to very precise temperature measurements.

3.4.2 Relative line intensities of subsequent ionization stages of the same element

In dense LTE plasmas of known electron density N_e, one can more precisely than in the previously described method, determine the plasma temperature by measuring the relative integrated intensities i and i' of, say, a line from a neutral atom and the following ion. In that case their ratio is (Griem 1997)

$$R = \frac{i'}{i} = \frac{\nu' A' g'}{\sqrt{\pi} \nu A g} (4\pi a_0^3 N_\mathrm{e})^{-1} \left(\frac{kT}{E_\mathrm{H}}\right)^{3/2} \exp\left(-\frac{E' + E_\infty - E - \Delta E_\infty}{kT}\right), \tag{3.4.6}$$

where g is the upper level statistical weight, a_0 is Bohr radius, E_H is the hydrogen ionization energy, E is the excitation energy, E_∞ and ΔE_∞ are the ionization energy of the "atom" and its reduction[13]. The point here is that the combination of the various energies appearing in the exponent is often substantially larger than kT, which simplifies error estimates.

If electron densities are not sufficient enough to ensure LTE conditions for ionization and excitation up to energy level E', a combination of PLTE for the two upper level populations relative to the groundstate populations of the following charge state and of the corona ionization equilibrium may be used. In that case the line ratio is (Griem 1997)

$$R = \frac{i'}{i} = \frac{\nu' A' g'}{\nu A g} \exp\left(-\frac{E' + E_\infty - E - \Delta E_\infty}{kT}\right) \frac{g_i S}{g_i' \alpha}, \tag{3.4.7}$$

[13]In the presence of the cloud of electrons, the ionization energy of an atom or ion reduces as a consequence of the Coulomb interaction.

where S and α are ionization and recombination rate coefficients, respectively. If we take for S and α the suitable coefficients for the collisional-radiative model, this relation can also be used for the ionized gas of intermediate electron densities between the coronal and LTE regimes (Griem 1997). A good example of such calculations is the ratio of He II 4686 Å and He I 5876 Å lines.

3.5 Boltzmann-Plot (BP) method in the case of the BLR

For the plasma of the length ℓ that emits along the line of sight, the flux (or the spectrally integrated emission-line intensity F_{ul}) of transition from the upper to the lower level ($u \rightarrow l$) can be calculated as (Griem 1997, Konjević 1999, Popović 2003, 2006ab):

$$F_{ul} = \frac{hc}{\lambda} g_u A_{ul} \int_0^{\ell} N_u(x) dx, \tag{3.5.1}$$

where λ is transition wavelength, g_u statistical weight of the upper level, A_{ul} transition probability, N_u is the number of emitters excited in the upper level which effectively contribute to the line flux (which are not absorbed), and h and c are the Planck constant and the speed of light, respectively. If we assume that population in the observed region (in all layers) follows the Saha-Boltzmann distribution one can write the following equation

$$N_u(x) \approx \frac{N_0(x)}{Z} \exp(-E_u/kT(x)), \tag{3.5.2}$$

thus, the equation (3.5.1) becomes

$$F_{ul} = \frac{hc}{\lambda} g_u A_{ul} \int_0^{\ell} \frac{N_0(x)}{Z} \exp(-E_u/kT(x)) dx. \tag{3.5.3}$$

Here Z is partition function, N_0 is total number density of radiating species, E_u is energy of the upper level in the transition, T is temperature and k is the Boltzmann constant.

In the realistic case one can not expect to have a homogenous distribution of physical parameters in such a vast region as the broad line region is, thus the number density of emitters and temperature of the BLR are not constant along the line of sight. For that reason, lets divide the BLR in small layers with the same physical conditions and emitter density. Then we can rewrite the equation (3.5.3) as

$$F_{ul} = \frac{hc}{\lambda} g_u A_{ul} \sum_{i=1}^{n} \frac{N_0(i)}{Z} \exp(-E_u/kT(i)) \ell_i. \tag{3.5.4}$$

If we assume that the temperature across the BLR vary as $T(i) = T_{\rm av} \pm \Delta T_i$ and that the number density vary as $N_0(i) = N_0^{\rm av} \pm \Delta N_0(i)$, where $T_{\rm av}$ and

$N_0^{\rm av}$ are mean temperature and number density of the region, then the equation (3.5.4) can be written as

$$F_{ul} = \frac{hc}{\lambda} g_u A_{ul} \frac{N_0^{\rm av}}{Z} \sum_{i=1}^{n} (1 + \delta N_0(i)) \exp\left[-\frac{E_u}{kT_{\rm av}} \frac{1}{(1 + \delta T_i)} \right] \ell_i, \tag{3.5.5}$$

where $\delta T_i = \Delta T_i / T_{\rm av}$ and $\delta N_0 = \Delta N_0 / N_0^{\rm av}$. If we assume that in a BLR the temperature and emitter density does not vary too much, i.e. $\Delta N_0 / N_0^{\rm av} << 1$ and $\Delta T_i / T_{\rm av} << 1$, the equation (3.5.5) becomes

$$F_{ul} = \frac{hc}{\lambda} g_u A_{ul} \frac{N_0^{\rm av}}{Z} \exp(-E_u / kT_{\rm av}) \ell. \tag{3.5.6}$$

Then the following relation, that is already mentioned Boltzmann plot (BP), can be used for the temperature diagnostics $T_{\rm av}$ in the BLR (Popović 2006b):

$$\log_{10}(F_n) = \log_{10} \frac{F_{ul} \cdot \lambda}{g_u A_{ul}} = B - A E_u, \tag{3.5.7}$$

where B and A are BP parameters. Parameter A, defined as

$$A = \frac{\log_{10}(e)}{kT} \approx \frac{5040}{T[\mathrm{K}]} \tag{3.5.8}$$

is the temperature indicator. F_n is the normalized flux, scaled with the atomic parameters of the certain transition. Therefore, for one line series (as e.g. Balmer line series) if the population of the upper energy states ($n \geq 3$)[14] adheres to a Saha-Boltzmann distribution than one can by applying the equation (3.5.7) to the line fluxes of one atomic spectral series, determine the temperature parameter A. From this parameter one can estimate the temperature (T) of the region where these lines are formed. Note here that $T_{\rm av}$ is the average excitation temperature in the BLR.

We should emphasize that the BP method does not take into account any *a priori* physics in the BLR, besides that the line series (e.g. Balmer lines that are used in this work) are originating in the same emitting region. Also, one should not confuse BP with the Balmer decrement, i.e. the ratio of the Balmer lines, usually the Hα and Hβ lines (eventually the Hγ too), as BP is applied to the whole line series and moreover, to the normalized line fluxes. On the other hand, radiative transfer issues and high optical depths of the Hydrogen lines complicate the picture of this emitting region, but some additional tests could be used that are in favor of the BP method (Popović et al. 2008). Furthermore, the "Case B" recombination[15] line ratios can produce similar

[14]Note here that since the emission deexcitation goes as $u \rightarrow l$ it is not necessary that level l has a Saha-Boltzmann distribution.

[15]Case B recombination is a good approximation to describe gas clouds with large optical depths. It assumes that every Lyman-line photon is scattered many times and converted into lower-series photon before it escapes from the gas cloud.

Boltzmann plots of the Balmer line series in some AGN whose BLR is close to "Case B" recombination (see Osterbrock 1989). But, in such cases, due to the physical conditions (densities and temperatures) in such BLR the constant A is too small ($A < 0.2$) and the Boltzmann plot cannot be applied for diagnostics of the temperature even if the BP can be properly applied (Popović 2003, 2006ab, Ilić et al. 2006b). Finally, it is logical to ask a question why the proposed BP method is applied to the hydrogen Balmer line series, when it is known that there are many problems to accurately measure their fluxes, as e.g. self-absorption or satellite lines. The answer to this question is simple and it is first of all the consequence of the technical constraints, as the Balmer line series is the most observed one being completely in the optical part of the spectrum. On the other hand, hydrogen is the most abundant element in the BLR too, so these lines are also very intensive.

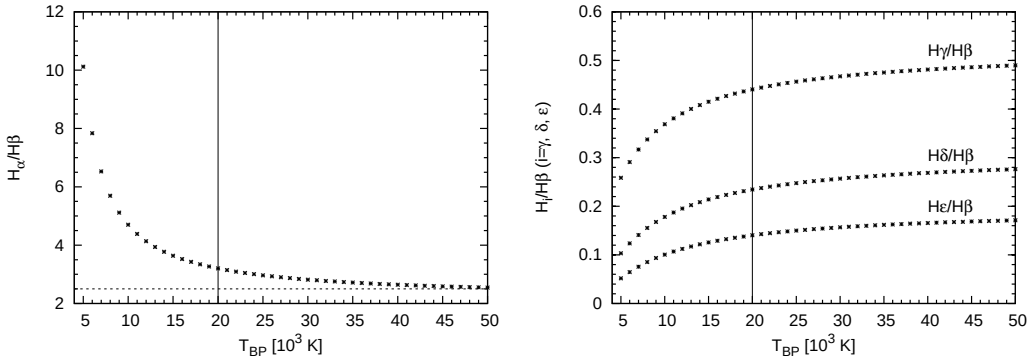

Figure 4: The Balmer line ratios as a function of the excitation temperature. The emission line fluxes are calculated using the equation (3.5.3). Left is the Hα/Hβ line ratio, while on the right the ratios of the Hγ/Hβ, Hδ/Hβ, and Hϵ/Hβ are presented. The limit of the 20,000 K temperature is presented with the vertical line, while on the left graph the constant Hα/Hβ = 2.5 ratio is plotted.

Using equation (3.5.3) we calculated the emission line fluxes of the Balmer line series, in order to see what line ratios are expected, especially for the case of the Hα/Hβ line ratio. It can be seen from equation (3.5.3) that the line ratios do not depend on the number density or length of the emitting region, but only on the temperature. Varying the temperature from 5,000 to 50,000 K, we calculated the fluxes of the Balmer lines from Hα to Hϵ. In the Figure 4 we present these Balmer lines normalized to the Hβ flux as a function of the temperature. The obtained values are in the range of the previously observed one in the case of AGN. It is clear from the Figure 4 that after the temperature of $\approx$ 20,000 K the line ratios are starting to be close to constant, thus independent of the temperature changes. Therefore, this temperature represents the limit for using the BP method for the Balmer series.

3.6 Numerical simulations of regions of ionized gas

As already mentioned in the introduction, spectroscopy offers very efficient methods to investigate objects that emit electromagnetic radiation, or to quote Gary J. Ferland: *"Most of the quantitative information we have about the cosmos comes from spectroscopy. Examples include absorption lines superimposed on distant quasars by intervening galaxies or the intergalactic medium, emission lines in nebulae, and the emission lines of the quasars."* (Ferland 2003).

In the case of active galaxies and emission nebulae, the electromagnetic spectrum is emitted from the ionized gas of a certain temperature, density and ionization level. The properties of that ionized gas, such as the kinetic gas temperature or energy level population, are influenced by all microscopic processes occurring in the gas. In order to estimate the physical properties and predict the outcoming spectrum of that region, it is necessary to simultaneously solve the equations of statistical and thermal equilibrium, the equations that describe the ionization and neutralization processes, as well as the heating and cooling processes. The analytical solution that would give such a spectrum are rarely possible, thus, one of the way to investigate the physical properties of emission regions is by using the numerical simulations.

The first numerical calculations of photoionized nebulae were attempted in the early 1960s, as soon as computers became capable of handling such simulations. Today there are roughly a half-dozen large codes that have been continuously developed since the 1970s. Some of them are: ION (Netzer & Ferland 1984, Rees et al. 1989, Netzer 1993), AANGABA (Gruenwald & Viegas 1992), MAPPINGS I (Binette et al. 1985, 1993ab), MAPPINGS II (Sutherland & Dopita 1993), XSTAR (Kallman & McCray 1982), NEBU (Petitjean et al. 1990), CLOUDY (Ferland et al. 1998), SUMA (Viegas & Contini 1994), and others. These are, of course, very complex computer codes that include all possible physical processes occurring in the photoionized gas (many include ionization induced by the shock waves too). However, problems with this approach are that the underlying physics is not always obvious, therefore, sometimes simple approximation could better describe the system than the complicated iterative process assigned by the numerical simulation, i.e. analytical approach to the spectral analysis should not be completely ignored.

Simply said, numerical simulations make it possible to understand complex physical environments starting from fundamental principles of physics. The spectral simulation code **CLOUDY** is designed to do just that. It is made to determine the physical conditions (temperature, level of ionization, and chemical state) within a non-equilibrium gas, possibly exposed to an external source of radiation (as is the case for e.g. H II regions or emission line region in AGN), and predict the resulting spectrum. For this research CLOUDY was

chosen, first of all, because of its relatively simple usage, but mostly because the team of scientists is constantly working on its development and improvement. Moreover, the code is open source and is available to everyone. All details about the code itself and the starting physical assumptions, as well as some details about its installation, usage and applications, are given in the Appendix B of this thesis.

3.6.1 CLOUDY program and AGN

With CLOUDY one could make good models of the AGN narrow and broad line regions, since the main ionization mechanism of these regions is photoionization by the continuum emission coming from the accretion disk and its corona (see e.g. Ferland & Persson 1989, Ferland et al. 1992, Kwan & Krolik 1981, Marziani et al. 1996, Dumont et al. 1998, Goad & Koratkar 1998, Ferland 1999, Korista & Goad 2000, 2004, Baldwin et al. 2004, Casebeer et al. 2006, Bruhweiler & Verner 2008). Even though the numerical simulations are now highly improved, there are still some important unsolved problems related to the BLR (Ferland 1999).

Some of the opened questions and problems are:
- the stratification of the BLR, the approach that CLOUDY has is over-simplified;
- the fact that the emission line profiles are so smooth, the spatial velocity distribution within BLR (HIL an LIL have different redshift);
- some emission line ratios, i.e. the disagreement of the theoretically predicted and observed emission lines. Here we specially emphasize the problem of the observed small ratio of some hydrogen line and ratio of UV and optical lines of ionized iron Fe II, which cannot be described with the photoionization models;
- energy budget problem, etc.

One of the most interesting problems is the observed small ratio of Lyα and Hβ lines (usually in the range 5 - 15), while models predict much higher values (30 - 50) (see Netzer et al. 1995 and all references within). Recent studies (Baldwin et al. 2004) show that using CLOUDY code with the assumption of strong velocity gradient or high microturbulent velocities, it is possible to reproduce the UV Fe II lines, while the optical Fe II emission is in that case still one order of magnitude smaller than observed one. Also, same authors show that in the case if Fe II emission is the result of the collisional ionization and excitation, the observations can be easily fitted, but again this cannot simultaneously explain the UV and optical Fe II emission. Finally, it is necessary to mention the "energy budget problem" (Netzer 1985, Collin-Souffrin 1986, Dumont et al. 1998, Gaskell et al. 2007), i.e. the observed ratio of the total BLR flux (that is mostly contributed by the optical emission lines and the Balmer continuum) and the Lyα line flux is larger from the predicted one. One of the

possible explanation of this problem is that apart from the photoionization, there is an additional heating mechanism of the line-emitting region. It could be that mechanisms like ionization induced by shock-waves or radio jets also contribute to the emission line formation (Dumont et al. 1998, Shapovalova et al. 2008).

4 CLOUDY simulations of the BLR physics

One of the main tasks of this thesis is to give and describe a simple method for the plasma diagnostics of the broad line region of active galaxies using only the observed broad emission lines. For that reason we start from the Boltzmann plot method, that is widely used in the laboratory plasma diagnostics and which can be applied on broad Balmer lines of some AGN (Popović 2003, 2006ab, Popović et al. 2008a). In order to test under which physical conditions the BP method can be applied, we generate grids of photoionization models of the BLR using the CLOUDY code[16]. We consider different gas densities, column densities and ionizing flux values in order to achieve that populations of the upper levels follow the Saha-Boltzmann distribution, that is necessary for the gas diagnostics using the BP method. Besides, we use the emission lines of neutral and ionized helium, that are also the result of the numerical simulations of the physical conditions in the BLR. The proposed method could be used for the BLR temperature and hydrogen gas density diagnostics, only with the use of the broad hydrogen Balmer lines and helium lines: He II λ4686 and He I λ5876. We consider these specific lines since they are always available being in the optical part of the spectrum, and covered almost in every observational program in the optical band. For more details see section 3.4 and 3.5.

4.1 Simulations of the photoionization model of the BLR

In order to analyze the physical conditions in the BLR for which we could apply the BP method, we generate grids of photoionization models of the BLR using the CLOUDY code (version C07.02.01: Ferland et al. 1998, Ferland 2006). Input parameters for the simulations are chosen to match the standard conditions in the BLR (Ferland 2006, Korista & Goad 2000, 2004). For the simulations, we assumed solar chemical abundances and constant hydrogen density, and we use the code's AGN template for the incident continuum shape. In order to compute grids of the emission-line spectrum we vary two input parameters: hydrogen gas density $n_{\rm H}({\rm cm}^{-3})$ and hydrogen-ionizing photon flux $\Phi_{\rm H}({\rm cm}^{-2}{\rm s}^{-1})$. The grid dimensions span 4 - 5 orders of magnitude in each direction, where hydrogen gas density varied in interval log $n_{\rm H} \in [8, 12]$ and hydrogen-ionizing photon flux in interval log $\Phi_{\rm H} \in [17, 22]$, with the step in in 0.2 dex increments for a total of 546 simulations. First simulations are done assuming that all clouds have a single column density $N_{\rm H} = 10^{23}{\rm cm}^{-2}$ which many authors claim to be the most probable one in the case of the BLR (Dumont et al. 1998, Korista & Goad 2000, 2004). But for more detail

[16]The code and its usage is described in details in Appendix A.

analysis, the same grids of models are produced for different column densities, where $N_{\rm H}$ is ranging from $10^{21} - 10^{25}$cm^{-2}, so in total 5 grids of 546 simulations are produced. One example of the input file with following parameters $n_{\rm H} = 10^{10}$ cm^{-3}, $\Phi_{\rm H} = 10^{19}$ cm^{-2}s^{-1} and $N_{\rm H} = 10^{23}$ cm^{-2} is:

```
table agn
hden 10
phi 19
print last iteration
stop column density 23
iterate to convergence
```

Since we are dealing here with large number of simulations (in total 2730), that are also CPU time demanding (on average 20 minutes per simulation), all grids of numerical simulations were done automatically. For that purpose, scripts in the dynamical program language *Perl* are written. The scripts are written in such way so that for the fixed column density both hydrogen gas density and hydrogen-ionizing photon flux are varied.

4.2 Results and analysis of numerical simulations

Our further work on the results of the CLOUDY models consists of an analysis of the emission line fluxes generated by the code. The code gives line ratio of all lines formed in the emitting region with given chemical abundance, hydrogen density and hydrogen-ionizing photon flux. The CLOUDY code gives all lines normalized to the Hβ flux, but since it has no influence in the BP analysis, we have used these line ratios in further analysis.

The main idea in the analysis of the simulation results is to apply the previously described BP method on the hydrogen Balmer lines fluxes calculated with CLOUDY. Basically, using the equation 3.5.7, that is applied on the Balmer lines (Hα, Hβ , Hγ, Hδ, Hε), we estimate the BP temperature ($T_{\rm BP}$ further in the text) of the region where these lines are forming (Figure 5). Beside Balmer lines, we consider the following simulated lines and quantities: flux ratio R of the helium lines He II λ4686 and He I λ5876, defined as $R = F(\mathrm{HeII}\lambda 4686)/F(\mathrm{HeI}\lambda 5876)$, temperature averaged over the BLR radius ($T_{\rm av}$ further in the text), ionization parameter Γ, defined as the dimensionless ratio of ionizing photons to hydrogen density $U \equiv \frac{\Phi(\mathrm{H})}{n(\mathrm{H})c}$, and temperatures of the zones of constant physical properties in the ionized cloud, closest and furthest from the central continuum source[17] ($T_{\rm max}$ and $T_{\rm min}$ respectively). We particularly consider these helium lines, since they are the lines of the same

[17]The code CLOUDY works by dividing a cloud into a large number of thin layers, called

element but in two different ionization states, thus their ratio He II λ4686/He I λ5876 is sensitive to the change in the temperature and density (see section 3.4.2, Griem 1997). Besides, these lines are in the same spectral range as hydrogen Balmer lines, thus if present they are always observed as well.

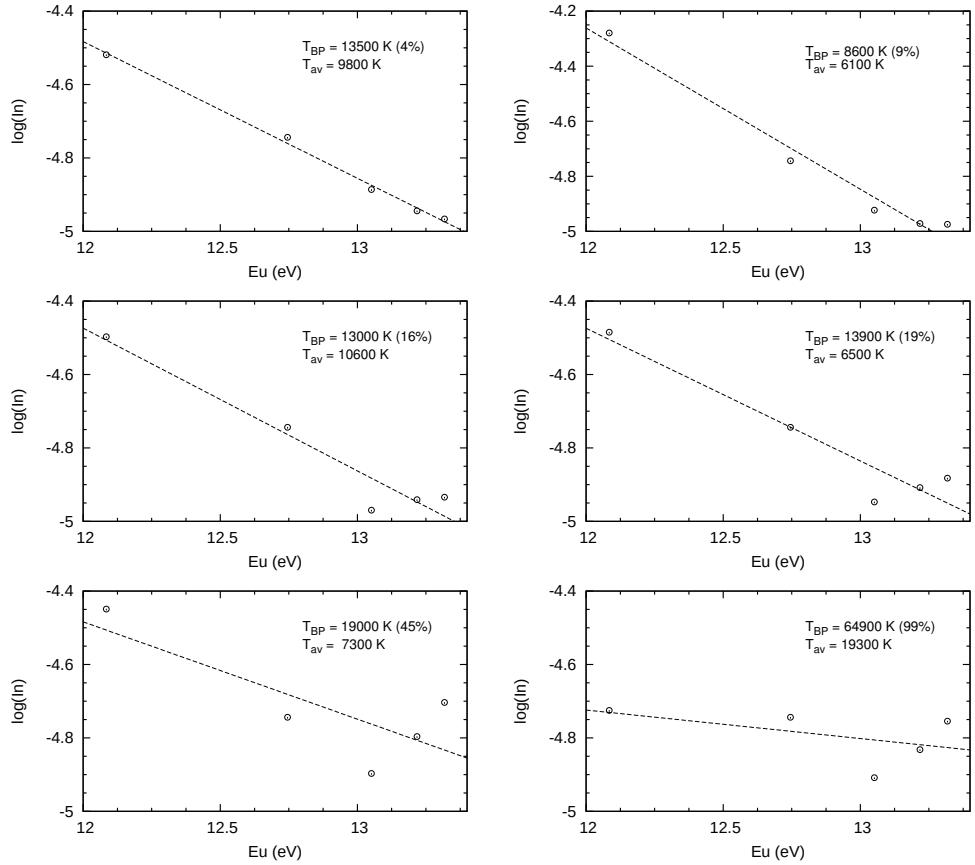

Figure 5: Some examples of the BP applied on the Balmer line ratios calculated with the CLOUDY models for different hydrogen gas density n_{H} and hydrogen-ionizing photon flux Φ_{H} but constant column density of $N_{\mathrm{H}} = 10^{23}\mathrm{cm}^{-2}$. The normalized intensities F_n are calculated from the equation 3.5.7 using the Balmer lines normalized on the Hβ flux. In the right corner of every plot, the BP temperature T_{BP}, the error of the BP fit and the average temperature T_{av} are given.

In order to extract the studied quantities from the large number of output files, it was necessary to write the script for automatic data extraction. This procedure first recognize the given key words in the output file, then reads

zones, which thickness is small enough to have almost constant physical conditions (More details in Appendix A).

the value of the searched quantity, and finally writes them in the separate table. Besides the input hydrogen gas density and hydrogen-ionizing photon flux, hydrogen Balmer lines fluxes (Hα, Hβ, Hγ, Hδ, Hε, helium line fluxes (He II λ4686, He I λ5876), average temperature, ionization parameter, thickness of the region, and optical depth in hydrogen Lyα and Hα lines are written in the table, as well as the temperatures of the first and last zone in the gas cloud. The separate table is made for each grid of simulations, in order to analyze the results for every column density separately. These scripts are also written in the dynamical program language *Perl*. Further on, for simulation results of every pair of n_H and Φ_H, the BP method (equations 3.5.7 i 3.5.8) is applied on the Balmer lines (Hα-Hε), and temperature parameter A and BP temperature T_{BP} are calculated. A few examples of the BP applied on the Balmer lines simulated with CLOUDY for column density of $N_H = 10^{23}\mathrm{cm}^{-2}$ are presented in Figure 5. In many cases a satisfactory fit of the equation 3.5.7 is not obtained, i.e. the BP fits have large errors. Notice how in few examples in Figure 5 for the case of the large error the temperature T_{BP} is high and much above expected in the BLR of AGN.

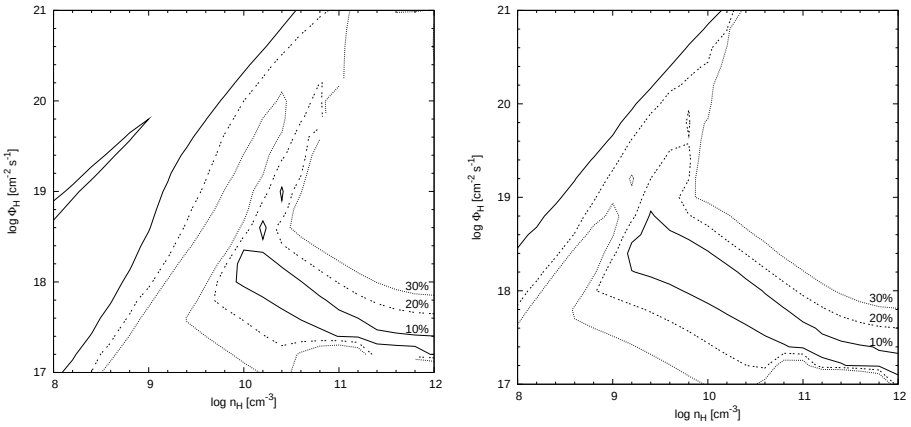

Figure 6: The error of the BP fit applied on the Balmer lines simulated with CLOUDY in the hydrogen-density vs. ionizing flux plane for the column density $N_H = 10^{21}\mathrm{cm}^{-3}$ (left) and $N_H = 10^{22}\mathrm{cm}^{-3}$ (right). Only the contours inside which the BP fit error is smaller than 10%, 20% and 30% are given.

This fact is even more noticeable for the higher values of hydrogen-density and ionizing photon flux. For this reason, we plot the error of the BP fit in the hydrogen density vs. ionizing flux plane in order to see for what values of these parameters the BP fit gives the smallest error (Figure 6 - 8). In Figure 6 - 8 we give only the contours inside which the BP fit error is smaller than 10%, 20% and 30%, taking into account results from all simulations (further in the analysis some constraints are introduced so that only a part of simulations were used). If we assume that the BP method could be considered valid if the

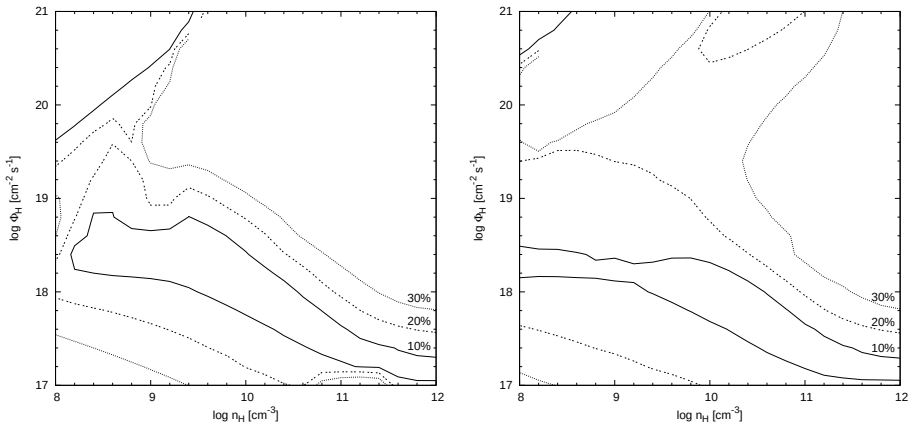

Figure 7: The same as in Figure 6 but for the column density $N_{\rm H} = 10^{23}{\rm cm}^{-3}$ (left) and $N_{\rm H} = 10^{24}{\rm cm}^{-3}$ (right).

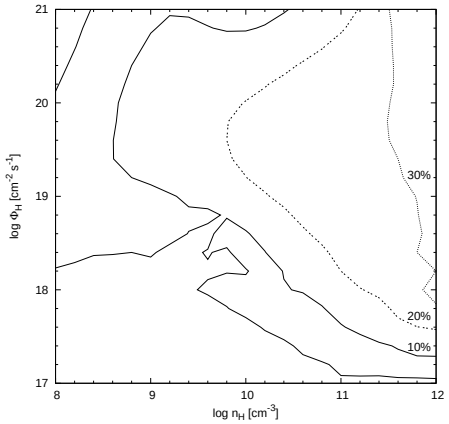

Figure 8: The same as in Figure 6 but for the column density $N_{\rm H} = 10^{25}{\rm cm}^{-3}$.

error of the fit is smaller than 10% (eventually in the absorbed spectra 20%), then it is clear from Figure 6 - 8 that the parameter space where this is valid is pretty constrained for different column densities $N_{\rm H}$. It indicates that for some physical conditions the BP method could be used for the temperature diagnostics, i.e. the populations of the higher hydrogen energy levels $n \geq 3$ could be approximately described with the Saha-Boltzmann distribution. We should note here that in the case where the error of the fit applied on fluxes of the Balmer lines is higher than 10 %, the BP does not give valid results and it cannot be used for the BLR temperature estimates.

Further in our analysis, we introduce several constraints for selection of the numerical simulation results to be studied in details.

1. The first constraint is that the error of the BP fitting of modeled spectra is less than 10% . Selected data set is denoted as "BP 10%" further in

the text).

2. Then, the second constraint is that the average temperature $T_{\rm av}$ of the emitting region, given by the numerical simulations is not higher than 20,000 K. This comes from the analysis of the sensitivity of the Balmer line ratios to the temperature changes given in the section 3.5 and in Figure 4. It gives that for higher temperatures, these ratios are not temperature sensitive, therefore the Saha-Boltzmann approximation cannot be applied (Popović 2006b).

3. Finally, the third constraints relates to the ratio of the helium lines. It is accepted that their ratio $R = F(\text{He II } \lambda4686)/F(\text{He I } \lambda5876)$ should be less than 2, that is the expected value obtained from the observations (see e.g. Kollatschny et al. 2001, Vanden Berk et al. 2001).

With all these three conditions, the number of simulations in the considered data sets decreases from 543, to 22 (4.03 %) in the case of column density $N_{\rm H} = 10^{21}{\rm cm}^{-2}$, to 35 (6.41 %) for $N_{\rm H} = 10^{22}{\rm cm}^{-2}$, to 54 (9.94 %) for $N_{\rm H} = 10^{23}{\rm cm}^{-2}$, to 50 (9.16 %) for $N_{\rm H} = 10^{24}{\rm cm}^{-2}$, and finally, to 73 (13.37 %) for $N_{\rm H} = 10^{25}{\rm cm}^{-2}$.

4.2.1 The case of the column density $N_{\rm H} = 10^{23}{\rm cm}^{-2}$

Since many authors give that the expected value for the column density in the plasma of the BLR is $N_{\rm H} = 10^{23}{\rm cm}^{-2}$ (Dumont et al. 1998, Korista & Goad 2000, 2004), we first consider the grid of simulation results performed for this column density. Thus, we consider the data set which follows the above three constraints, denoted as "BP 10%". On Figure 9 we plot the average temperature $T_{\rm av}$ of the emitting region, one of the outputs of the model, with respect to the ratio R of the He II $\lambda4686$ and He I $\lambda5876$ lines. If we would present on the same plot all the numerical simulation results of this grid, we would get high dispersion of the data and unrealistically large ratio of the helium lines. Thus, we fit the data set BP 10% with the linear function $T_{\rm av} = A_i + B_i \cdot R$, where $R = F(\text{He II } \lambda4686)/F(\text{He I } \lambda5876)$ is the flux ratio of these helium lines. We obtained the high level of correlation $r = 0.96$ and the best-fitting results are:

$$T_{\rm av}[10^3{\rm K}] = (3.49 \pm 0.20) + (7.12 \pm 2.88) \cdot R. \qquad (4.2.1)$$

Such high level of correlation tells us that if the BP fits well the Balmer lines, the correlation between the average temperature and the ratio of these helium lines could be used as a direct probe of the average temperature in the BLR, as these lines are in the same spectral region as Balmer lines, and are thus almost always covered with optical observations. On the other hand, one should also

consider that the formation region of the helium lines does not have to be necessarily the same as of the hydrogen lines (see e.g. Kollatschny et al. 2001).

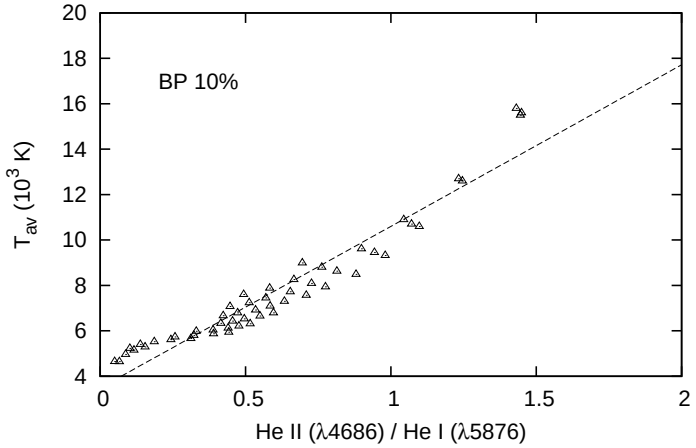

Figure 9: The average temperature $T_{\rm av}$ obtained from simulations versus the ratio of the He II λ4686 and He I λ5876 lines, for the case of the data set "BP 10%" for the column density $N_{\rm H} = 10^{23}{\rm cm}^{-3}$. The linear best-fitting is presented with the dashed line.

It is interesting to see how the BP temperature $T_{\rm BP}$ differs from the average temperature $T_{\rm av}$, so we plot the ratio of these temperature as a function of the hydrogen density for data sets BP 10% (Figure 10). The difference exists, but is more noticeable for higher hydrogen densities. For $n_{\rm H} \approx 10^{9.5}{\rm cm}^{-3}$ the ratio of these two temperatures is around 1.5, but for most of the values of $n_{\rm H}$ it is close to 1, while for the smallest values of hydrogen density this ratio drops to 0.6 (Figure 10). The difference between these two temperatures is expected since it is most likely that the Balmer lines, that determine the BP temperature, are formed only in part of the BLR, while the average temperature is averaged over the total BLR radius, so it is the characteristic of the whole region not just one its part, like BP temperature is.

On the other hand, if there would be any connection between the average temperature $T_{\rm av}$ and the BP temperature $T_{\rm BP}$ that could give us a useful tool for the average temperature diagnostics in the BLR of AGN. In order to check such connection, we plot $T_{\rm av} = f(T_{\rm BP})$ for the "BP 10%" data set, fitting it with the linear function (Figure 11). Even though the scattering is large for the higher temperatures, the obtained correlation is high $r = 0.80$. The obtained linear fitting result is:

$$T_{\rm av} = (-1498 \pm 997) + (1.01 \pm 0.11) \cdot T_{\rm BP}. \qquad (4.2.2)$$

Such relation could be used as a tool for a rough temperature estimate in the

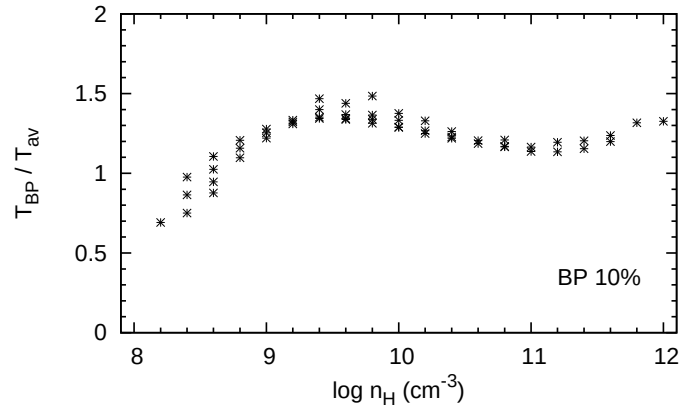

Figure 10: The ratio of the BP temperature $T_{\rm BP}$ and the average temperature $T_{\rm av}$ as a function of the hydrogen density for the data set "BP 10%" for column density $N_{\rm H} = 10^{23}{\rm cm}^{-3}$. It is clearly seen that the variation is in the range -30%, +50%.

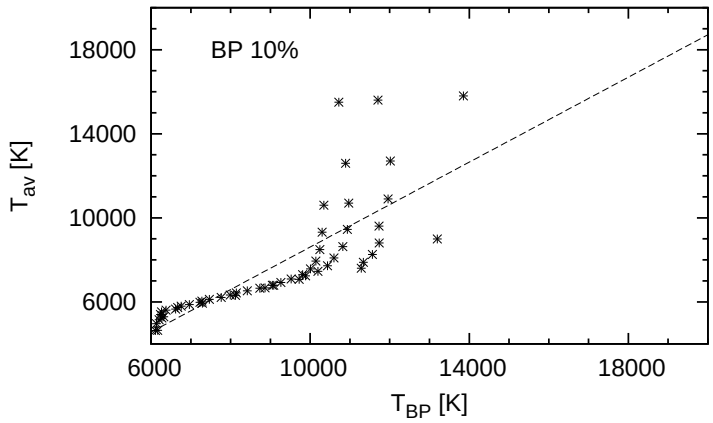

Figure 11: The average temperature $T_{\rm av}$ of the BLR plotted versus the BP temperature $T_{\rm BP}$ for the case of the data set "BP 10%" for column density $N_{\rm H} = 10^{23}{\rm cm}^{-3}$. The linear best-fitting is presented with the dashed line.

BLR. Therefore, if the normalized Balmer line ratios can be fitted with the equation 3.5.7 with the fitting error smaller than 10%, then from the slope of the fit (equation 3.5.8) one can determine the BP temperature, that represents the temperature of the region where Balmer lines are forming. Then, using the above relation 4.2.2, the average temperature of the region can be roughly estimated.

Figure 12 shows how temperatures are changing with the ionization parameter Γ. In the upper panel both temperatures are presented for the data set

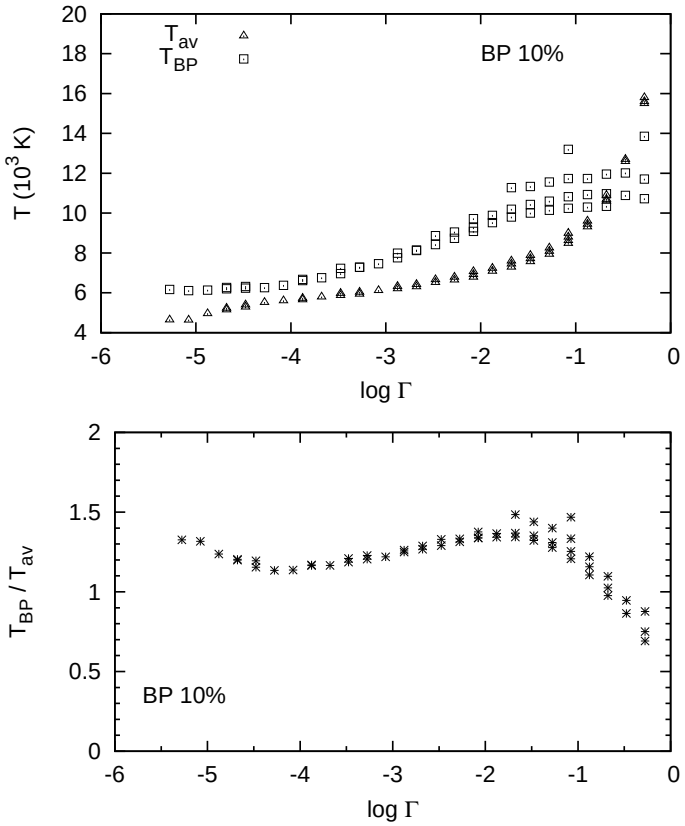

Figure 12: *Upper panel:* The temperature as a function of ionization parameter Γ. *Lower panel:* The ratio of the BP temperature $T_{\rm BP}$ and the average temperature $T_{\rm av}$ as a function of the ionization parameter Γ. Data were taken from the data set "BP 10%" for column density $N_{\rm H} = 10^{23}{\rm cm}^{-3}$.

"BP 10%", while in the lower panel the temperature's ratio is presented as a function of the ionization parameter for the same set. It can be seen from Figure 12 that the difference between these temperatures is not significant, but it is larger for lower values of the ionization parameter, particularly in the cases of high hydrogen densities and higher ionizing photon flux. In principle, the shape of this dependance is inverse from the one seen in Figure 10, that is expected since the ionization parameter is inversely proportional to the hydrogen density by its definition. It is interesting that the BP temperature is mainly larger than the average temperature. One of the reasons for this could be that the layers in which the Balmer lines are formed are deeper in the clouds and more closer to the ionizing continuum source. Also, this difference could come from the fact that the BP temperature is by its definition the excitation temperature, while the average temperature calculated by CLOUDY is the average electron temperature.

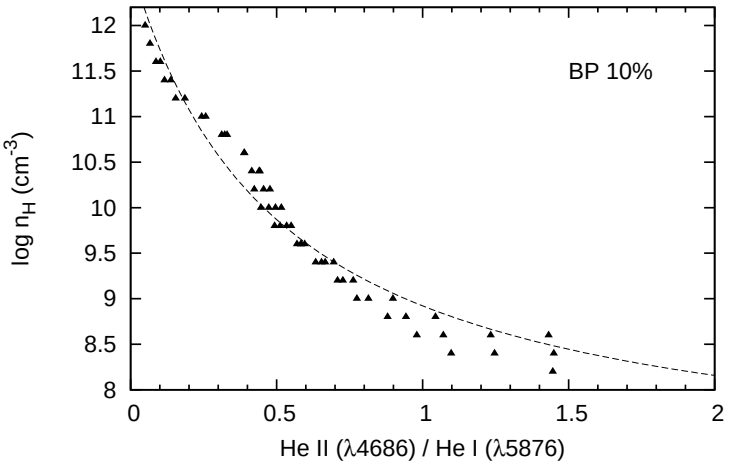

Figure 13: The hydrogen density as a function of the ratio of the He II λ4686 and He I λ5876 lines for the data set "BP 10%" for column density $N_{\rm H} = 10^{23}{\rm cm}^{-3}$. The dashed line represents the best-fitting with the function $\log n_H({\rm in}\ 10^7\ {\rm cm}^{-3}) = 2.86/(0.53+R)$, where R is the ratio between these two helium lines.

Another possible probe of the physical conditions in the BLR can be obtained from the relation between the hydrogen density and the He II λ4686 and He I λ5876 line ratio. For that reason, we plot the logarithm of the hydrogen density and the ratio R in Figure 13. The data are fitted with the function $\log n_{\rm H} = d/(c+R)$, where n_H is given in the units of $10^7{\rm cm}^{-3}$. The best-fitting result is:

$$\log n_{\rm H}({\rm in}\ 10^7{\rm cm}^{-3}) = \frac{2.909 \pm 0.098}{(0.514 \pm 0.027) + R}. \qquad (4.2.3)$$

Actually, this kind of dependence is expected in the case when the energy levels are described with Saha-Boltzmann equation (see section 3.5). The ratio of these two helium lines represents the ratio of the two ionization states that, according to the Saha-Boltzmann equation, should decrease with the electron density [18] as $R \sim 1/n_{\rm e}$ and increase with the temperature as shown in Figure 9. This relation could be very useful for the estimate of the hydrogen density in the BLR of AGN using only the observed BELs.

[18] In this case we can assume that hydrogen is nearly totally ionized, thus $n_{\rm e} \approx n_{\rm H}$.

4.2.2 General relations for column densities in the range of $N_{\rm H} = 10^{21} - 10^{25}{\rm cm}^{-3}$

We investigate the line ratios of hydrogen Balmer and helium He II/He I lines using all grids of numerical simulations for different column densities $N_{\rm H}$. Basically, the column density defines the optical thickness of the region, so that for higher column density the optical thickness in the emission lines increases. Once again the constraints for the selection of the numerical simulation results are: the error of the BP fit less than 10%, the average temperature less than 20,000 K and the ratio of helium lines $R = F(\text{He II } \lambda4686)/F(\text{He I } \lambda5876)$ less than 2. Such selected data set is marked as "BP 10%". In Figure 14 the full circles represent the simulations for which the above criteria are met. It is also clearly seen in Figure 14 that there is a certain regularity in the values of the input parameters $\Phi_{\rm H}$ and $n_{\rm H}$. It can be seen that when ionization photon flux increases, the hydrogen gas density decreases, and viceversa.

Figure 15 show the average temperature $T_{\rm av}$ of the emitting region as a function of the ratio of the He II $\lambda4686$ and He I $\lambda5876$ lines for different column densities. Furthermore, every data set "BP 10%" is fitted with the linear function $T_{\rm av} = A_i + B_i \cdot R$. The best-fitting parameters A_i and B_i are given in Table 1, while Figure 16 gives their dependance on the column density. From Figure 16 one can see that there is a tendency to have linear dependance on the column density for both parameters, which means that the fitting results could be all represented by single column density.

Table 1: The best-fitting parameters A_i and B_i of the function $T_{\rm av} = A_i + B_i \cdot R$ for different column densities $N_{\rm H}$.

$\log N_{\rm H}$ [cm^{-2}]	A_i [K]	B_i [K]
21	4422±689	10468±1697
22	3215±562	10701±1049
23	3486±200	7116±288
24	4646±92	3355±139
25	5208±119	1899±152

The best fit with linear function (Figure 16) gives the following results for the dependance of the parameter A_i and B_i on the column density: $A_i = (-2713\pm5712)+(300\pm248)\cdot N_{\rm H}$, $B_i = (63018\pm9092)+(-2448\pm395)\cdot N_{\rm H}$. From this we can get the general relation for calculation of the average temperature $T_{\rm av}$ from the helium line ratio R, that depends on the column density $N_{\rm H}$ as:

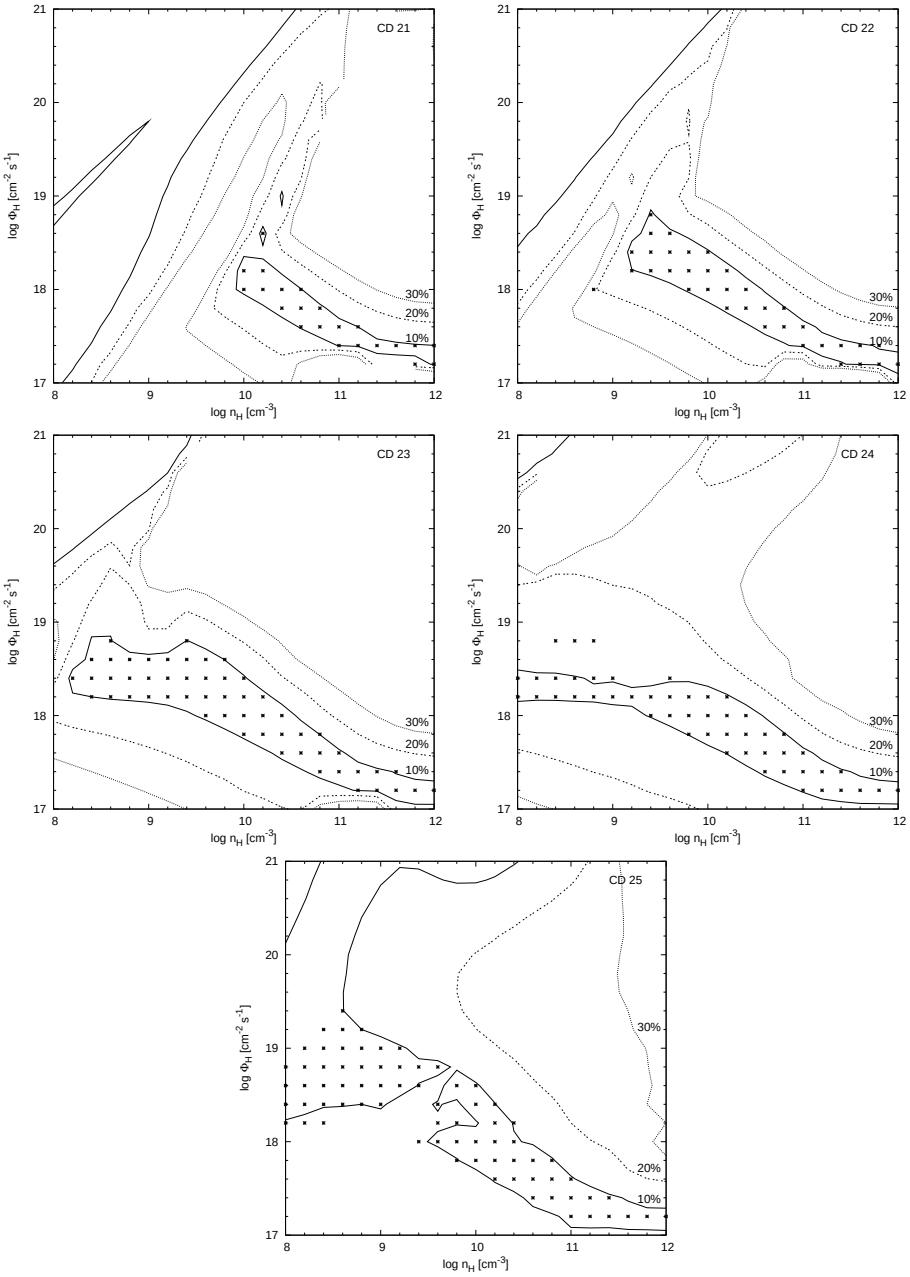

Figure 14: The error of the BP fit in the hydrogen-density vs. ionizing flux plane for the column density $N_{\rm H} = 10^{21} - 10^{25}{\rm cm}^{-3}$ with contours inside which the BP fit error is smaller than 10%, 20% and 30% are given (same as in Figure 6-8), but here with full circles only the simulation results that satisfied the three given constraints are given: the BP fit error less than 10%, $T_{\rm av} <$ 20000K, as well as the helium line ratio $R = F(\text{He II } \lambda 4686)/F(\text{He I } \lambda 5876)$ less than 2.

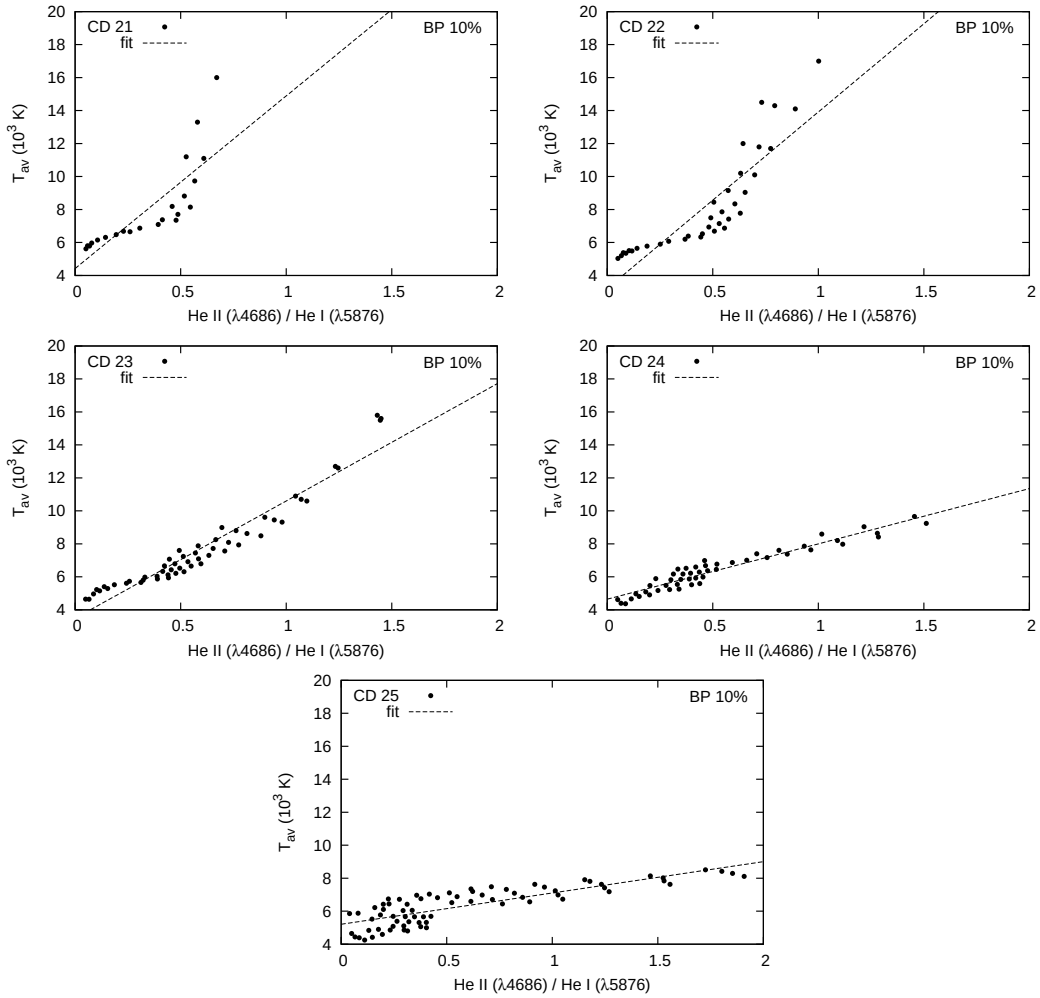

Figure 15: The average temperature $T_{\rm av}$ of the emitting medium plotted versus the ratio of the He II λ4686 and He I λ5876 lines, for the case of the data set "BP 10%" for the column densities $N_{\rm H} = 10^{21} - 10^{25}{\rm cm}^{-3}$. The best-fitting linear function $T_{\rm av} = A_i + B_i \cdot R$ is presented with the dashed line. Column densities are given in the upper left corner.

$$T_{\rm av}[10^3{\rm K}] = (-2.71\pm5.71)+(0.30\pm0.25)\cdot N_{\rm H}+[(63.02\pm9.09)-(2.45\pm.40)\cdot N_{\rm H}]\cdot R. \quad (4.2.4)$$

To estimate the hydrogen density from the ratio of the helium He II λ4686 and He I λ5876 lines, the dependance on the column density is analyzed as well. Figure 17 gives the hydrogen density as a function of the the He II λ4686/He I λ5876 line ratio for the data set "BP 10%" for different column densities ($N_{\rm H} \in [10^{21} - 10^{25}]{\rm cm}^{-2}$). Then every data set is fitted with the function $\log n_{\rm H} = D_i/(C_i + R)$ (Figure 17 and 18). It can be seen from Figure 17 and

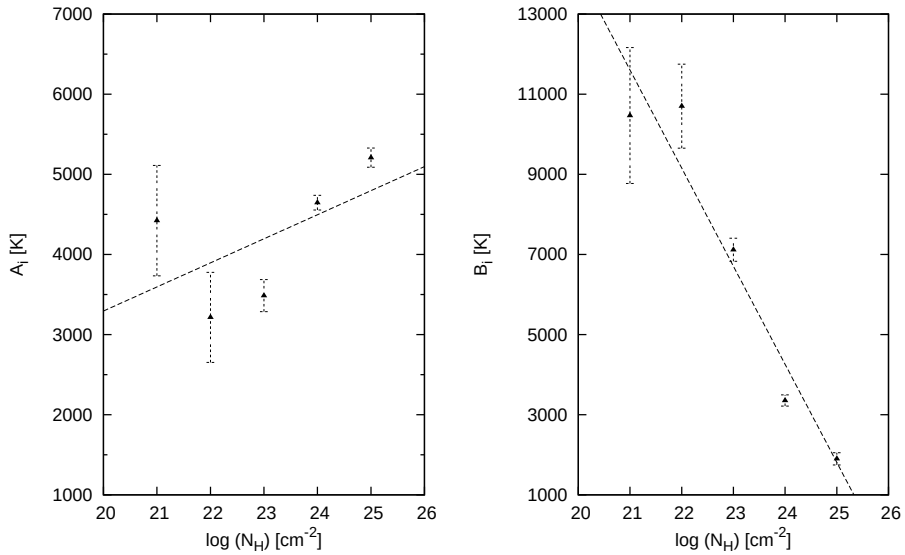

Figure 16: The dependance of the fitting parameters A_i (left) and B_i (right) on the column density $N_{\rm H}$.

18 that even when the column density changes, the same dependance of the hydrogen density on the helium line ratio R remains. The fitting parameters C_i and D_i are given in Table 2, as well as in Figure 19. As it can been seen in Figure 19 there is a tendency to have a linear dependance on the column density for both parameters, which means that the fitting results could be all represented by single column density. The best-fitting results with the linear function gives the following dependance of the parameters C_i and D_i on the column density (Figure 19):

$$C_i = (3.82 \pm 0.74) + (-0.14 \pm .03) \cdot N_{\rm H}$$
$$D_i = (19.46 \pm 2.89) + (-0.70 \pm 0.10) \cdot N_{\rm H}.$$

From this we can get the general relation for calculation of the hydrogen density $n_{\rm H}$ from the helium line ratio R, which now depends on the column density $N_{\rm H}$ as:

$$n_{\rm H} = \frac{(19.46 \pm 2.89) + (-0.70 \pm 0.1) \cdot N_{\rm H}}{[(3.82 \pm 0.74) + (-0.14 \pm 0.03) \cdot N_{\rm H} + R]}. \qquad (4.2.5)$$

In Figure 20 we present the dependance of the ratio of the Hα/Hβ emission lines on the temperature parameter A. Data from all grids of numerical simulations for every column densities $N_{\rm H}$ are given, and are denoted with different symbols in Figure 20. The values of the Hα/Hβ emission line ratio for different temperatures calculated with the Saha-Boltzmann equation (section 3.5, equation 3.5.3) are also given with the dashed line in Figure 20. It can

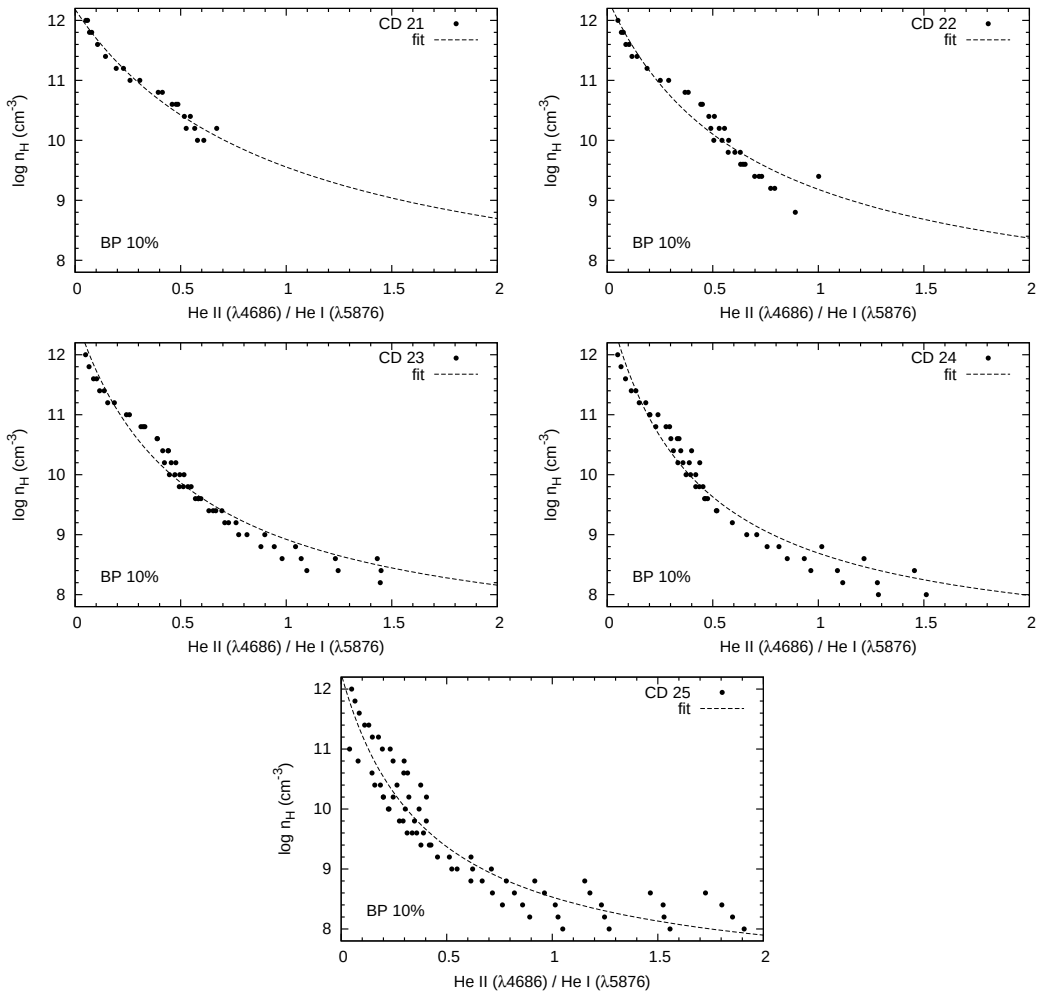

Figure 17: The hydrogen density as a function of the ratio of the He II $\lambda 4686$ and He I $\lambda 5876$ lines for the data set "BP 10%" for column densities $N_{\rm H} = 10^{21} - 10^{25}{\rm cm}^{-3}$. Column densities are given in the upper right corner. The dashed line represents the best-fitting with the function $\log n_{\rm H} = D_i/(C_i + R)$, where R is the ratio between these two helium lines.

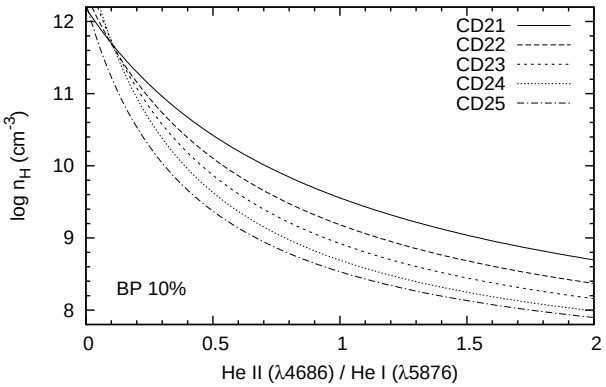

Figure 18: The hydrogen density as a function of the ratio of the He II λ4686 and He I λ5876 lines. The lines represent the best-fitting for the data set of different column density $N_{\rm H}$.

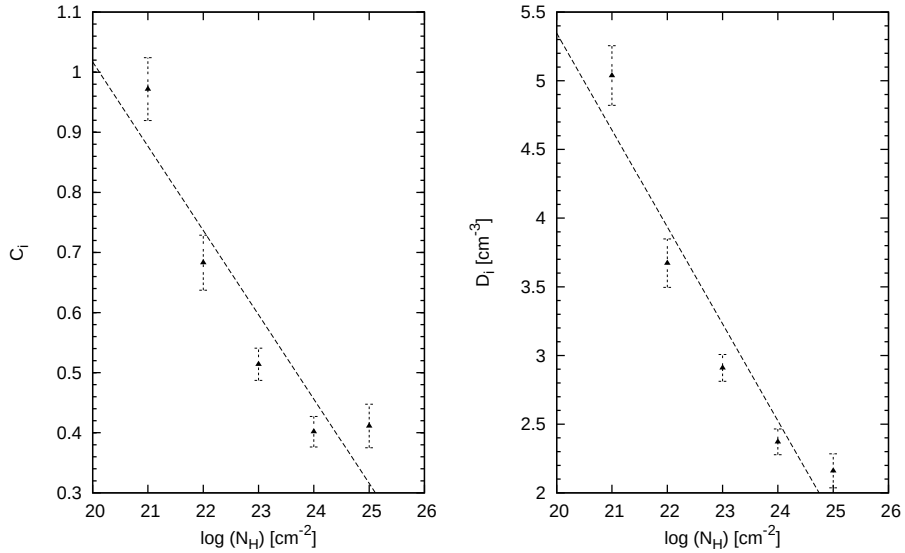

Figure 19: The dependance of the fitting parameters C_i (left) and D_i (right) on the column density $N_{\rm H}$.

Table 2: The best-fitting parameters C_i and D_i of the function $\log n_{\rm H} = D_i/(C_i + R)$ for different column densities $N_{\rm H}$.

$\log N_{\rm H}$ [cm^{-2}]	D_i [cm^{-3}]	C_i
21	5.04±0.22	0.97±0.05
22	3.67±0.18	0.68±0.05
23	2.91±0.10	0.51±0.03
24	2.37±0.09	0.40±0.03
25	2.16±0.12	0.41±0.04

be clearly seen from Figure 20 that the simulated ratio of the Hα/Hβ lines for which the error of the BP fit is smaller than 10% follows the theoretical curve obtained from the Saha-Boltzmann equation. This gives some indication that for certain physical conditions, the population of the upper energy levels of hydrogen could follow the Saha-Boltzmann distribution.

The quantities also obtained with these numerical simulations are temperatures of the first and last zone in the BLR. It is already mentioned that CLOUDY works by dividing a gas cloud into a large number of thin layers, called zones, with constant physical conditions. Here we consider the temperature of the first zone, i.e. the zone closest to the central ionization source and thus of maximal temperature $T_{\rm max}$, and the temperature of the last zone, i.e. the zone furthest from the center and thus of the minimal temperature $T_{\rm min}$. In Figure 21 all so far considered temperatures are given ($T_{\rm max}$, $T_{\rm av}$, $T_{\rm BP}$, $T_{\rm min}$) as a function of the hydrogen density $n_{\rm H}$ for data set "BP 10%" in the case of column densities $N_{\rm H} = 10^{21} - 10^{25}$cm^{-3}. It is obvious from Figure 21 that the BP temperature is between the minimal and maximal temperature, which another fact in favor of the validity of this temperature, i.e. this temperature can give us some indications of the temperature in the broad line region. The same applies for the average temperature, though such dependance is expected by its definition.

4.2.3 Method of the BLR plasma diagnostics

In this PhD thesis, we propose a straightforward and simple semi-empirical method, that would use only the observed hydrogen Balmer and helium lines, for estimation of the plasma physical properties in the BLR of AGN.

For generating the grids of numerical simulations of physical conditions in the BLR of AGN, we consider different hydrogen gas densities and hydrogen-ionizing photon flux, as well as different column densities, in order to obtain the situation that the populations of the upper energy levels of neutral hy-

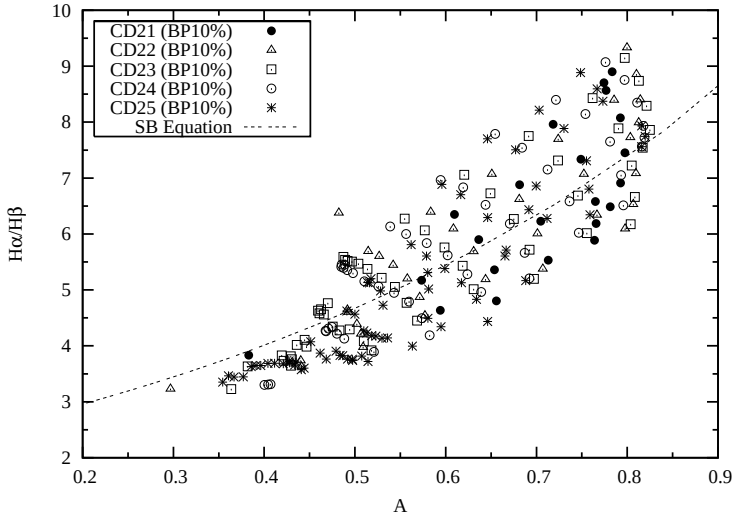

Figure 20: The ratio of the Hα/Hβ emission lines as a function of the temperature parameter A for the data set "BP 10%" for different column densities $N_{\rm H}$. The data for different column densities are denoted with different symbols. The values of the Hα/Hβ line ratio calculated for different temperatures with the Saha-Boltzmann equation (section 3.5, equation 3.5.3), are presented with the dashed line.

drogen follow approximately Saha-Boltzmann equation, that is the necessary prerequisite for the temperature diagnostics with the Boltzmann plot method. This method is applied on the simulated broad emission lines, and it has been shown that in the limited number of case this method can be applied on the hydrogen Balmer lines (Figure 6 - 8). For cases for which the following conditions are met: the BP fit error less than 10%, the average temperature $T_{\rm av}$ less than 20,000 K, and the helium line ratio $R = F(\text{He II } \lambda4686)/F(\text{He I } \lambda5876)$ less than 2, the ratio of the helium lines R is considered, and it has been shown that for those cases the ratio R could be used for the estimates of the average temperature and hydrogen density in the BLR (equations 4.2.1 - 4.2.5, Figure 9, 11 i 13).

Therefore, in order to estimate the physical properties in the BLR directly from the observed BELs, one should do the following (Ilić et al. 2008a,b):

1. measure fluxes of the broad Balmer lines (from Hα to Hϵ) and apply the Boltzmann plot method (calculate the normalized fluxes and fit them with the equation 3.5.7). If the error of the fit is smaller than 20% [19] then one can calculate the BP temperature $T_{\rm BP}$ using the equation 3.5.8;

[19] Even though in numerical simulations the error was taken to be smaller than 10%, in real measurements one could take larger range of fitting errors due to the additional observational and line flux measurement errors.

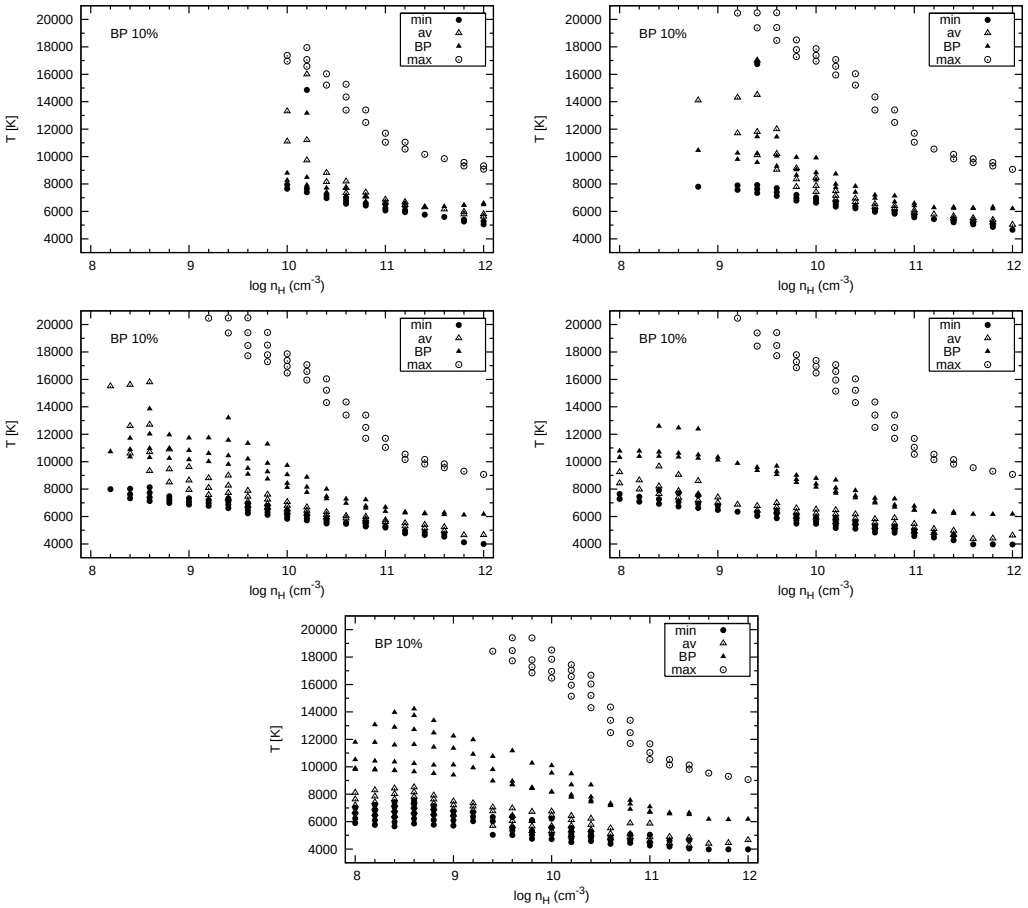

Figure 21: The dependance of different temperatures on the hydrogen density n_{H} for data set "BP 10%" in the case of the column densities $N_{\mathrm{H}} = 10^{21} - 10^{25}\mathrm{cm}^{-3}$. Different temperatures ($T_{\max}$, T_{av}, T_{BP}, $T_{\min}$) are denoted with different symbols given in the upper right corner.

2. if the previous is valid, then measure also the line fluxes of the broad helium lines He II λ4686 and He I λ5876, taking special care when extracting the contribution of the narrow helium lines and Fe II multiplet in the vicinity of the He II λ4686 line, and then calculate their ratio R;

3. estimate the average temperature $T_{\rm av}$ and hydrogen density of the broad line region using the measured helium line ratio R and the equations 4.2.1 - 4.2.5.

This is the first time that similar method has been proposed for the estimations of the temperature and density of hydrogen in the BLR that uses only the measured fluxes of the broad emission lines. However, here we should emphasize some of the possible problems in the application of this method:

1. one problem is the fact that it is still not clear whether the hydrogen Balmer and helium lines are coming from the same or different emission region (see e.g. Kollatschny 2003). Moreover, it is possible that even the hydrogen lines of the Balmer series are not originating in the same region (e.g. Hα and Hβ);

2. another possible problem is the self-absorption that is seen as the decrease of the flux in the center of the emission line. But, this effect is more intensive and noticeable in the case of the lines of Lyman series, e.g. Lyα line since the probability of the absorbtion of the Lyα photon is much higher;

3. also, the large optical depth of some lines can produce influence on the total line fluxes, and thus, in that way also the BP estimates;

4. finally, one should be aware that there are possible differences between temperatures in some type of plasmas. For example, ratios of the hydrogen lines of the Balmer series via BP method give an indication of the excitation temperature, while the ratio of these helium lines indicates the ionization temperature.

One of the possible way to test the influence of the above problems (e.g. first and third problem) is to compare the shape of the line profiles. If, for example, the shape of the Balmer line profiles is the same, that indicates that these lines are probably coming from the same region. Regardless the above mentioned problems, the proposed method could be use for the rough estimate of the physical parameters in the BLR directly from the observations.

5 Selection of objects, observations and data reductions

In this work we analyze the observations of 48 AGN taken from the SDSS spectral database, as well as the spectral observations of the variable galaxies NGC 5548 and NGC 4151, obtained in the period of 8 and 11 years, respectively. In this section, some basic properties of the considered objects are given, as well as the observations and data reduction.

5.1 The SDSS sample

In order to compare the numerical simulation results with the observed data, we consider the sample of AGN studied by La Mura et al. (2007a,b). The sample consisted of 90 AGN taken from the 3rd data realese[20] of the SDSS (Sloan Digital Sky Survey) spectral database[21]. For these objects, La Mura et al. (2007a,b) have measured the BLR temperature parameter A using the BP method. They have found that in the case of around 50% AGN, the BP method can be applied. In this work, for the same sample we measure the fluxes of the helium lines (He II λ4686 and He I λ5876) and apply the method for plasma diagnostics described in the previous section.

[20] http://www.sdss.org/dr3

[21] The Sloan Digital Sky Survey (SDSS) is the most ambitious astronomical survey ever undertaken. It provides detailed optical images covering more than a quarter of the sky, and a 3-dimensional map of about a million galaxies and quasars. As the survey progresses, the data are released to the scientific community and the general public in annual increments. Funding for the SDSS and SDSS-II has been provided by the Alfred P. Sloan Foundation, the Participating Institutions, the National Science Foundation, the U.S. Department of Energy, the National Aeronautics and Space Administration, the Japanese Monbukagakusho, the Max Planck Society, and the Higher Education Funding Council for England. The SDSS Web Site is http://www.sdss.org/. The SDSS is managed by the Astrophysical Research Consortium for the Participating Institutions. The Participating Institutions are the American Museum of Natural History, Astrophysical Institute Potsdam, University of Basel, University of Cambridge, Case Western Reserve University, University of Chicago, Drexel University, Fermilab, the Institute for Advanced Study, the Japan Participation Group, Johns Hopkins University, the Joint Institute for Nuclear Astrophysics, the Kavli Institute for Particle Astrophysics and Cosmology, the Korean Scientist Group, the Chinese Academy of Sciences (LAMOST), Los Alamos National Laboratory, the Max-Planck-Institute for Astronomy (MPIA), the Max- Planck-Institute for Astrophysics (MPA), New Mexico State University, Ohio State University, University of Pittsburgh, University of Portsmouth, Princeton University, the United States Naval Observatory, and the University of Washington. This research has made use of NASA's Astrophysics Data System

5.1.1 Observations and selection of objects

Observations are performed as survey campaigns at the 2.5m f/5 modified Ritchey-Chretien altitude-azimuth telescope, located at the Apache Point Observatory, New Mexico (USA). Data are obtained with a spectrograph, whose sensor uses a mosaic made up by four SITe/Tektronix 2048 x 2048 CCDs, which covers a wavelength range running from 3800 $\AA$ to 9200 $\AA$. A system of 640 optical fibers, each having an aperture of $3''$, subdivides the telescope's field of view, so that each exposure yields 640 spectra corresponding to as many areas in the sky. The spectral resolution R of the observations ranges from 1850 to 2200.

The objects were selected from the SDSS database according to the following requirements: (i) objects had to be located at redshift $z < 0.4$, in particular it was required that the entire profiles of lines belonging to the Balmer series were covered by the available spectral range; (ii) the spectra where the Balmer series was clearly recognized, at least up to the Hδ line, have been considered; (iii) the profile of a broad component had to be detectable for each Balmer line; (iv) such profiles had not to be affected by distortions, due, for example, to bad pixels on the sensors, as well as by the presence of strong foreground or background sources.

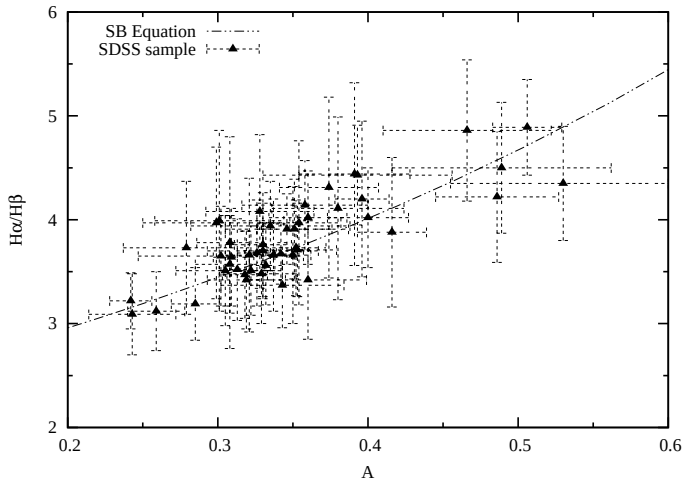

Figure 22: The Hα/Hβ emission line ratio as a function of the BP temperature parameter A for the SDSS sample of 48 galaxies (open triangles). The values of this ratio calculated with the equation 3.5.3, i.e when Saha-Boltzmann distribution can be assumed, are presented with the dashed line.

For the sample of 90 AGN from the SDSS spectral database, the fluxes of the broad Balmer lines are measured (detail procedures of the broad line component extraction and flux measurements are described in the papers La

Mura et al. 2007a,b) and the BP temperature parameter A, i.e. the BP temperature of the BLR has been estimated using BP analysis. In further analysis we consider only those objects for which we assume that the BP method can be applied ($\approx 50\%$ of the whole sample), and those are the objects that have the error of the BP fit smaller than 20% and the BP temperature smaller than 20,000 K, that is in total 48 objects. For those objects we plot the ratios of the Hα/Hβ emission lines against the BP temperature (open triangles in Figure 22). As it can be seen from this figure, the results are in good agreement, and they clearly follow the Hα /Hβ line ratio calculated using the equation 3.5.3 (dashed line in Figure 22), that is derived assuming the Saha-Boltzmann distribution.

5.2 Active galaxy NGC 5548

Active galaxy NGC 5548 is one of the most observed and studied Seyfert 1.5[22] galaxies (see e.g. Shapovalova et al. 2004, Bentz et al. 2007a, Sergeev et al. 2007), therefore the kinematical and physical properties of its BLR have been investigated by many authors (e.g. Netzer & Maoz 1990, Netzer et al. 1990, Krolik et al. 1991, Shields & Ferland 1993, O'Brien et al. 1994, Dumont et al. 1998, Korista & Goad 2000, 2004, Vestergaard & Peterson 2005, Sergeev et al. 2007, Gaskell et al. 2007). The specific property of this galaxy is the strong variability of the continuum and emission line fluxes. For instance, the variability of emission line fluxes is so high that this galaxy changes its type from Seyfert 1.5 (broad emission lines with superposed narrow lines) to Seyfert 1.8 galaxy (weak broad lines with strong superposed narrow lines) which is clearly seen in Figure 23.

This galaxy was the main target of the intensive, 13-year, monitoring campaign performed by *The International AGN Watch Consortium* with the main objective to study the variability of the optical continuum flux and Hβ line flux (Peterson et al. 2002). As a result of this campaign, using the reverberation mapping technique, the BLR size of this galaxy is determined from the time lag between the continuum and broad line flux variations. It is estimated the BLR size has been changed in the period 1989 - 2001, in the range 6 - 26 light days (Peterson et al. 2002). Using these results and assuming the virial approximation, the mass of the black hole in the center of the NGC 5548 is estimated to be $M_\bullet \approx 7 \times 10^7 M_\odot$ (Peterson & Wandel 1999, Bentz et al. 2007a).

There are many interesting, and somehow contradictive, investigations of

[22]Seyfert 1.5 galaxies are the transition type between type 1 and 2 Seyfert galaxies. Their main property are the broad permitted lines with prominent narrow peak.

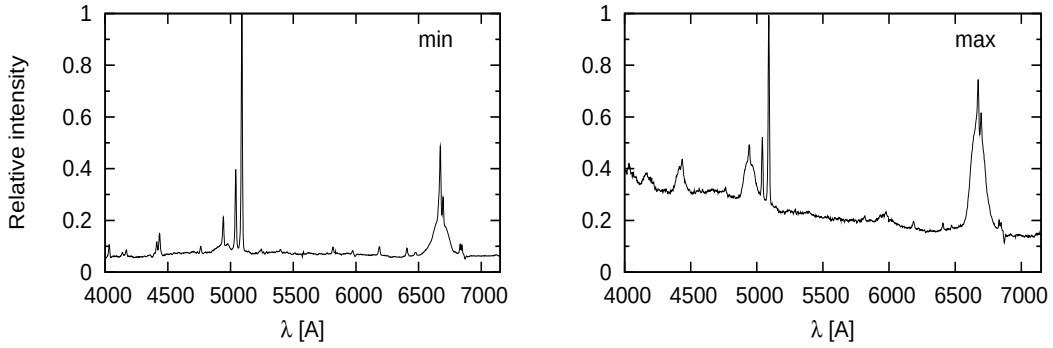

Figure 23: The spectrum of active galaxy NGC 5548 in minimum (left) and maximum (right) activity.

the properties of the broad line region of this galaxy. It has been shown that the BLR of NGC 5548 cannot be described only with the photoionization model since the measured line fluxes, as well as the variability seen in lines and underlying continuum, are inconsistent with the prediction of the photoionization model. Therefore, it is possible that another, non radiatively heated region could contribute to the BLR line spectrum (Dumont et al. 1998). On the other hand, some authors claim that the "locally optimally emitting clouds" (LOCs) BLR model, proposed by Baldwin et al. (1995) is valid for the BLR of NGC 5548. E.g. Korista & Goad (2000) simulated the light curves of the UV emission lines using the LOCs model, and they have shown that there is a good agreement between the predicted and observed light curves and time delays.

In order to connect the variations of the physical properties of the BLR and the variations seen in the spectrum of active galaxy NGC 5548, we apply the BP method to the broad Balmer lines and performed numerical simulations. We use the observations performed in the period from 1996 to 2004 (Shapovalova et al. 2004), and show that in the case of the broad Balmer lines of NGC 5548, the BP method could be used for the BLR temperature estimates. Also, the physical properties in the BLR are simulated using CLOUDY. In order to try to explain the variability of the measured temperature in the BLR, the obtained simulated temperature is compared to the temperature estimated from the BP method.

At the end of the introductory section on NGC 5548, we give some basic data of this galaxy, such as diameter, position and redshift, that are presented in Tabele 3[23].

[23]The data were taken from NED (NASA/IPAC Extragalactic Database) that can be found on the website http://nedwww.ipac.caltech.edu/

Table 3: Basic properties of active galaxy NGC 5548.

Other names	UGC 09149 Mrk 9027
Position	α: 14h 17m 59.5s δ: $+25^{o}$ 08″ 12′
Heliocentric Radial Velocity	5149 ± 7 km s^{-1}
Redshift (z)	0.017175 ± 0.000023
Major Diameter	1.4′
Minor Diameter	1.3′
Visual magnitude	13.3
Classification	SA0 ; Sy1.5
Galactic extinction E(B-V)	0.020
Angular distance	71.9 Mpc
Luminosity distance	74.5 Mpc

5.2.1 Observations and data reduction

Optical spectra of NGC 5548 were taken with the 6 m and 1 m telescopes of Special Astrophysical Observatory (SAO) in Russia (in period 1996-2004) and with INAOE's 2.1 m telescope at the Guillermo Haro Observatory (GHO) at Cananea, Sonora, Mexico (in period 1998-2004)[24]. The spectra were obtained with a long slit spectrograph equipped with CCDs. The typical wavelength range covered was from 4000 Å to 7500 Å, while the spectral resolution was 4.5-15 Å, and the S/N ratio was >50 in the continuum near the Hα and Hβ lines. During observations the seeing was in the range of 1.4 - 3.5 arcsec. Spectrophotometric standard stars were observed every night. Details concerning the spectroscopic observations are given in Shapovalova et al. (2004). The errors of the continuum at 5100 Å and line fluxes measurements were about 3-5%. From the spectral database collected during the monitoring program of NGC 5548 (≈150 spectra) we selected only 24 spectra (Table 4), which satisfy the following criteria: (i) good photometric conditions; (ii) S/N > 10 in the continuum near the Hϵ line; (iii) spectrum covers the wavelength range from λ4000 Åto λ7000 Å; and (iv) the broad component of the Balmer lines from Hα to Hϵ are presented. The basic data of the spectroscopic observations are given in Table 4.

The spectrophotometric data reduction was carried out either with the soft-

[24]All spectra of NGC 5548 were obtained under already mentioned AGN spectral monitoring program with the aim to study the variability of the optical continuum flux and broad Balmer Hα and Hβ emission lines.

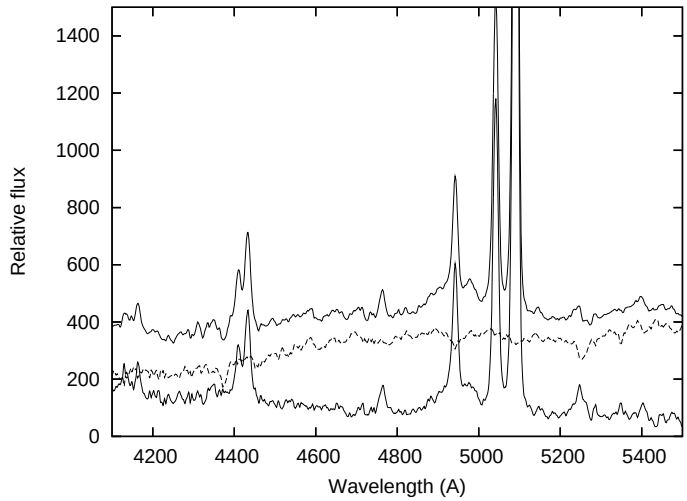

Figure 24: The continuum flux of NGC 5548 in minimum before (top solid line) and after (bottom solid line) subtraction of the host galaxy continuum (dashed line).

ware developed at the SAO RAS by Vlasyuk (1993), or with IRAF[25] for the spectra obtained in Mexico. The image reduction process included bias subtraction, flat-field corrections, cosmic ray removal, 2D wavelength linearization, sky spectrum subtraction, stacking of the spectra for every set-up, and flux calibration based on standard star observations. The procedure of absolute calibration of the spectra is described in details in Shapovalova et al. (2004). Some details about data reduction and spectra extraction in general can be found in Ilić (2005). Apart from standard data reduction procedures, we also remove from the observed spectra the contribution of the continuum of the host galaxy at wavelengths 4250 Å and 5100 Å in order to have only the AGN-component of the optical continuum. This was done using the measurements of the host galaxy contribution in the AGN continuum at 5100 Å of NGC 5548 from Romanishin et al. (1995, see their Fig. 5) with appropriate correction for the aperture effect, and the spectrum of the normal E galaxy NGC 4339, that is justified since the central colors of the host galaxy NGC 5548 in minimum activity state (B-V≈0.9; V-I≈1.2) are similar to the colors of an elliptical galaxy (Romanishin et al. 1995). Details about the correction of the host galaxy contribution to the continuum emission is given Popović et al. (2008a). In Figure 24 the spectra of NGC 5548 before and after the substraction of the stellar continuum contribution are presented.

[25]Image Reduction and Analysis Facility - *http://iraf.noao.edu*

Table 4: The basic data of the spectroscopic observations of NGC 5548: the name of the file, the date of the observation, the Julian date, the telescope used in observation, the aperture size, the spectral range, and the resolution. The column "Code" refers to the telescope used for the observations: L - 6m telescope SAO RAS (Russia), GH - 2.1m telescope GHO (Cananea, Mexico).

File (spectrum)	UT-Date	JD (2400000+)	Code	Aperture (arcsec)	Sp.range (Å)	Resolution (Å)
960213	1996Feb14	50127.579	L	1.5"x6.0"	3100-7200	6
960214	1996Feb14	50128.432	L	1.5"x6.0"	3100-7200	6
960319	1996Mar19	50162.382	L	2.0"x6.0"	3600-7400	8
960321	1996Mar21	50164.395	L	2.0"x6.0"	3600-7400	8
960710	1996Jul10	50275.283	L	2.0"x6.0"	3600-7000	8
980120	1998Jan21	50834.632	L	2.0"x6.0"	3800-7600	8
980222	1998Feb23	50867.535	L	2.0"x6.0"	3800-7600	8
980504	1998May04	50938.293	L	2.0"x6.0"	3700-7600	8
980508	1998May08	50942.461	L	2.0"x6.0"	3700-7700	8
980725	1998Jul26	51020.703	GH	2.5"x6.0"	3960-7231	15
980726	1998Jul27	51021.712	GH	2.5"x6.0"	3930-7219	15
200126	2000Jan27	51570.959	GH	2.5"x6.0"	4070-7350	15
210513	2001May14	52043.859	GH	2.5"x6.0"	3980-7300	15
210613	2001Jun14	52074.772	GH	2.5"x6.0"	4022-7330	15
210614	2001Jun15	52075.738	GH	2.5"x6.0"	4010-7330	15
21-07	2001Jul16	52107.320	L	2.0"x6.0"	3630-8050	8
220304	2002Mar05	52338.780	GH	2.5"x6.0"	3976-7305	15
220404	2002Apr05	52369.850	GH	2.5"x6.0"	3976-7305	15
220405	2002Apr06	52370.780	GH	2.5"x6.0"	3976-7305	15
220624	2002Jun24	52450.420	L	2.0"x6.0"	3800-7600	8
230126	2003Jan27	52666.96	GH	2.5"x6.0"	3976-7305	15
230127	2003Jan28	52667.930	GH	2.5"x6.0"	3976-7305	15
230325	2003Mar26	52724.900	GH	2.5"x6.0"	3976-7305	15
230522	2003May23	52782.750	GH	2.5"x6.0"	3976-7305	15

5.3 Active galaxy NGC 4151

Active galaxy NGC 4151 is the brightest and closest Seyfert 1.5 galaxy. This makes this galaxy very suitable for different investigation in various spectral bands (e.g. Hutchings et al. 1998, Kaiser et al. 2000, Ulrich 2000, Mundell et al. 2003, Ulvestad et al. 2005). Some basic data of this galaxy, such as diameter, position and redshift, that are presented in Tabele 5[26].

Like NGC 5548, the active galaxy NGC 4151 shows strong continuum and line flux variability in the period of just couple of days (Peterson 1988, Clavel et al. 1990, Maoz et al. 1991, Shapovalova et al. 1996, Ulrich & Horne 1996, Sergeev et al. 2001, Lyuty 2005). In the last 20 years, this galaxy was the subject of many monitoring programs with the main aim to determine the size of the BLR using the reverberation mapping technique, i.e. by measuring the time delay between the emission line fluxes, in response to the variations of the continuum flux. It is interesting to notice that different authors have obtained different results for the BLR size by studying different spectral ranges in different time intervals (for review of the all results see Shapovalova et al. 2008). But one thing is certain, the BLR of this galaxy is very compact, with dimensions of only couple of light days, and very complex and stratified, in the sense that different emission lines are coming from different regions inside of the BLR (e.g. Kaspi et al. 1996, Metzroth et al. 2006, Shapovalova et al. 2008).

Table 5: Basic properties of active galaxy NGC 5548.

Position	α: 12h 10m 32.6s δ: $+39^{o}$ $24'$ $21''$
Heliocentric Radial Velocity	995 ± 3 km s^{-1}
Redshift (z)	0.003319 ± 0.000010
Major Diameter	$6.3'$
Minor Diameter	$4.5'$
Visual magnitude	11.5
Classification	SAB ; Sy1.5
Galactic extinction E(B-V)	0.028
Angular distance	16.9 Mpc
Luminosity distance)	17.1 Mpc

Shapovalova et al. (2008) found that the relation between the line and

[26]The data were taken from NED (NASA/IPAC Extragalactic Database) that can be found on the website http://nedwww.ipac.caltech.edu/

continuum flux is not linear in the whole continuum flux range, i.e. the change of the line flux does not correspond to the change of the continuum flux (Figure 25). It can be seen in Figure 25 that the line flux steepens at low continuum fluxes and saturates at the high continuum flux. Furthermore, even when we extrapolate linearly the continuum flux to zero, it seems that the line flux is still larger than zero. All this could be due ti the fact that the ionizing incident flux is very intense, so the medium reprocesses the irradiating flux into continua (Balmer, Pashen...) and not only into lines.

Moreover, it has been shown that when assuming the photoionization model for the BLR of NGC 4151 and computing the line fluxes (e.g. the Hβ line) for different optical luminosities and BLR radii, one gets the line fluxes much smaller than the observed one (Shapovalova et al. 2008). The measured Hβ line flux is in the range $(2.25 - 10.80) \times 10^{-12}$erg s^{-1}cm^{-2}. Figure 26 gives the measured Hβ flux at Earth as a function of density for different optical luminosites and BLR radii. It is clear from Figure 26 that the observed flux is always much higher than the computed one, even for the highest densities 10^{14} cm^{-3}. One possible explanation of such behavior could be that a non-photoionized region is also contributing to the total Balmer line fluxes. Such a "mechanically heated" region was already proposed by Dumont et al. (1998) to account for the strong intensities of the Balmer lines in NGC 5548. In the case of NGC 4151, this region could be associated with the radio-jet, since the high resolution radio images of this galaxy indeed reveal a 0.2-pc two-sided base to the well-known arc-second radio jet (Ulvestad et al. 2005). Therefore, it could be that the BLR is made of two-components: the usual one, ionized by the radiation of the accretion disc and its corona, and another component, possibly associated with a rotating subrelativistic outflow surrounding the jet (Murray & Chiang 1997), where ionization and heating could be due either to relativistic particles or to a shock at the basis of the jet, and thus, they could not be directly correlated to the ionizing continuum coming from the center.

Also, Popović (2003) has made some estimate of the physical properties in the BLR of this galaxy using the BP method, applied on the 5 broad Balmer lines Hα to Hε (Popović 2003). The observations were done February 10, 1998 with the Hubble Space Telescope. In this case, when BP method was applied on 5 Balmer lines, the obtained temperature parameter is $A = 0.357$, and the corresponding temperature is $T \approx 14100$ K.

In this work, in order to connect the change of the physical conditions in the BLR with the change of the NGC 4151 spectrum, we applied the BP method to the large set of the broad Balmer lines. For this we used the high-quality observations obtained in a long-term spectral monitoring (11 years, from 1996 to 2006) of NGC 4151 (Shapovalova et al. 2008, Popović et al. 2008b). But, on the other hand, only fluxes of the first three lines of Balmer series could be measured. We show later that, in the case of these three broad Balmer lines

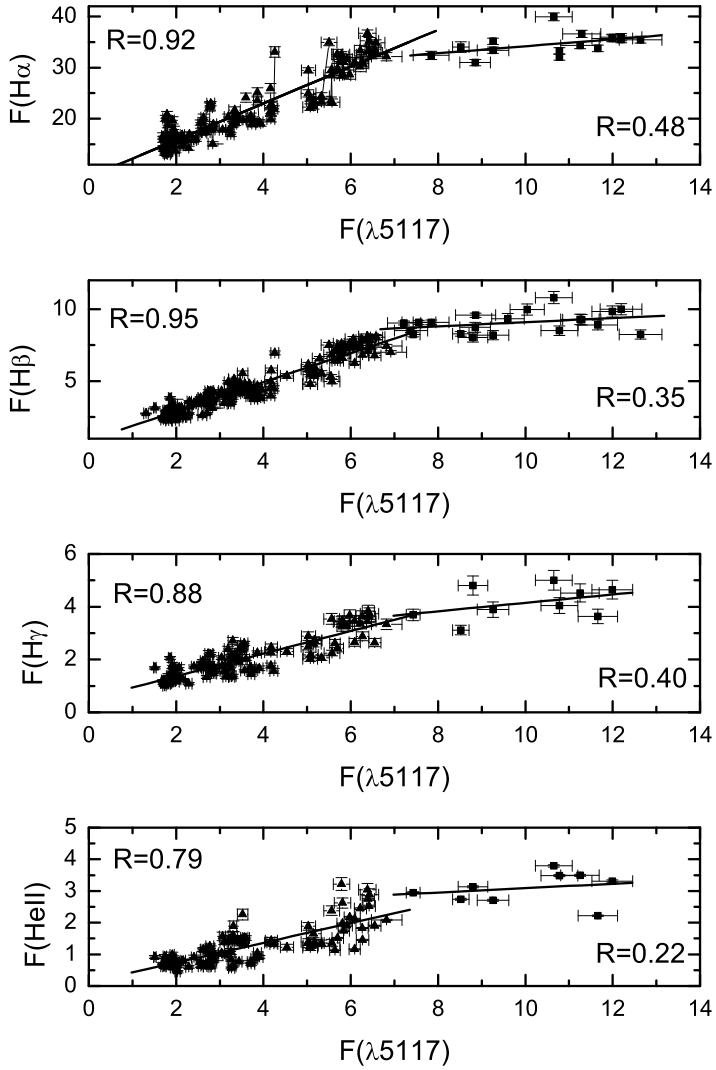

Figure 25: The Hα, Hβ, Hγ, HeIIλ4686 fluxes versus the continuum flux at λ =5117 Å for AGN NGC 4151. The line fluxes are given in units of 10^{-12}erg cm^{-2}s^{-1}, and the continuum flux in units of 10^{-14}erg cm^{-2}s^{-1}A^{-1} (Shapovalova et al. 2008).

of NGC 4151, the BP method could not be used for the BLR temperature estimates.

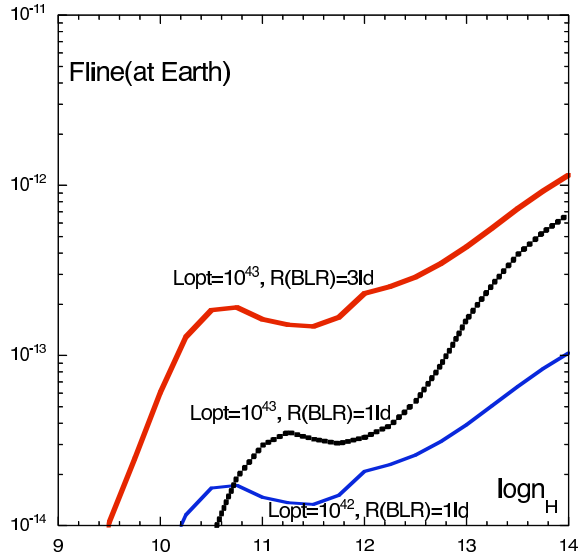

Figure 26: The computed Hβ flux for the conditions of NGC 4151 at Earth as a function of the density in cm^{-3} for different optical luminosities and BLR sizes (Shapovalova et al. 2008).

5.3.1 Observations, data reduction and flux measurments

In this thesis we used spectroscopic observations of NGC 4151 that covered the period of 11 years. The observations and flux measurements were carried out by Shapovalova et al. (2008) in the period from January 11, 1996 (Julian Date = JD 2450094) to April 20, 2006 (JD 2453846). In total 180 blue spectra (that contain region around Hγ and Hβ lines) and 137 red spectra (that contain region around Hα line) were taken during 220 nights, with the 6 m and 1 m telescopes of SAO, Russia (1996–2006), with the 2.1 m telescope of the Guillermo Haro Astrophysical Observatory (GHAO) at Cananea, Sonora, México (1998–2006), and with the 2.1 m telescope of the Observatorio Astronómico Nacinal at San Pedro Martir (OAN-SMP), Baja California, México (2005–2006). The spectra were obtained with a long–slit spectrograph equipped with CCDs. The typical observed wavelength range was 4000 - 7500 Å, the spectral resolution was R=5–15 Å, and the S/N ratio was $>$ 50 in the continuum near the Hα and Hβ lines. The spectral observations from 2004 to 2006 with the GHAO's 2.1 m telescope were carried out with two variants of the equipment: 1) with a grism of 150 l/mm (a low dispersion of R=15 Å); 2) with a grism of 300 l/mm (a moderate dispersion of R=7.5Å). Spectrophotometric standard stars were observed every night.

The spectrophotometric data reduction was carried out with the software developed at the SAO RAS by Vlasyuk (1993), or with IRAF for the spec-

tra observed in México. The image reduction process included bias subtraction, flat-field corrections, cosmic ray removal, 2D wavelength linearization, sky spectrum subtraction, addition of the spectra for every night, and relative flux calibration based on standard star observations.

The standard technique of flux calibration spectra using standard stars is not precise enough for the study of AGN variability, since even under good photometric conditions the accuracy of spectrophotometry is not better than 10%. Therefore, the absolute calibration was performed, using the fluxes of the narrow emission lines for scaling the AGN spectra. The narrow emission lines are known to remain constant on time scales of tens of years (Peterson 1993), since the forbidden line emitting region is extended to more than a hundred light years. Thus, the authors assume that the flux of the [OIII]λ5007 line was constant during the monitoring period, so they used this line in order to obtain a homogeneous set of spectra with the same wavelength calibration and the same [OIII]λ5007 flux. All procedures of obtaining the absolutely calibrated spectra, the correction for the position angle, seeing and aperture effects are described in details in Shapovalova et al. (2008). Finally, in order to estimate the narrow line contributions to the broad line fluxes, the spectral template for the narrow lines was constructed, using the blue and red spectra in the minimum activity state (May 12, 2005), where the broad Hβ component was very weak, and the broad components from the higher Balmer line series were absent. Also, the continuum flux at 5117 Å was measured.

From this large set of spectral data, we chose only 68 for the BP analysis. The criteria used for the data selection was that all three Balmer lines (Hα, Hβ i Hγ) were observed on the same date. The fluxes of these lines are given in Table 8 (Shapovalova et al. 2008, Popović et al. 2008b).

6 Data analysis, results and discussion

In the following section we give the analysis of the data and the results of this thesis. More precisely, we will present how previously described method for plasma diagnostics could be applied on the observations.

6.1 The SDSS sample

6.1.1 The measurements of helium lines fluxes

For the data sample defined in section 5.1.1, we measure the fluxes of the helium lines He II λ4686 and He I λ5876. The fluxes are measured with the astronomical software DIPSO[27], being particularly careful in the case of He II λ4686 line, where there is contamination from Fe II multiplet and nearby Hβ line. The local continuum has been subtracted from the spectra, as well as the contribution of the host galaxy (for details see La Mura et al. 2007a,b).

In order to measure the broad He II λ4686 line flux more accurately, we perform Gaussian decomposition (including Fe II template) in order to subtract the contribution of the Fe II multiplet, Hβ and He II λ4686 narrow lines (Gaussian decomposition is already described in details in many paper; see e.g. Ilić 2005, 2006, Popović et al. 2001, 2002, 2004). In Gaussian decomposition, great attention was given to fitting the helium narrow component, Fe II multiplet and the blue wing of the Hβ line (Figure 27). A standard deviation σ is taken as an error of the line flux measurements. The results are given in Table 6. From total 48 objects, the cases when helium lines could not be measured are excluded from the further analysis (e.g. when lines were too noisy or the contribution of Fe II could not be properly subtracted). For this reason, the number of object in our sample is reduced to 20 objects (Ilić et al. 2008a).

6.1.2 Plasma diagnostics using helium lines

In Figure 28 we plot the ratio of the helium lines R as a function of the BP temperature $T_{\rm BP}$ for the 20 objects from the SDSS sample. As can be seen in Figure 28 there is a linear function between BP temperature and the helium line ratio, whit the correlation coefficient is $r = 0.50$. This trend is in an agreement with the BLR physics, where for higher temperatures one should expect to have stronger He II than He I lines. We should note here that if we

[27]The software package DIPSO is part of the STARLINK program collection that contains very useful spectroscopic procedures. All information about the package can be found at the website*http://www.starlink.ac.uk*.

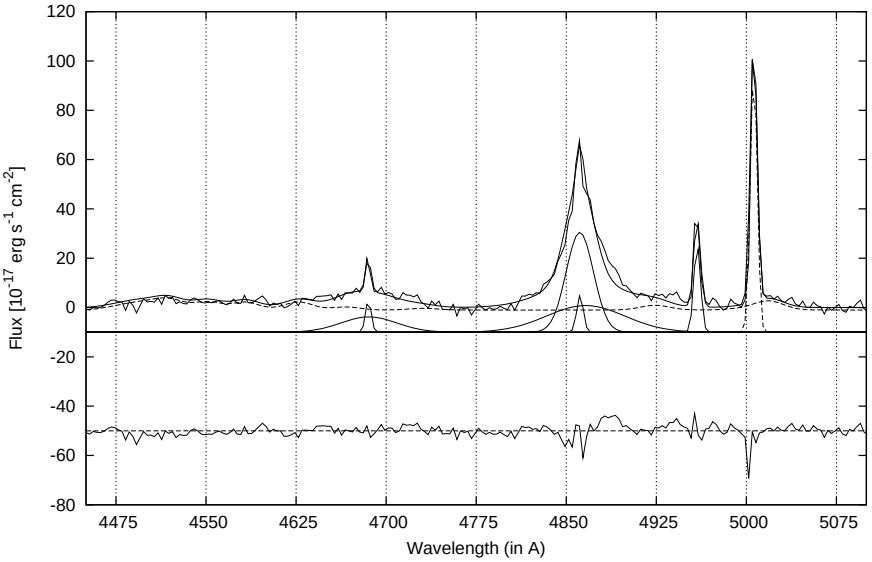

Figure 27: An example of the Gaussian decomposition of the Hβ line region in the case of the object SDSSJ1300+5641. The Gaussian components are shown below the observed spectrum. The helium line He II λ4686 is fitted with two Gaussians. The Fe II template is presented with dashed line, while the residual spectrum is given at the bottom.

exclude the point that is clearly high above the best-fitting line (see Figure 28), the correlation coefficient is slightly higher $r = 0.62$.

The method for diagnostics of the plasma in the broad line region (described in section 5.3) is applied on the sample of 20 AGN taken from the SDSS data set. For objects from this sample, the BP method could be applied and fluxes of the helium He II λ4686 and He I λ5876 lines could be measured. Using equations 4.2.1 - 4.2.3 we estimate the average temperature $T_{\rm av}$ and hydrogen gas density in the BLR of galaxies from the sample, assuming that we have column density $N_{\rm H} = 10^{23}{\rm cm}^{-2}$. The results of our measurements are presented in Table 6 in the last three columns. The hydrogen density is estimated using the equation 4.2.3, while the temperature is obtained from equations using 4.2.1 and 4.2.2. As one can see from Table 6, there is a scatter between temperatures estimated with different equations, but mostly both values are in the frame of estimated error bars. In the case of the temperature estimations, taking into account that correlation between the average temperature $T_{\rm av}$ and the helium line ratio R obtained from the models (see Figure 9) is higher than between the average temperature $T_{\rm av}$ and the BP temperature $T_{\rm BP}$ (see Figure 11), we assume that the values obtained using equation 4.2.1 (T^1_{av} in Table 6) are more realistic. The estimated BLR temperatures are in the range of $T_{\rm BLR} = 4000 - 18000$ K , while the hydrogen gas density is in the range of

Table 6: The measurements of the broad component of the helium lines (He II λ4686 and He I λ5876) for the SDSS sample. The temperature $T^1_{\rm av}$ is calculated using 4.2.1 (column 8), while $T^2_{\rm av}$ is calculated using 4.2.2. The BP temperature $T_{\rm BP}$ is taken from La Mura et al. (2007b). The line fluxes are given in units 10^{-17}erg cm^{-2}s^{-1} .

Object name	$T_{\rm BP}[K]$	F(HeI5876)	F(HeII4686)	log $n_{\rm H}$[cm^{-3}]	$T^1_{\rm av}$ [K]	$T^2_{\rm av}$ [K]
SDSSJ0013-0951	17000±2000	165.1 ±18.7	137.8 ± 6.8	9.2 ±0.9	9400± 1000	15700± 2000
SDSSJ0037+0008	15000±2000	150.4 ±15.9	89.1 ± 12.6	9.6 ±1.3	7700± 1000	13700± 2000
SDSSJ0110-1008	14000± 1000	919.4 ±51.5	402.0 ± 50.8	10.1 ±0.8	6600± 600	12700± 1000
SDSSJ0142-1008	15000± 2000	4243.2 ±205.2	1487.6± 160.7	10.4 ±0.7	6000± 400	13700± 2000
SDSSJ0150+1323	11000± 1000	1017.6 ±95.2	279.1 ± 39.7	10.7 ±0.9	5400± 500	9700± 1000
SDSSJ0409-0429	15000± 2000	656.8 ±72.6	636.0 ± 48.5	9.0 ±1.1	10400±1300	13700± 2000
SDSSJ0832+4614	16000± 2000	616.7 ±38.0	465.6 ± 26.0	9.3 ±0.6	8900± 600	14700± 2000
SDSSJ1118+5803	14000± 2000	2156.2 ±147.7	2707.2± 137.1	8.6 ±0.7	12400±1100	12700± 2000
SDSSJ1122+0117	15000± 1000	589.8 ±49.1	501.3 ± 126.0	9.1 ±1.9	9500±2000	13700± 1000
SDSSJ1223+0240	19000± 3000	169.4 ±19.9	148.2 ± 24.6	9.1 ±1.6	9700±1800	17700± 3000
SDSSJ1300+5641	17000± 1000	498.0 ±44.7	398.3 ± 44.2	9.2 ±1.1	9200± 1100	15700± 1000
SDSSJ1300+6139	15000± 3000	677.0 ±12.7	253.0 ± 31.4	10.3 ±0.6	6100± 400	13700± 3000
SDSSJ1307+0107	11000± 2000	501.1 ±16.5	67.6 ± 15.0	11.5 ±0.6	4400± 200	9700± 2000
SDSSJ1341-0053	16000± 1000	266.3 ±19.4	56.2 ± 18.5	11.0 ±1.3	5000± 600	14700± 1000
SDSSJ1342-0053	16000± 2000	145.9 ±14.9	96.1 ± 16.9	9.5 ±1.5	8200± 1300	14700± 2000
SDSSJ1349+0204	10000± 1000	1116.8 ±57.0	365.6 ± 55.0	10.5 ±0.8	5800± 500	8700± 1000
SDSSJ1619+4058	13000± 2000	657.6 ±127.6	408.6 ± 46.9	9.6 ±1.6	7900± 1400	11700± 2000
SDSSJ1654+3925	15000± 2000	633.7 ±62.0	526.4 ± 31.5	9.2 ±0.9	9400± 900	13700± 2000
SDSSJ1719+5937	10000± 1000	1214.0 ±165.1	288.5 ± 80.2	10.9 ±1.4	5200± 700	8700± 1000
SDSSJ1720+5540	16000± 1000	1134.7 ±106.6	325.3 ± 59.0	10.6 ±1.0	5500± 600	14700± 1000

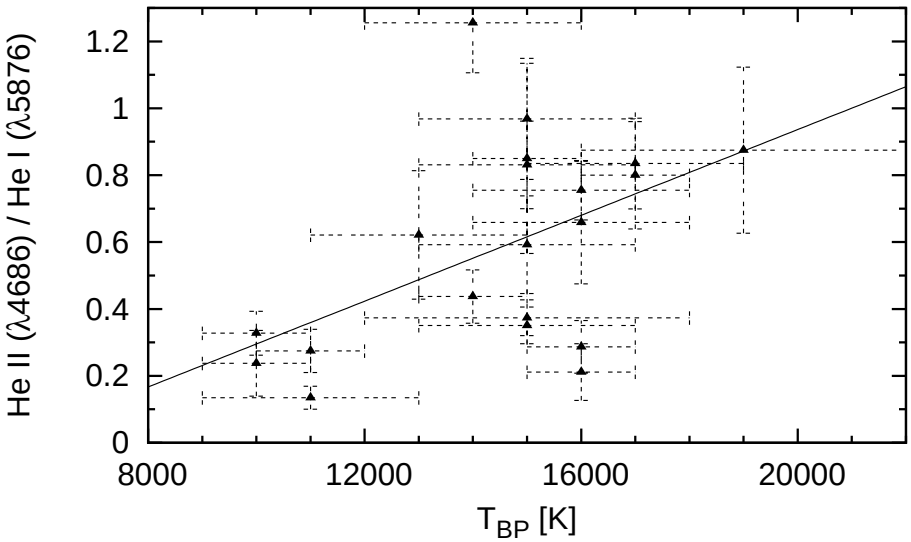

Figure 28: The He II lines ratio R as a function of the BP temperature $T_{\rm BP}$ for the SDSS sample. The linear best-fitting is presented with solid line.

$n_{\rm H} = 10^{8.6} - 10^{11.5}$ cm^{-3} (Ilić et al. 2008a). These values are in good agreement with the previous estimates of the physical conditions in the BLR (see e.g. Osterbrock & Ferland 2006).

6.2 Physics of the BLR of galaxy NGC 5548

6.2.1 The measurements of fluxes and velocities of the emission line broad component

In order to investigate only the broad part of the Balmer emission lines, we need to subtract the continuum and the narrow Balmer and satellite lines. To estimate the contribution of these lines we used a template of narrow and satellite lines (Figure 29) estimated from two independent measurements in the case of the minimum intensity of the broad Balmer lines. In this template the Fe II lines in the Hβ spectral region are included. The optical Fe II lines showed variability with smaller amplitude than that of the Hβ (around 50%-75% of Hβ, Vestegaard & Peterson 2005). Testing the contribution of the Fe II residuals (after subtraction of the template), we concluded that it may contribute about 2-5% to the total measured line flux of the Hβ line. Furthermore, we *a priori* take into account that the continuum subtraction contributes to the error-bars within 10% of the measured fluxes. In general, we can expect this value in weak Balmer lines (e.g. Hε), but in the case of the Hα and Hβ lines, it should

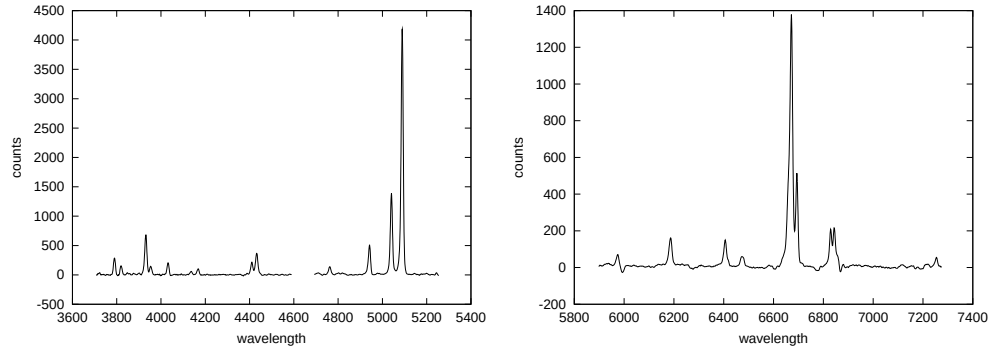

Figure 29: The adopted narrow emission line template (Balmer and satellite lines) for the region of Hβ - Hε (left panel) and Hα lines (right panel).

be even smaller.

The fluxes of the Balmer lines were measured several times, but it is important to emphasize that independent measurements were performed by two persons. Then, the error-bars were calculated as:

$$\Delta F_i = \Delta F_i^{\rm mes} + 0.1 \cdot F_i^{\rm mes}, \tag{7.2.1}$$

where F_i^{mes} is the measured flux, ΔF_i^{mes} is statistical error (within 1σ) obtained from several measurements and $0.1F_i^{mes}$ is taken to be the error of the continuum and narrow line template subtraction. The flux ratios of the Balmer lines and the fluxes of the Hβ from different periods are given in Table 7. The error-bars presented in the Table 7 were obtained as (see e.g. Agekyan 1972, Bevington & Robinson 2003):

$$\Delta R_i = R_i \cdot \sqrt{\left(\frac{\Delta F_i}{F_i^{\rm mes}}\right)^2 + \left(\frac{\Delta F_{\rm H\beta}}{F_{\rm H\beta}^{\rm mes}}\right)^2}, \tag{7.2.2}$$

where R_i is the ratio of $F_i/F_{\rm H\beta}$ ($i = \alpha, \gamma, \delta, \varepsilon$) lines. The fluxes are scaled using the atomic parameters of the transition according to the equation 3.5.7. The obtained scaled flux is denoted with F_n, which error-bars ($\Delta \log_{10}(F_n)$) have been calculated as:

$$\Delta \log_{10}(F_n) = \frac{\Delta F_i}{F_i^{\rm mes} \times \log_e 10}. \tag{7.2.3}$$

Furthermore, we apply the Boltzmann plot method on measurements of every line series and determine the temperature parameter A according to the equation 3.5.7. The parameter A is obtained from the best fit of the measured values, while ΔA is the asymptotic standard error (within 1σ). Both of these values are also given in Table 7. Some examples of Boltzmann plots of the Balmer line series of NGC 5548 from different epochs are presented in Figure 30.

For this analysis, we used only those observed spectra where the spectral region from Hε to Hα was covered, except for the two spectra (see Table 7) that covered only the interval from Hδ to Hα. We used the aforementioned spectra in order to have the data in years 2000 and 2001.

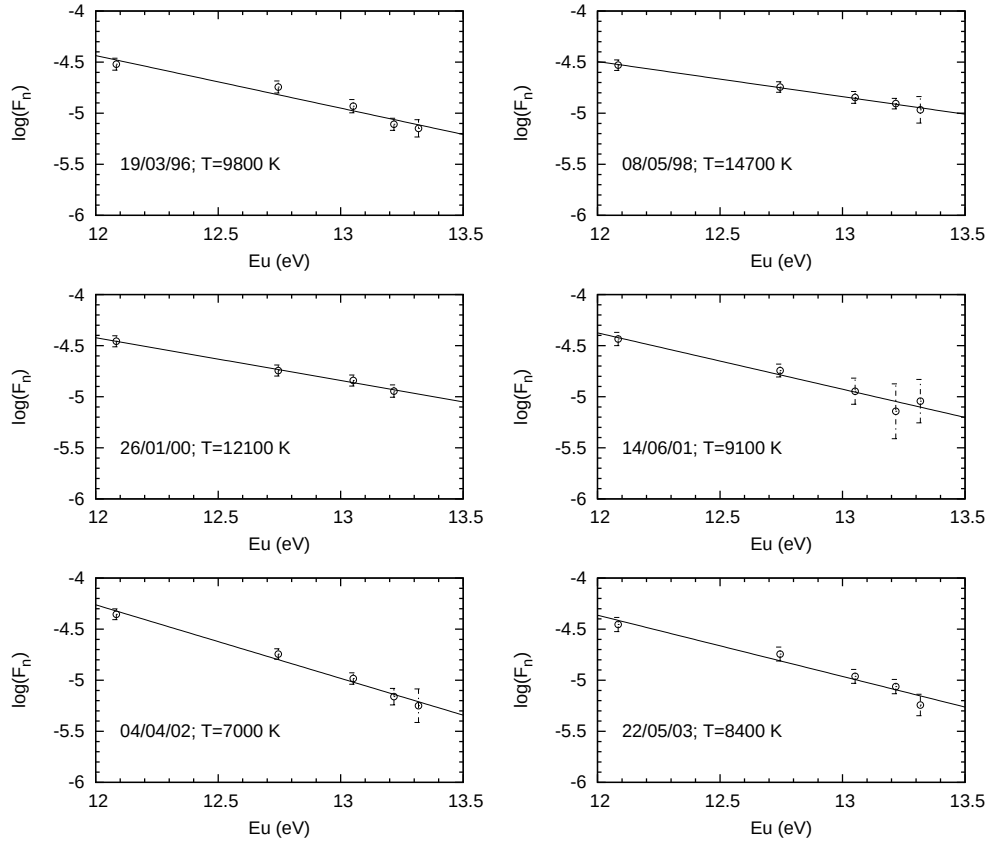

Figure 30: The examples of Boltzmann plots of the Balmer line series of NGC 5548 from different epochs. F_n is calculated using the equation 3.5.7 after the normalization of all Balmer lines to the $H\beta$ flux ($F_{ul}(\mathrm{H}\beta) = 1$).

We note here that the reddening effect can influence the Balmer line ratio (e.g. Crenshaw & Kraemer 2001, Crenshaw et al. 2001, 2002, Popović 2003) and consequently the temperature parameter obtained with the BP method. In the case of NGC 5548 the Galactic reddening is negligible E(B-V) = 0.020 mag (Burstein & Heiles 1982; Schlegel et al. 1998), and here it is not considered. Concerning the intrinsic reddening, it is not negligible for this galaxy. Recently Gaskell found that it is E(B-V) = 0.17 mag (Gaskell et al. 2007). But, since we are here investigating the changes in the BP during an interval, the intrinsic reddening can be neglected as it should not vary too much in a relatively short period of around 8 years, thus, it should not influence the temperature changes.

Table 7: The measured flux of the Balmer lines and continuum at λ4230 and λ5190 Å of NGC 5548, as well as the temperature parameter A. The Hβ line flux is given in 10^{-13}erg cm^{-2}s^{-1} and the continuum flux in 10^{-15}erg cm^{-2}s^{-1}.

Spectrum	$F_{H\alpha}/F_{H\beta}$	$F_{H\gamma}/F_{H\beta}$	$F_{H\delta}/F_{H\beta}$	$F_{H\varepsilon}/F_{H\beta}$	$F_{H\beta}$	A	$F_c(\lambda\ 4230)$	$F_c(\lambda\ 5190)$
960213	3.405±0.406	0.396±0.047	0.174±0.021	0.071±0.027	7.998±0.950	0.456±0.095	12.51±1.01	10.33±0.84
960214	3.689±0.625	0.456±0.074	0.148±0.025	0.091±0.016	7.598±1.220	0.450±0.085	13.94±1.13	10.19±0.83
960319	3.647±0.492	0.341±0.051	0.133±0.018	0.077±0.015	7.281±0.983	0.515±0.068	12.52±1.01	10.99±0.89
960321	3.126±0.384	0.386±0.048	0.187±0.029	0.072±0.016	7.055±0.864	0.414±0.100	11.86±0.96	9.65±0.78
960710	4.203±0.569	0.465±0.063	0.204±0.027	0.084±0.011	9.891±1.322	0.462±0.082	17.68±1.43	13.73±1.11
980120	3.672±0.446	0.393±0.048	0.220±0.038	0.062±0.008	8.420±1.023	0.474±0.138	15.35±1.24	11.81±0.96
980222	3.624±0.429	0.376±0.072	0.210±0.027	0.082±0.023	9.694±1.146	0.426±0.075	14.06±1.14	11.22±0.91
980504	3.523±0.398	0.401±0.048	0.201±0.024	0.125±0.042	9.650±1.090	0.337±0.013	20.58±1.67	15.56±1.26
980508	3.571±0.427	0.416±0.055	0.212±0.025	0.117±0.035	7.998±0.950	0.344±0.014	19.87±1.61	14.79±1.20
980725	3.961±0.471	0.417±0.049	0.167±0.020	0.072±0.009	9.969±1.179	0.508±0.088	15.38±1.24	12.37±1.00
980726	3.727±0.438	0.338±0.047	0.153±0.018	0.039±0.012	9.235±1.083	0.633±0.177	15.21±1.23	12.85±1.04
200126	4.223±0.528	0.420±0.052	0.194±0.027	-	7.167±0.886	0.418±0.022	9.83±0.80	7.63±0.62
210513	5.718±1.134	0.314±0.099	0.109±0.049	0.146±0.096	2.900±0.437	0.586±0.161	5.94±0.48	5.11±0.41
210613	4.493±0.622	0.414±0.056	0.150±0.077	-	3.874±0.524	0.512±0.073	7.86±0.64	6.09±0.49
210614	4.439±0.664	0.330±0.097	0.123±0.076	0.098±0.048	3.408±0.499	0.551±0.070	8.38±0.68	6.81±0.55
21-07	4.028±0.521	0.390±0.065	0.166±0.024	0.055±0.009	5.901±0.749	0.572±0.127	10.04±0.81	8.03±0.65
220304	5.411±0.784	0.289±0.042	0.125±0.022	0.035±0.012	3.616±0.520	0.826±0.143	5.52±0.45	5.19±0.42
220404	5.347±0.654	0.303±0.039	0.118±0.022	0.061±0.023	7.998±0.950	0.720±0.049	4.20±0.34	4.13±0.33
220405	5.619±0.895	0.329±0.052	0.126±0.023	0.057±0.019	3.311±0.523	0.735±0.064	4.05±0.33	3.94±0.32
220624	4.781±1.127	0.057±0.017	0.062±0.011	0.029±0.012	2.691±0.472	1.042±0.276	4.13±0.33	4.69±0.38
230126	6.546±0.984	0.292±0.066	0.168±0.032	0.140±0.048	2.421±0.364	0.584±0.117	6.77±0.55	5.99±0.48
230127	6.794±1.176	0.208±0.040	0.162±0.030	0.130±0.032	2.136±0.369	0.641±0.167	6.00±0.49	5.49±0.44
230325	4.532±0.707	0.238±0.039	0.160±0.026	0.079±0.031	3.252±0.505	0.586±0.077	6.91±0.56	6.33±0.51
230522	4.248±0.677	0.318±0.050	0.148±0.024	0.062±0.015	4.782±0.758	0.599±0.073	8.06±0.65	6.99±0.57

We also measured the velocity of the emitters in the BLR. These measurements were performed in order to present A as a function of Full Width Half Maximum (FWHM) and Full Width Zero Intensity (FWZI). The graphs A vs. FWHM and FWZI are useful because of:

(i) the Balmer line ratios are velocity dependent in AGN (Stirpe 1990, 1991) and this may be related to the physical conditions (temperature, density and kinematics) as well as to the radiative transfer effects;

(ii) illustration of the physical conditions in the BLR plasma. As it was pointed out by Popović (2003) if $A < 0.3$, the recombination "Case B" plus the intrinsic reddening may explain BP. The "Case B" recombination of Balmer lines can bring the $\log(F_n)$ *vs* E_u as a linear decreasing function (see Table 4.4 in Osterbrock 1989).

In order to compare the temperature parameter A with the velocity of gas, very high data quality is required to measure FWHM, especially FWZI. The data quality is different for different spectra of NGC 5548, consequently, for velocity measurements we used only the Hα and Hβ lines. We first normalized the broad profiles of these lines and converted the wavelength axis to the velocity scale $X = (\lambda - \lambda_0)/\lambda_0$ (Figure 31). We measured FWHM and FWZI of both lines, and we calculated the average values for each spectrum (Figure 31). We note here that there was no significant difference between the profiles of Hα and Hβ lines, that indicates that the line forming region of Hα and Hβ is the same.

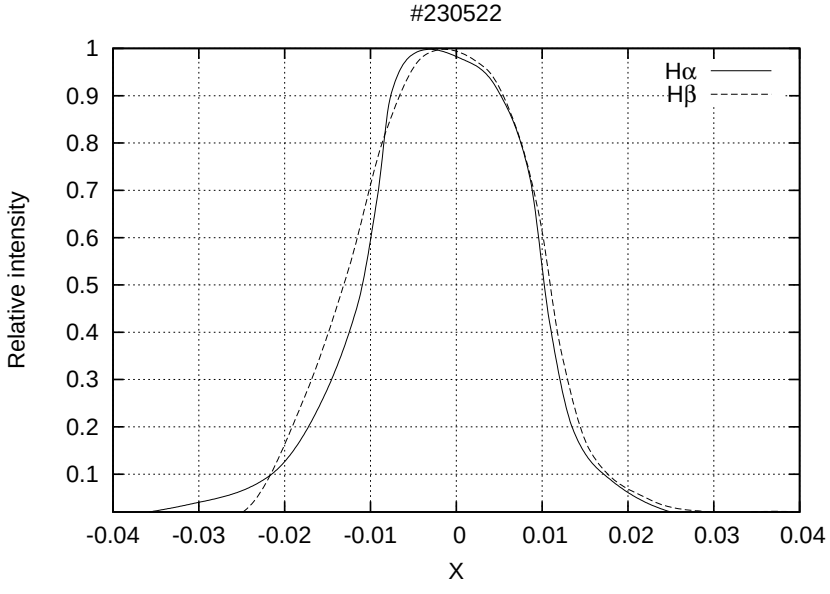

Figure 31: The profiles of Hα and Hβ lines of NGC 5548 observed on 22/05/2003.

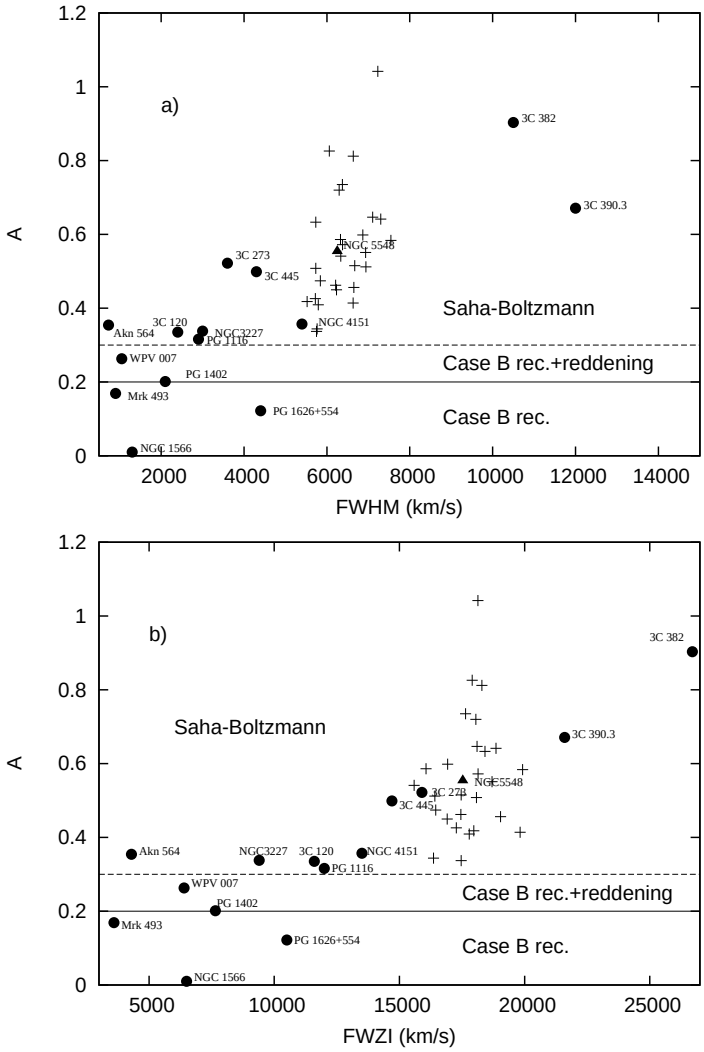

Figure 32: The graph A=f(FWHM,FWZI). The data from different periods are denoted with crosses, while the averaged value for NGC 5548 is presented with full triangles. The data presented with full circles are taken from Popović (2003) just for illustration.

6.2.2 BP temperatures of NGC 5548

One can see in Figures 30 and 32 that BPs graphics indicate that the population of the excited levels from the Balmer series follows the Saha-Boltzmann distribution. We found that in all considered periods, the temperature parameter is $A > 0.3$. It means that the recombination "Case B" plus an intrinsic reddening cannot explain the line flux ratio of the Balmer lines. Also, we investigate the dependence of the temperature coefficient as a function of FWHM and FWZI (Figure 32). As one can see from Figure 32, there is no significant

correlation between widths and A. That is expected since macroscopic bulk motions are mainly constrained by kinematics, which in the case of the BLR of this galaxy is probably a disk-like geometry as it was suggested by Shapovalova et al. (2004). On the other hand, it may indicate that changes in the self-absorption in the Balmer lines has no significant variation during the period. The averaged value obtained from all periods (full triangle in Figure 32) is in a good agreement with the trend of the AGN sample given in Popović (2003). Such a trend (increasing A with FWHM and FWZI) may indicate that physical conditions are dependent on kinematical characteristics of the BLR. This may be connected with distances from the massive black hole, e.g. the broader Balmer lines indicate higher macroscopic bulk motions which can be expected in the regions closer to the massive black hole. Moreover, when we plot the Hα/Hβ line ratio as a function of the temperature parameter A (Figure 33), we get that all the points are distributed around the theoretical curve obtained when assumed that the Saha-Boltzmann distribution is valid (section 3.5, Figure 4). It is obvious from Figure 33 that the data point from 2002 (spectrum #220624) is far from the SB curve, but this point clearly does not belong to the group of other points, that can also be seen in Figure 32.

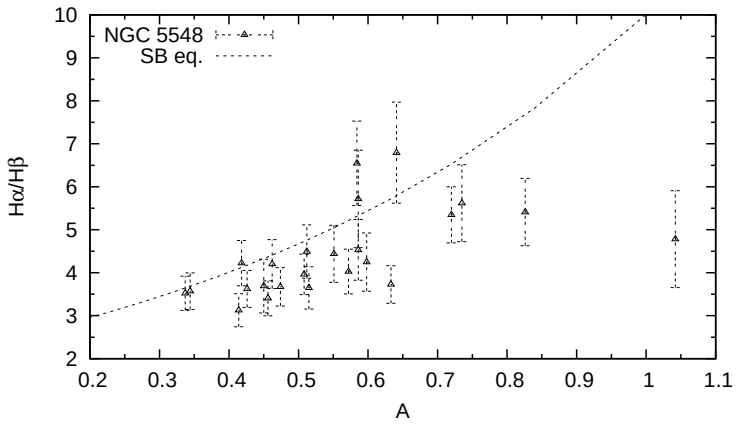

Figure 33: The Hα/Hβ line ratio as a function of the temperature parameter A for NGC 5548 in the observed period of 8 years. The dashed line gives this ratio calculated when the Saha-Boltzmann distribution is assumed (section 3.5, Figure 4).

We could estimate the temperature of the emitting region using the equation 3.5.8. In Figure 34 we plot the temperature variation in the period of 8 years: as one can see the averaged temperature is ≈10000 K, and is changing by around 50% in the considered period. The maximum value of the temperature was reached in 1998 and minimum in 2002. The obtained temperatures agree well with the ones expected in the BLR ($\sim 10^4$ K).

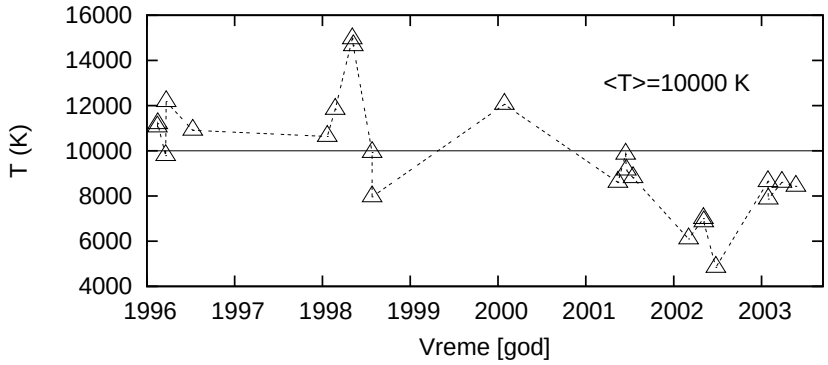

Figure 34: The temperature variation of active galaxy NGC 5548 from 1996 till 2004. The maximum value of the temperature was reached in 1998 when Balmer lines were most intensive.

On the other hand, from the BP fits, we obtained the parameter B. As it can be seen from equations 3.5.3 - 3.5.6 the parameter B depends on the number density of radiating species and the partition function ($B = \log(hcN_0/Z)$). Both values are the same for the Balmer line series at one moment, but they are changing during the time, since we expect that the physical properties in the emitting BLR plasma of NGC 5548 are changing (seen as variability in the broad spectral lines). In principle the partition function depends on the temperature and the level configuration (in our case the partition function Z is summed up to $n = 2$). It is hard to find some real information about variation in the number density in the BLR plasma using the B parameter, but still one can have impression about magnitude of variations of these two quantities. Taking into account equations 3.5.3 - 3.5.6 and also the fact that we normalized Balmer line fluxes to the Hβ flux, we can write $\log(N_0/Z) \sim B_{E_l} + \log(F_{\mathrm{H}\beta})$, where B_{E_l} is intercept corresponding to the energy of the lower level, since Z is given for $n = 2$, $E_l = 10.2$ eV. Using this relation we found the difference between maximal and minimal value of $\log(N_0/Z)$ to be $\Delta \log(N_0/Z) = \log(N_0/Z)_{\max} - \log(N_0/Z)_{\min} \sim 0.9$. This can be expected, e.g. if we roughly approximate that Z stay constant, then maximal variation of number density is $\sim$8 times, this is in an agreement with observed magnitude of variation in spectral lines of NGC 5548 (e.g. the flux of the Hβ was changing $\sim$5 times).

6.2.3 Continuum vs. temperature

Here we start from the fact that the response of the broad lines to continuum variations in NGC 5548 suggests that the BLR is very close to the continuum source (Ferland et al. 1992), or it may even indicate that a part of optical continuum is originating in the BLR as well. We assume that the continuum is

originating in an accretion disk, e.g. Kong et al. (2004) explained the variation in the optical spectral index with the variation in the accretion parameter of the inner part of the disc. On the other hand, the Balmer lines may also be emitted from outer part of the accretion disc (Shapovalova et al. 2004), then the temperature variation measured from BP should be connected with the continuum variation. Therefore, we investigate the continuum intensity as a function of obtained temperatures. In an accretion disk, temperature depends on the radius (see e.g. Shakura & Sunyaev 1973) but if the continuum is emitted mostly from the inner part of the disk and Balmer lines mostly from the outer part, one can approximate that $T_{\rm c}$ correlates with the BLR temperature, i.e. $T_{\rm c} \propto T_{\rm BLR}$.

To find the correlation, we measured the flux in a window from 4240 Å to 4260 Å (rest-frame wavelengths) and calculated the average value for 4250 Å as well as in the spectral range from 5090 Å to 5110 Å (rest-frame wavelengths) with the average value at 5100 Å. In order to have only the AGN-component of the optical continuum, one should subtract the continuum of the host galaxy from the observed continuum of the NGC 5548 nucleus (Popović et al. 2008a).

The total continuum flux ($F_{\rm t}(\lambda)$) emitted at λ can be represented as a sum of the BLR ($F_{\rm BLR}$), central source ($F_{\rm c}(\lambda)$) and stellar continuum ($F_{\rm s}(\lambda)$). As we noted above, the stellar continuum is subtracted therefore the total continuum flux is:

$$F_{\rm t}(\lambda, T) = F_{\rm c}(\lambda, T_{\rm c}) + F_{\rm BLR}(\lambda, T_{\rm BLR}). \tag{7.2.4}$$

Assuming that the optical continuum is originating far enough from the center of an accretion disk, one can use the next relation for the central source of continuum (see Peterson 2004, the equation 4.6 and corresponding discussion):

$$F_{\rm c}(\lambda, T) \sim {\rm const} \times \frac{T_{\rm c}^{8/3}}{\lambda^{1/3}}. \tag{7.2.5}$$

Furthermore, if we neglect the contribution of the BLR continuum, the continuum flux ratio measured at λ_1 and λ_2 is:

$$\frac{F_{\rm t}(\lambda_1, T)}{F_{\rm t}(\lambda_2, T)} \sim (\frac{\lambda_2}{\lambda_1})^{1/3} = {\rm const}. \tag{7.2.6}$$

There is no evidence that the continuum temperature is proportional to the BLR temperature, but one can assume that they are in correlation ($T_{\rm c} \sim T_{\rm BLR}$), therefore we will present the continuum intensity vs. the BLR temperature.

In Figure 35, we present the AGN-component continuum flux variation as a function of the measured temperatures. Figure 35a shows the continuum flux variation at λ4250 Å; Figure 35b shows the continuum flux variation at 5100 Å; Figure 35c shows the variation of the ratio of these two continuum fluxes. As one can see from Figure 35a,b the AGN-component continuum tends to

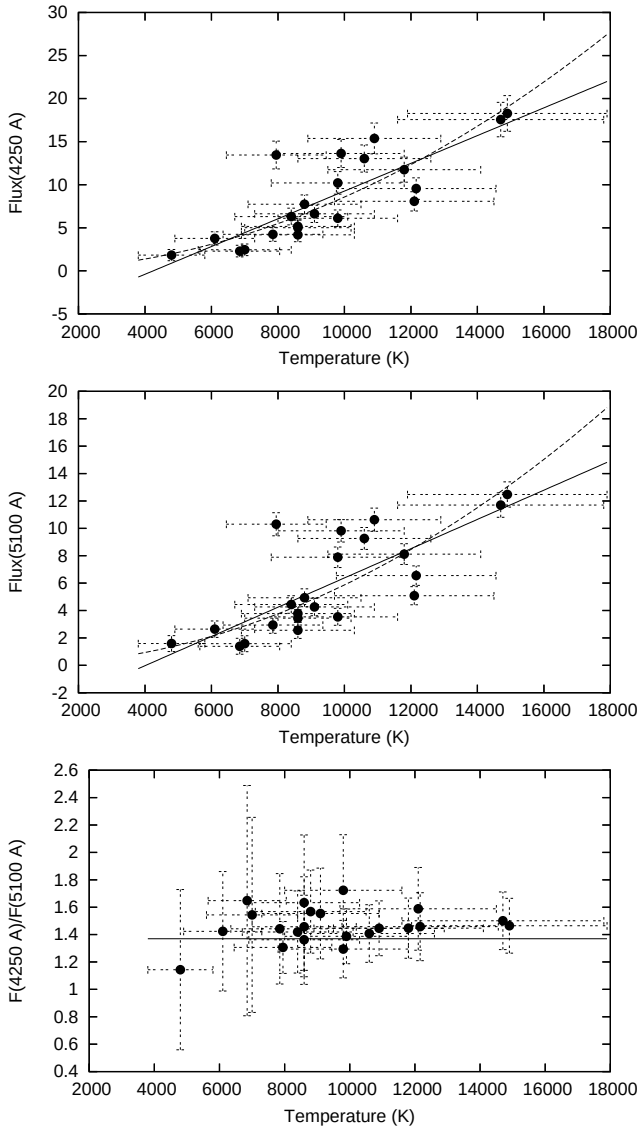

Figure 35: The continuum flux measured at 4250 Å and 5100 Å as a function of the temperature measured with the BP method (first two panels), and the ratio $I_{\rm C}(4250)/I_{\rm C}(5100)$ as a function of the temperature (bottom panel). The measured values are denoted with full circles. The assumed linear function and the function given with the equation 7.2.5 are presented with full and dashed line, respectively (first two panels). In the bottom panel the full line represents the best fit with the equation 7.2.6.

be a linear function of the temperature. We found a high level of correlation between the continuum and temperature variability ($r = 0.85$). Also, we fitted the measured data with the continuum function as given by the equation 7.2.5 and presented it with dashed line in Figure 35a,b, finding that the equation 7.2.5 fits well the observed data. Furthermore, as one can see from Figure 35c the AGN-component continuum intensity ratio at 4250 and 5100 Å follows the expected function given by the equation 7.2.6, i.e. remains constant as a function of the temperature. This also indicates the disk emission. But, here we should note that the temperature measured from the BLR fits very well the physical changes in the continuum.

This can be expected because of the following reason: whether illuminated by a variable hard X-ray source at the center, or by some other mechanisms, the optical/UV continuum varies with the ionizing spectrum. Then, one can observe the continuum becoming "bluer" as it becomes brighter. This is consistent with an increase in the temperature of the thermal accretion disk as the central source (X-rays and the ionizing continuum emitting inner disk) brightens. The obtained high level of correlation between the AGN-component continuum and temperature, as well as of the ratio of the AGN-component continuum at different wavelengths and temperatures, support a dominant emission by an accretion disk in the BLR, as already suggested (Shapovalova et al. 2004). Also, recent investigations of the spectral energy distribution of NGC 5548 done by Gaskell et al. (2007) show that its BLR is not spherical (which is often assumed for the BLR geometry), but has a flatter distribution and spreads until the inner regions of the torus. On the other hand, as it was noted by Ulrich (2000) for the case of NGC 4151 the high correlation between X-ray emission (originated in an accretion disk) and the temperature of the BLR is expected. Here, we showed for the first time that this correlation exist in the optical part of the continuum.

On the other hand, the correlation obtained from our measurements may also be explained by the following: the emitting gas in the BLR becomes hotter when the central source brightness and the flux of incident photons increases. At the same time the sizes of the Strömgren zones increase in depth, increasing the optical depths in the Balmer lines. Their emitting efficiencies thus diminish with increasing incident flux, but the effect on Hα is greater than that on Hβ, which is greater than the effect on Hγ (because Hα optical depth remains greater than Hβ, etc., e.g. Ferland et al. 1979). In this case one can expect that the ratio of Balmer lines fluxes is a function of the continuum ratio measured in the blue and red part of the spectrum. To check it we presented the flux ratios of the continuum measured at 4250Å and 5100 Å as a function of $H\alpha/H\beta$, $H\alpha/H\gamma$ and $H\alpha/H\delta$ flux ratios in Figure 36. As one can see from Figure 36, a slight tendency exists for the line ratios F(Hα)/F(H$_i$), $i = \beta, \gamma, \delta$F(H$\alpha$)/F(Hi), to be smaller when the continuum is bluer, but it

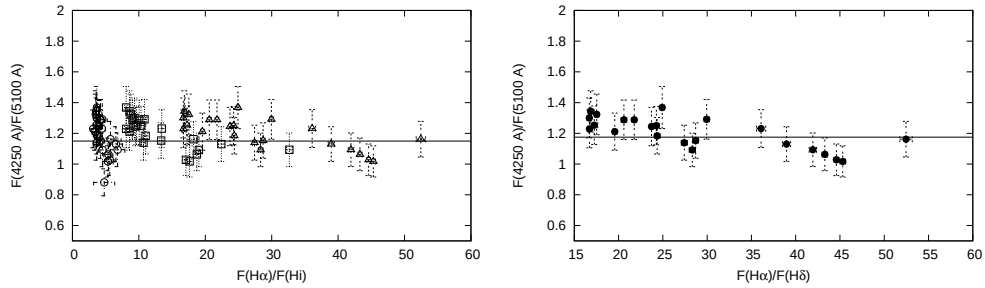

Figure 36: *Left:* The ratio of measured continuum flux as a function of the line flux ratios $H\alpha/H\beta$ (open circles), $H\alpha/H\gamma$ (open triangles), and $H\alpha/H\delta$ (open squares). *Right:* The case for $H\alpha/H\delta$ flux ratio is presented separately.

is a very tiny effect. It indicates that we have the real correlation between the temperature and AGN-component continuum flux, that is presented in Figure 35.

6.2.4 The simulation of the BLR of NGC 5548

We use CLOUDY code to simulate the physical conditions in the BLR of NGC 5548 in order to estimate the BLR average temperature, and then to compare it with the temperature estimated with the BP method. The aim of these numerical simulations is not to find the best fit for the observed data, but rather the physical reason of the variation measured in the BLR temperature. For numerical simulations and comparison with our results, we used independently obtained physical and kinematical parameters taken from Peterson et al. (2002).

The main input parameters of these models are: the radius of the BLR ($R_{\rm BLR}$), the ionizing photons flux ($Q_{\rm h}$), and hydrogen density ($n_{\rm H}$)[28]. The radius of the BLR is taken from reverberation results of Peterson et al. (2002)[29]. For calculations of the ionizing photons flux the optical continuum mean flux F_λ(5100 Å) taken from Peterson et al. (2002) and the correlation between the $Q_{\rm h}$ and the bolometric luminosity $L_{\rm bol}$ (Padovani & Rafanelli 1988) are used, assuming that the bolometric luminosity is $L_{\rm bol} \approx 9 \times \lambda \times L_\lambda$, where λ = 5100 Å (Collin & Hure 2001). Additionally, the mean optical continuum flux is corrected for the host galaxy starlight contribution at λ =5100 Å, $F_{\rm gal} = 3.4{\times}10^{-15}$ergs s^{-1} cm^{-2} (Romanishin et al. 1995). For the calculation of the distance to the galaxy the following cosmological parameters are assumed H_0 = 65 km s^{-1} Mpc^{-1}, Ω_m = 0.3 and Ω_λ = 0.7. For the simulations it is

[28]Definitions of these parameters are given in Appendix A

[29]From the data set, the measurements in the Year 12 (2000) are not consider since the value of the BLR radius was very low.

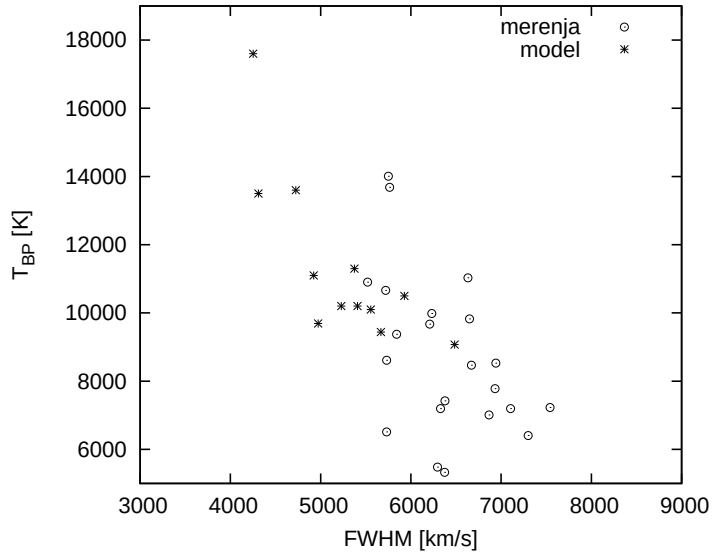

Figure 37: The BLR temperature as a function of the FWHM. The circles represent the measured values presented in section 6.2.1, while the asterisks are the simulated values using the input data of Peterson et al. (2002), where the BP temperature is predicted by CLOUDY and the velocity is calculated with the virial equilibrium assumption.

assumed that all clouds have a single column density $N_{\rm H} = 10^{23}{\rm cm}^{-2}$ (Dumont et al. 1998, Korista & Goad 2000, 2004). In order to calculate the velocity (that is represented with FWHM) the mean value for the mass of the black hole $M_\bullet = 7 \times 10^7 M_\odot$ (Peterson & Wandel 1999) is considered, as well as the assumption that the BLR is in the virial equilibrium. One of the outputs of these numerical simulations is the temperature averaged over the BLR radius $T_{\rm av}$. using this temperature and according to the equation 4.2.2, we calculate the BP temperature $T_{\rm BP}$, and that temperature is used for further analysis.

First, the models were done by fixing the hydrogen density (e.g. $n_{\rm H} = 10^9{\rm cm}^{-3}$) and varying other parameters. But, the temperature variability could not be reproduced only with the variation of the continuum flux. Therefore, further simulations are performed, assuming that the hydrogen density $n_{\rm H}$ varies from $n_{\rm H} = 10^{8.8}{\rm cm}^{-3}$ up to $n_{\rm H} = 10^{10}{\rm cm}^{-3}$, where these values correspond to maximal and minimal continuum flux, respectively.

The results are presented in Figure 37, where the BLR temperature is given as a function of the FWHM. From Figure 37 it is clearly seen that the calculated results follow the trend of the temperatures measured with BP method. However, one should emphasize that small variations in the hydrogen density could cover a wider range in the temperature. The lowest measured temperatures (most of the data below $T = 8000$K) are from the period between

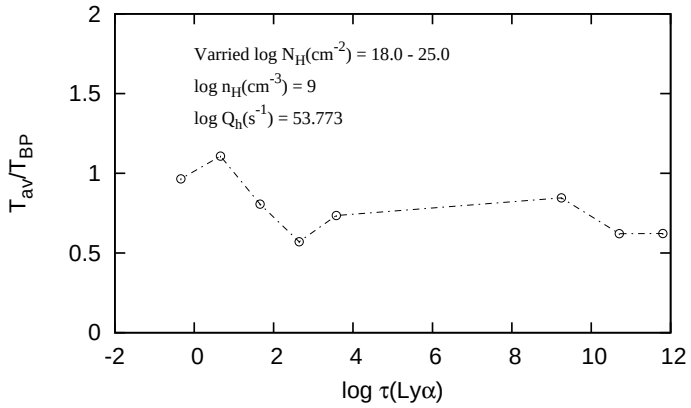

Figure 38: The difference between the mean temperature predicted by the code, T_{av}, and the temperature determined when BP method is applied to the Balmer line ratios predicted by the code T_{BP}, as a function of the Lyα optical depth, for the fixed hydrogen density $n_H = 10^9 cm^{-3}$ and the ionizing photons flux $Q_h \approx 7.8 \times 10^{53} s^{-1}$, where the column density N_H was varied from 10^{18} to $10^{25} cm^{-2}$.

2000 and 2003 for which Peterson et al. (2002) did not make reverberation measurements, hence those data were not attempted to be reproduced with the models.

Also, it is interesting to see how the difference between the mean temperature predicted by the code, T_{av}, and the BP temperature determined from the simulated Balmer line ratios, T_{BP}, is changing with the column density[30]. As can be seen in Figure 38 the ratio of these temperatures is mostly close to unity and does not depend on the Lyα optical depth. Therefore, one can say that the difference between the mean temperature predicted by the CLOUDY and the temperature determined with BP method is not significant, especially for the lowest values of the hydrogen density.

Due to the increase of the hydrogen density, the intensity of the Hα increases with respect to the Hβ line, while other Balmer lines are less influenced, since the collisional processes contribute more to the lower excitation levels. The difference between these two temperatures in case of higher densities could be due to the fact that the line ratios could not be explained only with the photoionization model (Dumont et al. 1998), or it might be that other processes, apart from collisional excitation, contribute to the line formation. In any case, the change in the temperature could be explained with the change of the hydrogen density, but one should be very careful when choosing the input parameters in the simulations. Goad & Koratkar (1998) have shown that changes of the

[30]The column density basically determines the optical depth of the Lyα line, given a fixed hydrogen density.

line fluxes of NGC 5548 is not only the consequence of changes in the ionizing continuum source luminosity, but rather could be due to a change in the spectral energy distribution of the ionizing continuum or physical properties of the BLR gas (Goad & Koratkar 1998). Anyhow, we conclude that the BLR temperature of NGC 5548 estimated with the BP method could be reproduced with the CLOUDY simulations. Finally, the results of the CLOUDY simulations lead to conclusion that the BP method could be used in some cases as a probe for temperature in the BLR (Ilić 2007).

6.3 Physics of the BLR of galaxy NGC 4151

6.3.1 BP coefficients of NGC 4151

Since it has been already shown that the Boltzmann plot method can be applied to one observation of the active galaxy NGC 4151 (Popović 2003), we use here the BP method for every series of measurements. The method is applied on first three lines of the Balmer series and the temperature parameter A is calculated from the equation 3.5.7, and it could give us some indications about the BLR temperature in this galaxy. The temperature parameter A is obtained from the best-fitting of the normalized fluxes (equation 3.5.7), and the error ΔA is the asymptotic standard deviation (within 1σ). The best-fitting results and fluxes of the first three Balmer lines are given in Table 8. In Figure 39 we give the examples of Boltzmann plots for NGC 4151 from different epochs, with different fitting errors p[31], where $p \in [1.4 - 36.5]\%$. It can be clearly seen from Figure 39 that the linear best-fitting of three points is not good enough. On the other hand, Figure 40 represents the variation of the temperature parameter A in the considered period of 11 years, where the average value of the parameter is $A \sim 0.434$, while the dependance of the temperature parameter A from the continuum flux at 5117 Å is given in Figure 41. If we plot the flux ratio of the Balmer lines Hα and Hβ versus the temperature parameter A, we get that all the points are distributed around (where majority is above) the theoretical curve calculated with the assumption that the Saha-Boltzmann distribution is valid for the upper levels in the line transition (section 3.5, Figure 4).

The obtained values for the temperature parameter A are expected for the BLR in general, and Figure 42 show that the Hα/Hβ flux ratio is close to the theoretical predictions if the Saha-Boltzmann distribution is valid, which is one of the requirements for the BP method. However, the errors of the best-fitting are too high, since the linear fitting using the equation 3.5.7 is used for only three Balmer lines (Table 8). Here we use only the first three Balmer lines instead of usual five (e.g. the previous case of active galaxy NGC 5548)

[31]The error is the standard deviation of the least square fitting.

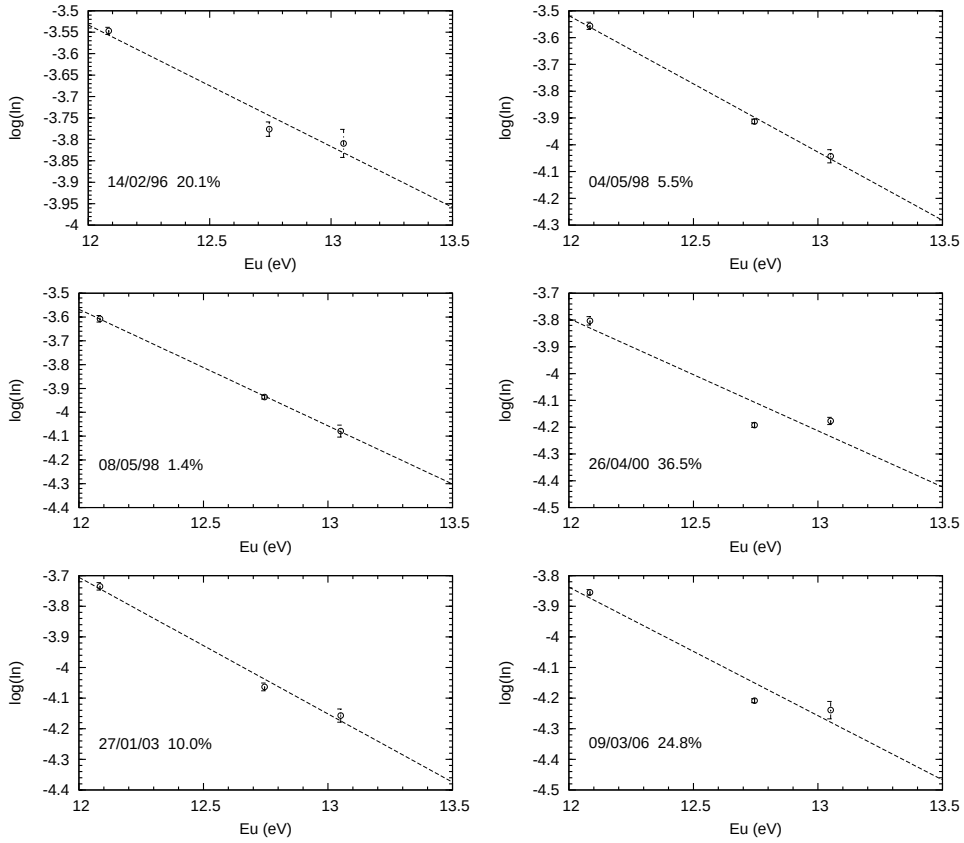

Figure 39: The examples of Boltzmann plots of the Balmer line series of NGC 4151 from different epochs. F_n is calculated using the equation 3.5.7 after the normalization of all Balmer lines to the $H\beta$ flux ($F_{ul}(\mathrm{H}\beta) = 1$).

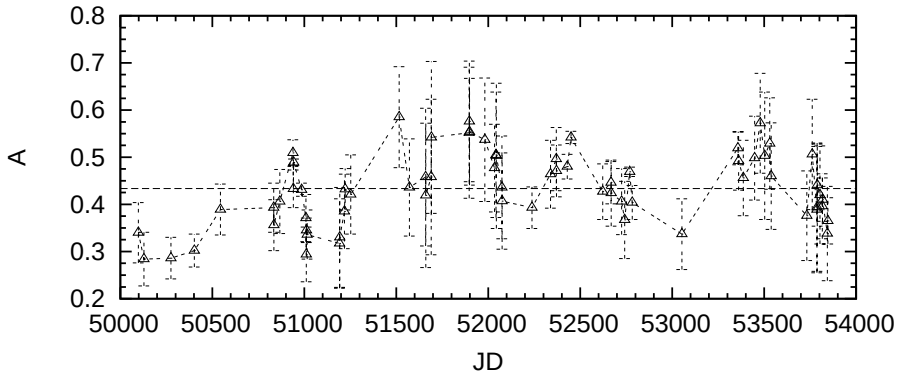

Figure 40: The variation of the temperature parameter A of active galaxy NGC 4151 in the period of 11 years (1996 - 2006).

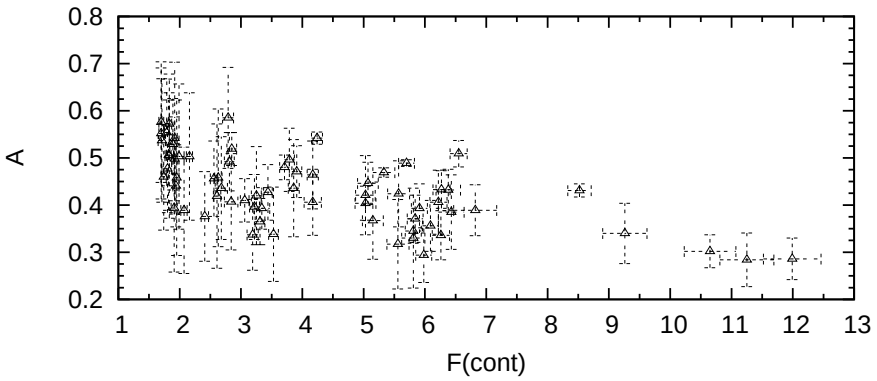

Figure 41: The temperature parameter A as a function of the continuum flux at 5117 Å (given in 10^{-14}erg s^{-1}cm^{-2}) for active galaxy NGC 4151.

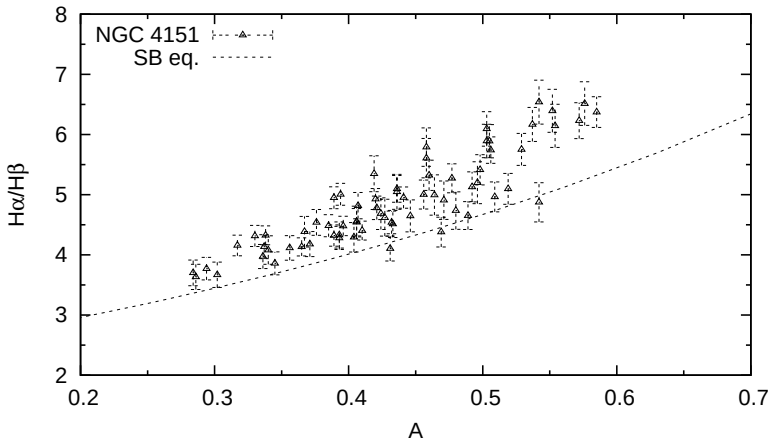

Figure 42: The ratio of Hα/Hβ lines as a function of temperature parameter A for galaxy NGC 4151 observed in the period of 11 years. The dashed line gives this ratio calculated when Saha-Boltzmann distribution is assumed (section 3.5, Figure 4).

and that should significantly decrease the linear fitting error. But here on the contrary we have much higher errors than in the case when five lines are used. This leads to a conclusion that the BP method is not a reliable tool to estimate the BLR temperature and it can not be applied in the case of the AGN NGC 4151. One possible explanation for this could be that the broad line region of NGC 4151 is complex, i.e. there are at least two regions with different physical properties that contributes to the total flux of the Balmer lines.

Table 8: The fluxes of Balmer lines (Hα, Hβ and Hγ) of active galaxy NGC 4151, the temperature parameter A and its error (given in %). The date of observations is given in Julian dates (2400000JD have been subtracted) and the flux is in 10^{-12}erg cm^{-2}s^{-1}. The measured fluxes are taken from Shapovalova et al. (2008).

#	date	$F_{H\alpha}$	$F_{H\beta}$	$F_{H\gamma}$	A	p[%]
1	50097.6	33.41 ± 0.63	8.19 ± 0.32	3.89 ± 0.29	0.340 ± 0.064	18.8
2	50128.0	34.34 ± 0.65	9.28 ± 0.36	4.52 ± 0.34	0.284 ± 0.057	20.1
3	50275.3	35.72 ± 0.68	9.83 ± 0.38	4.65 ± 0.35	0.286 ± 0.044	15.4
4	50402.6	39.95 ± 0.76	10.89 ± 0.42	5.00 ± 0.38	0.302 ± 0.035	11.6
5	50543.6	32.15 ± 0.80	7.44 ± 0.12	3.34 ± 0.20	0.389 ± 0.054	13.9
6	50833.6	31.65 ± 0.98	7.31 ± 0.14	3.26 ± 0.19	0.393 ± 0.052	13.2
7	50834.6	31.03 ± 0.96	7.54 ± 0.14	3.47 ± 0.20	0.356 ± 0.054	15.2
8	50867.4	33.34 ± 1.03	7.34 ± 0.14	3.36 ± 0.20	0.406 ± 0.068	16.8
9	50938.3	33.60 ± 1.04	6.77 ± 0.13	2.64 ± 0.15	0.509 ± 0.028	5.5
10	50940.5	30.78 ± 0.95	6.82 ± 0.13	2.88 ± 0.17	0.433 ± 0.040	9.2
11	50942.5	29.87 ± 0.93	6.42 ± 0.12	2.43 ± 0.14	0.489 ± 0.007	1.4
12	50985.3	34.03 ± 1.05	8.29 ± 0.16	3.12 ± 0.18	0.431 ± 0.014	3.2
13	51008.7	31.09 ± 0.96	7.44 ± 0.14	3.36 ± 0.20	0.371 ± 0.050	13.5
14	51010.7	28.62 ± 0.89	7.59 ± 0.14	3.68 ± 0.21	0.294 ± 0.058	19.7
15	51011.6	28.82 ± 0.89	7.47 ± 0.14	3.26 ± 0.19	0.345 ± 0.026	7.5
16	51015.7	31.15 ± 0.97	7.84 ± 0.15	3.64 ± 0.21	0.336 ± 0.052	15.5
17	51191.9	28.47 ± 0.51	6.85 ± 0.16	3.54 ± 0.20	0.317 ± 0.095	29.9
18	51193.0	28.47 ± 0.51	6.60 ± 0.15	3.46 ± 0.20	0.330 ± 0.106	32.1
19	51218.6	35.24 ± 0.63	7.86 ± 0.18	3.74 ± 0.21	0.385 ± 0.079	20.5
20	51221.7	36.73 ± 0.66	8.09 ± 0.19	3.45 ± 0.20	0.432 ± 0.044	10.2
21	51252.9	29.45 ± 0.53	6.16 ± 0.14	2.89 ± 0.16	0.421 ± 0.084	19.9
22	51515.6	22.94 ± 0.41	3.60 ± 0.08	1.58 ± 0.09	0.585 ± 0.107	18.3
23	51571.9	23.57 ± 0.85	4.67 ± 0.10	2.26 ± 0.06	0.436 ± 0.103	23.6
24	51659.8	20.19 ± 0.73	3.60 ± 0.08	1.88 ± 0.06	0.458 ± 0.146	31.9
25	51660.8	19.04 ± 0.69	3.56 ± 0.07	1.94 ± 0.06	0.419 ± 0.153	36.5
26	51689.7	17.89 ± 0.64	3.09 ± 0.06	1.68 ± 0.05	0.458 ± 0.165	36.0
27	51690.7	19.68 ± 0.71	3.01 ± 0.06	1.53 ± 0.04	0.542 ± 0.161	29.7
28	51895.9	15.92 ± 0.57	2.49 ± 0.05	1.20 ± 0.04	0.552 ± 0.139	25.2
29	51897.0	16.61 ± 0.60	2.55 ± 0.05	1.18 ± 0.03	0.576 ± 0.128	22.2
30	51898.0	16.22 ± 0.58	2.64 ± 0.06	1.20 ± 0.04	0.554 ± 0.113	20.4
31	51981.7	14.31 ± 0.41	2.32 ± 0.04	1.11 ± 0.05	0.537 ± 0.131	24.4
32	52034.6	12.97 ± 0.38	2.46 ± 0.04	1.13 ± 0.05	0.477 ± 0.093	19.5
33	52041.8	13.31 ± 0.39	2.26 ± 0.04	1.11 ± 0.05	0.505 ± 0.133	26.4
34	52043.7	13.71 ± 0.40	2.25 ± 0.04	1.16 ± 0.05	0.503 ± 0.154	30.6
35	52074.7	17.38 ± 0.50	3.41 ± 0.05	1.67 ± 0.07	0.436 ± 0.109	25.0

Table 8: Continued.

#	date	$F_{H\alpha}$	$F_{H\beta}$	$F_{H\gamma}$	A	p[%]
36	52075.7	15.08 ± 0.44	3.13 ± 0.05	1.54 ± 0.06	0.407 ± 0.102	25.1
37	52237.6	21.66 ± 0.63	5.06 ± 0.08	2.22 ± 0.09	0.393 ± 0.044	11.2
38	52338.7	19.93 ± 0.54	3.99 ± 0.16	1.77 ± 0.10	0.464 ± 0.072	15.5
39	52369.7	19.39 ± 0.52	3.73 ± 0.15	1.60 ± 0.09	0.496 ± 0.067	13.5
40	52370.7	19.29 ± 0.52	3.93 ± 0.15	1.67 ± 0.09	0.471 ± 0.055	11.7
41	52429.7	20.55 ± 0.55	4.34 ± 0.17	1.72 ± 0.09	0.480 ± 0.026	5.4
42	52450.4	21.93 ± 0.59	4.50 ± 0.18	1.57 ± 0.09	0.542 ± 0.013	2.4
43	52622.0	19.95 ± 0.54	4.32 ± 0.17	1.91 ± 0.10	0.427 ± 0.059	13.8
44	52666.9	22.26 ± 0.62	4.79 ± 0.14	2.03 ± 0.10	0.446 ± 0.045	10.1
45	52667.9	23.24 ± 0.65	4.96 ± 0.14	2.25 ± 0.11	0.424 ± 0.070	16.5
46	52724.8	22.59 ± 0.63	4.96 ± 0.14	2.28 ± 0.11	0.406 ± 0.070	17.3
47	52741.8	23.50 ± 0.66	5.36 ± 0.16	2.60 ± 0.12	0.367 ± 0.082	22.3
48	52769.3	24.39 ± 0.68	5.57 ± 0.16	2.06 ± 0.10	0.469 ± 0.010	2.1
49	52782.7	24.98 ± 0.70	5.82 ± 0.17	2.49 ± 0.12	0.404 ± 0.036	8.9
50	53053.0	20.35 ± 0.53	4.92 ± 0.11	2.40 ± 0.09	0.337 ± 0.075	22.3
51	53357.6	18.91 ± 0.49	3.71 ± 0.09	1.46 ± 0.06	0.519 ± 0.035	6.7
52	53361.5	17.85 ± 0.46	3.48 ± 0.08	1.48 ± 0.06	0.492 ± 0.062	12.6
53	53386.9	19.21 ± 0.52	3.84 ± 0.08	1.74 ± 0.06	0.456 ± 0.080	17.5
54	53447.8	16.62 ± 0.45	3.07 ± 0.06	1.38 ± 0.04	0.498 ± 0.089	17.9
55	53478.7	15.08 ± 0.41	2.42 ± 0.05	1.07 ± 0.04	0.572 ± 0.106	18.5
56	53503.3	14.79 ± 0.40	2.51 ± 0.05	1.24 ± 0.04	0.503 ± 0.135	26.9
57	53530.7	15.07 ± 0.41	2.62 ± 0.05	1.17 ± 0.04	0.529 ± 0.097	18.3
58	53538.3	13.25 ± 0.36	2.49 ± 0.05	1.21 ± 0.04	0.460 ± 0.113	24.6
59	53732.0	15.84 ± 0.43	3.49 ± 0.07	1.73 ± 0.06	0.376 ± 0.095	25.3
60	53761.5	16.59 ± 0.35	2.89 ± 0.05	1.37 ± 0.09	0.506 ± 0.117	23.1
61	53786.9	15.64 ± 0.33	3.16 ± 0.05	1.69 ± 0.11	0.389 ± 0.134	34.5
62	53787.5	16.57 ± 0.35	3.31 ± 0.05	1.77 ± 0.12	0.394 ± 0.136	34.5
63	53788.5	16.39 ± 0.34	3.31 ± 0.05	1.54 ± 0.10	0.441 ± 0.087	19.7
64	53803.8	16.90 ± 0.35	3.43 ± 0.05	1.68 ± 0.11	0.420 ± 0.104	24.8
65	53816.4	17.83 ± 0.37	3.98 ± 0.06	1.84 ± 0.12	0.396 ± 0.069	17.4
66	53817.4	17.79 ± 0.37	4.04 ± 0.06	1.76 ± 0.12	0.410 ± 0.046	11.2
67	53843.7	19.68 ± 0.41	4.55 ± 0.07	2.34 ± 0.15	0.338 ± 0.100	29.5
68	53846.4	19.01 ± 0.40	4.60 ± 0.07	2.08 ± 0.14	0.365 ± 0.049	13.4

7 Conclusions

The physical conditions of the broad line region of active galactic nuclei were studied and some methods for rough estimates a of the physical parameters were presented. Combining the results of the numerical simulations of the BLR using CLOUDY (numerical code for the simulation of the outcoming spectrum of the photoionized gas) and observed spectral properties of some AGN, we propose a simple and straightforward tool that could be used to estimate the physical parameters (temperature and density) of the BLR, using the observed hydrogen and helium lines. In this research we use the observations of active galaxies NGC 5548 and NGC 4151 obtained with the 6 m SAO telescope in Russia and 2.1 m INAOE telescope in Mexico, as well as the sample of 20 AGN taken from the SDSS spectral database. The most important results of this thesis are:

(i) using CLOUDY program to simulate the physical conditions of the plasma in the BLR of AGN, we showed that for some hydrogen densities $n_{\rm H}$ and ionizing photon flux $\Phi_{\rm H}$, the fluxes of Balmer lines can be fitted with the Boltzmann plot (BP) with the error less than 10% (Figure 6 - 8);

(ii) analyzing simulation results with the BP fitting error less than 10%, we concluded that the Balmer lines and the ratio of the helium lines R = F(He II λ4686)/F(He I λ5876) could be used to probe the physical properties of the BLR, i.e. temperature and hydrogen gas density, that is applied for the first time in this research;

(iii) the proposed method (section 4.2.3), as well as the method given by Laor (2006) are the only method for direct estimation of thermodynamical parameters in the BLR from the broad emission lines, that are avoiding complex numerical simulations;

(iv) the presented method was applied to the sample of 20 active galaxies taken from the SDSS database. The estimated BLR temperature is in the range $T_{\rm BLR} = 4000 - 18000$ K and the hydrogen density is $n_{\rm H} = 10^{8.6} - 10^{11.5}$ cm^{-3}. These results are in an agreement with the previous estimates of the physical conditions in the BLR (see e.g. Osterbrock & Ferland 2006);

(v) the BP method was applied on the broad component of the Balmer lines of the variable active galaxy NGC 5548 observed in the period from 1996 to 2004, and it was shown that the BP method can be applied for the BLR of this galaxy, i.e. the population of the upper energy levels ($n > 2$) of hydrogen follow the Saha-Boltzmann distribution;

(vi) the BLR temperature of NGC 5548 was changing from 5000 K (in 2002) to 15000 K (in 1998) in the period of 8 years. The average temperature is 10000 K, that is the expected vale for the BLR, while the maximal BLR temperature was when the Balmer lines were the most intensive. We showed that there is a high level of correlation ($r = 0.85$) between the change of the AGN optical continuum flux and the BLR temperature. This is the first time that such a correlation was shown to exist, and it could indicate the presence of the accretion disk in the BLR of NGC 5548, that was also suggested before (Shapovalova et al. 2004);

(vii) we simulated the physical conditions of the plasma in the BLR of active galaxy NGC 5548 with CLOUDY code for different epochs, and we showed that the BLR temperature estimated with the BP method could be reproduced with the numerical simulations, and we showed that the change in the BLR temperature could be the result of the hydrogen density variations;

(viii) the BP method was also applied on the broad component of the Balmer lines of the variable active galaxy NGC 4151 observed in the period 1996 - 2006. We showed that in the case of NGC 4151, the BP method cannot be properly used for the BLR temperature diagnostics. One possible explanation for this could be that two different regions with different physical properties contribute to the total flux of Balmer lines in the case of NGC 4151.

This kind of tool for temperature and hydrogen density estimates in the BLR of AGN, that is based on the observed broad Balmer line series and helium lines, is given for the first time in this work. We hope that we gave a contribution to better understanding of the physical processes inside this region and to the general structure of AGN. In the future work, we should study more the heating mechanisms (i.e. ionization) of the BLR, as well as the connection of the physical properties and the kinematics and geometry of the BLR. Moreover, we should give more attention to the connection between the optical emission of the BLR and emissions in other spectral bands, e.g. in X-ray or radio band.

8 References

[1] Agekyan, T.A. 1972, Osnovi teorii oshibok, Nauka, Moscow

[2] Baldwin, J. A., Ferland, G. J., Korista, K. T., Carswell, R. F., Hamann, F., Phillips, M. M., Verner, D., Wilkes, B. J., Williams, R. E., 1996, ApJ, 461, 664

[3] Baldwin, J. A., Ferland, G. J., Korista, K. T., Hamann, F., LaCluyzé, A., 2004, ApJ, 615, 610

[4] Baldwin, J. A., Ferland, G. J., Korista, K. T., Verner, D. A., 1995, ApJL, 455, 119

[5] Baldwin, J. A., Ferland, G. J., Martin, P. G., Corbin, M., Cota, S., Peterson, B. M., Slettebak, A., 1991, ApJ, 374, 580

[6] Bentz, M. C., Denney, K. D., Cackett, E. M., Dietrich, M., Fogel, J. K. J. et al., 2007a, ApJ, 662, 205

[7] Bentz, M. C., Denney, K. D., Peterson, B. M., Pogge, R. W., 2007b, in The Central Engine of Active Galactic Nuclei, ASP Conference Series, eds. L. C. Ho and J.-M. Wang, 373, 380

[8] Bentz, M. C., Peterson, B. M., Pogge, R. W., Vestergaard, M., Onken, C. A., 2006, ApJ, 644, 133

[9] Bevington, P. R., Robinson, D. K., 2003, Data reduction and error analysis for the physical sciences, 3rd ed., Boston, MA: McGraw-Hill

[10] Binette, L., Dopita, M., Tuohy, I. R., 1985, ApJ, 297, 476

[11] Binette, L., Wang, J., Villar-Martin, M., Martin, P. G., Magris, C. G., 1993a, ApJ, 414, 535

[12] Binette, L., Wang, J., Zuo, L., Magris, C. G., 1993b, AJ, 105, 797

[13] Binney, J., Merrifield, M., 1998, Galactic Astronomy, Princeton: Princeton Univ. Press

[14] Blandford, R. D., McKee, C. F., 1982, ApJ, 255, 419

[15] **Bon, E., Popović, L. Č., Ilić, D., 2006, New Astronomy Rev.,50, 716**

[16] Brotherton, M. S., Wills, B. J., Steidel, R., Sargent, W. L. W., 1994, ApJ, 423, 131

[17] Bruhweiler, F., Verner, E.,2008, ApJ, 675, 83

[18] Burstein, D., Heiles, C., 1982, AJ, 87, 1165

[19] Casebeer, D. A., Leighly, K. M., Baron, E., 2006, ApJ, 637, 157

[20] Chen, K., Halpern, J. P., 1989, ApJ, 344, 115

[21] Chen, K., Halpern, J. P., Filippenko, A. V., 1989, ApJ, 339, 742

[22] Clavel, J., Boksenberg, A., Bromage, G. E., Elvius, A., Penston, M. V., Perola, G. C., Santos-Lleo, M., Snijders, M. A. J., Ulrich, M. H, 1990, MNRAS, 246, 668

[23] Collin-Souffrin S., 1986, A&A, 166, 115

[24] Collin, S., Hure, J.-M., 2001, A&A, 372, 50

[25] Crenshaw, D. M., Kraemer, S. B., 2001, ApJ, 562, 29

[26] Crenshaw, D. M., Kraemer, S. B., Bruhweiler, F. C., Ruiz, J. R., 2001, ApJ, 555, 633

[27] Crenshaw, D. M., Kraemer, S. B., Gabel, J. R., Schmitt, H. R., Filippenko, A. V., Ho, L. C., Shields, J. C., Turner, T. J., 2004, ApJ, 612, 152

[28] Crenshaw, D. M., Kraemer, S. B., Turner, T. J., Collier, S., Peterson, B. M. et al. 2002, ApJ, 566, 187

[29] Dumont, A-M., Collin-Souffrin, S., Nazarova, L., 1998, A&A, 331, 11

[30] Dopita, M. A., Sutherland, R. S., 2003, Astrophysics of the Diffuse Universe, Springer Berlin Heidelberg

[31] Eracleous, M., Halpern, J. P., 1994, ApJS, 90, 1

[32] Eracleous, M., Halpern, J. P., 2003, ApJ, 599, 886

[33] Eracleous, M., Halpern, J. P., 2004, ApJS, 150, 181

[34] Fanaroff, B. L., Riley, J. M., 1974, MNRAS, 167, 31

[35] Ferland, G. J., 1999, in Quasars and Cosmology, ASP Conference Series, eds. G. Ferland and J. Baldwin, 162, 147

[36] Ferland, G. J., 2003, ARA&A, 41, 517

[37] Ferland, G. J., 2006, Hazy, A Brief Introduction to Cloudy 06.02, University of Kentucky Internal Report

[38] Ferland, G. J., Korista, K. T., Verner, D. A., Ferguson, J. W., Kingdon, J. B., Verner, E. M., 1998, PASP, 110, 761

[39] Ferland, G. J., Netzer, H., 1979, ApJ, 229, 274

[40] Ferland, G. J., Netzer, H., Shields G. A., 1979, ApJ, 232, 382

[41] Ferland, G. J., Persson, S. E., 1989, ApJ, 347, 656

[42] Ferland, G. J., Peterson, B. M., Horne, K., Welsh, W. F., Nahar, S. N., 1992, ApJ, 387, 95

[43] Gabel, J. R., Kraemer, S. B., Crenshaw, D. M., George, I. M., Brandt, W. N. et al., 2005, ApJ, 631, 741

[44] Gaskell, C. M., 1988, in Active Galactic Nuclei , ed. H.R. Miller & P.J. Wiita (Berlin:Springer), 61

[45] Gaskell, C. M., 1996, ApJL, 464, 107

[46] Gaskell, C. M., Klimek, E. S., Nazarova, L. S., 2007, sent to ApJ, astro-ph/0711.1025

[47] Goad, M. R., Koratkar, A. P., 1998, ApJ, 495, 718

[48] Goad, M. R., O'Brien, P. T., Gondhalekar, P. M., 1993, MNRAS, 263, 149

[49] Goad, M. R., Wanders, I., 1996, ApJ, 469, 113

[50] Griem, H. R., 1997, Principles of plasma spectroscopy, Cambridge: Cambridge University Press

[51] Gruenwald, R. B., Viegas, S., 1992, ApJS, 78, 153

[52] Hutchings, J. B., Crenshaw, D. M., Kaiser, M. E., Kraemer, S. B., Weistrop, D., Baum, S., Bowers, C. W., Feinberg, L. D., Green, R. F., Gull, T. R., Hartig, G. F., Hill, G., Lindler, D. J., 1998, ApJL, 492, 115

[53] **Ilić, D., 2005, Magistarska teza "Kinematičke i fizičke osobine emisionih oblasti aktivne galaksije Mrk 817"**

[54] **Ilić, D., 2006, Aktivna galaktička jezgra: primer galaksije Mrk 817, Beograd: Zadužbina Andrejević, 79 str, ISSN 1450 - 653X, 173, ISBN 86 - 7244 - 560 - 0**

[55] **Ilić, D., 2007, Serb. Astron. J., 175, 15**

[56] **Ilić, D., La Mura, G., Popović, L. Č., Shapovalova, A. I., Ciroi, S., Chavushyan, V. H., Rafanelli, P., Burenkov, A. N., Mercado, A., 2006, IAUS, 238, 383.**

[57] **Ilić, D., Popović, L. Č., Bon, E., Mediavilla, E., Chavushyan, V. H., 2006, MNRAS, 371, 1610**

[58] **Ilić, D., Popović, L. Č., Ciroi, S., La Mura, G, Rafanelli, P., 2008a, in preparation**

[59] **Ilić, D., Popović, L. Č., Ciroi, S., Rafanelli, P., 2008b, Rev Mex AA - Conf. Ser., 32, 102**

[60] Kaiser, M. E., Bradley, L. D. II, Hutchings, J. B., Crenshaw, D. M., Gull, T. R., Kraemer, S. B., Nelson, C. H., Ruiz, J., Weistrop, D., 2000, ApJ, 528, 260

[61] Kallman, T. R., McCray, R., 1982, ApJS, 50, 263

[62] Kaspi, S., 2007, ASPC, 373, 13

[63] Kaspi, S., Maoz, D., Netzer, H. et al. 1996, ApJ, 470, 336

[64] Kaspi, S., Maoz, D., Netzer, H., Peterson, B. M., Vestergaard, M., Jannuzi, B. T., 2005, ApJ, 629, 61

[65] Kaspi, S., Smith, P. S., Netzer, H., Maoz, D., Jannuzi, B. T., Giveon, U., 2000, ApJ, 533, 631

[66] Kollatschny, W., 2003, A&A, 407, 461

[67] Kollatschny, W., Bischoff, K., Robinson, E. L., Welsh, W. F., Hill, G. J., 2001, A&A, 379, 125

[68] Kong, M.-Z., Wu, X.-B., Han, J.-L, Mao, Y.-F., 2004, CJA&A, 4, 518

[69] Konjević, N., 1999, Phys. Rev., 316, 339

[70] Korista, K. T., Goad, M. R., 2000, ApJ, 536, 284

[71] Korista, K. T., Goad, M. R., 2004, ApJ, 606, 749

[72] Krolik, J. H., 1999, Active Galactic Nuclei: From the Central Black Hole to the Galactic Environment, Princeton University Press, Princeton, New Jersey

[73] Krolik, J. H., Horne, K., Kallman, T. R., Malkan, M. A., Edelson, R. A., Kriss, G. A., 1991, ApJ, 371, 541

[74] Kwan, J., 1984, ApJ, 283, 70

[75] Kwan, J., Krolik, J., 1981, ApJ, 250, 478

[76] **La Mura, G., Popović, L. Č., Ciroi, S., Rafanelli, P., Ilić, D., 2007a, AIPC, 938, 82**

[77] **La Mura, G., Popović, L. Č., Ciroi, S., Rafanelli, P., Ilić, D., 2007b, ApJ, 671, 104**

[78] Laor, A., 2006, ApJ, 643, 112

[79] Lyuty, V. M., 2005 Pis'ma in Astronom. Zhurnal 31, 723 (rus)

[80] Maoz, D., Netzer, H., Mazeh, T., Beck, S., Almoznino, E., Leibowitz, E., Brosch, N., Mendelson, H., Laor, A., 1991, ApJ, 367, 493

[81] Marziani, P., Sulentic, J. W., Dultzin-Hacyan, D., Calvani, M., Moles, M., 1996, ApJS, 104, 37

[82] McGill, K. L., Woo, J., Treu, T., Malkan, M. A., 2008, ApJ, 673, 703

[83] Metzroth, K. G., Onken, C. A., Peterson, B. M., 2006, ApJ, 647, 901

[84] Mundell, C. G., Wrobel, J. M., Pedlar, A., Gallimore, J. F., 2003, ApJ, 583, 192

[85] Murray, N., Chiang, G., 1997, ApJ, 474, 91

[86] Nahar,S. N., Pradhan, A. K., 1997, ApJS, 111, 339

[87] Netzer, H., 1975, MNRAS, 171, 395

[88] Netzer, H., 1985, ApJ, 289, 451

[89] Netzer, H., 1993, ApJ, 411, 594

[90] Netzer, H., Brotherton, M. S., Wills, B. J., Han, M., Wills, D., Baldwin, J. A., Ferland, G. J., Browne, I. W. A., 1995, ApJ, 448, 27

[91] Netzer, H., Ferland, G. J., 1984, PASP, 96, 593

[92] Netzer, H., Maoz, D., 1990, ApJL, 365, 5

[93] Netzer, H., Maoz, D., Laor, A., Mendelson, H., Brosch, N., Leibowitz, E., Almoznino, E., Beck, S., Mazeh, T., 1990, ApJ, 353, 108

[94] Netzer, H., Peterson, B. M., 1997, Astronomical Time Series, ed. D. Maoz, A. Sternberg, E. M. Leibowitz (Dordrecht: Kluwer), 85

[95] O'Brien, P. T., Goad, M. R., Gondhalekar, P. M., 1994, MNRAS, 268, 845

[96] Osterbrock, D. E., 1989, Astrophysics of Gaseous Nebulae and Active Galactic Nuclei, University Science Books, Sausalito, California

[97] Osterbrock, D. E., Ferland, G. J., 2006, Astrophysics of Gaseous Nebulae and Active Galactic Nuclei (2nd ed.), University Science Books, Sausalito, California

[98] Padovani, P., Rafanelli, P., 1988, A&A, 205, 53

[99] Peterson, B. M., 1993, PASP, 105, 207

[100] Peterson, B. M., 1988, PASP, 100, 18

[101] Peterson, B. M., 2004, An Introduction to Active Galactic Nuclei, Cambridge University Press

[102] Peterson, B. M., Bentz, M. C., Desroches, L.-B., Filippenko, A. V., Ho, L. C., Kaspi, S., Laor, A., Maoz, D., Moran, E. C., Pogge, R. W., Quillen, A. C., 2005, ApJ, 632, 799

[103] Peterson, B. M., Berlind, P., Bertram, R., Bischoff, K., Bochkarev, N. G. et al., 2002, ApJ, 581, 197

[104] Peterson, B. M., Ferrarese, L., Gilbert, K. M., Kaspi, S., Malkan, M. A., Maoz, D., Merritt, D., Netzer, H., Onken, C. A., Pogge, R. W., Vestergaard, M., Wandel, A., 2004, ApJ, 613, 682

[105] Peterson, B. M., Wandel, A., 1999, ApJ, 521, 95

[106] Petitjean, P., Boisson, C., Péqugnot, D., 1990, A&A, 240, 433

[107] Popović, L. Č., 2003, ApJ, 599, 140

[108] Popović, L. Č., 2006a, ApJ, 650, 1217 (an Erratum)

[109] Popović, L. Č., 2006b, Serb. Astron. J., 173, 1

[110] Popović, L. Č. et al. 2008b, in preparation

[111] **Popović, L. Č., Mediavilla, E. G., Bon, E., Ilić, D., 2004, A&A, 423, 909**

[112] Popović, L. Č., Mediavlilla, E. G., Bon, E., Stanić, N., Kubičela, A., 2003, ApJ, 599, 185

[113] Popović, L. Č., Mediavlilla, E. G., Kubičela, A., Jovanović, P. 2002, A&A, 390, 473

[114] Popović, L. Č., Stanić, N., Kubičela, A., Bon, E., 2001, A&A, 367, 780

[115] **Popović, L. Č., Shapovalova, A. I., Chavushyan, V. H., Ilić, D., Burenkov, A. N., Mercado, A., Ciroi, S., Bochkarev, N. G., 2008a, PASJ, 60, 1**

[116] Popović, L. Č., Vince, I., Atanacković-Vukmanović, O., Kubičela, A., 1995, A&A, 293, 309

[117] Rees, M., Netzer, H., Ferland, G. J., 1989, ApJ, 347, 640

[118] Romanishin, W., Balonek, T. J., Ciardullo, R., Miller, H. R., Peterson, B. M., Sadun, A. C., Stirpe, G. M., Takagishi, K., Taylor, B. W., Zitelli, V., 1995, ApJ, 455, 516

[119] Sergeev, S. G., Pronik, V. I., Sergeeva, E.A. 2001, ApJ, 554, 245

[120] Sergeev, S. G., Doroshenko, V. T., Dzyuba, S. A., Peterson, B. M., Pogge, R. W., Pronik, V. I., 2007, ApJ, 668, 708

[121] Seyfert, C. K., 1943, ApJ, 97, 28

[122] Shakura N. I., Sunyaev R. A., 1973, A&A, 24, 337

[123] Shapovalova, A. I., Burenkov, A. N., Bochkarev, N. G., 1996, Bull. Spec. Astrophys. Obs., 41, 28

[124] Shapovalova, A. I., Doroshenko, V. T., Bochkarev, N. G., Burenkov, A. N., Carrasco, L. et al., 2004, A&A, 422, 925

[125] Shapovalova, A. I., Popović, L. Č., Collin, S., Burenkov, A. N., Chavushyan, V. H. et al., 2008, A&A, 486, 99

[126] Shields, J. C., Freland, G. J., 1993, ApJ, 402, 425

[127] Schlegel, D. J., Finkbeiner, D. P., Davis, M., 1998, ApJ, 500, 525

[128] Stirpe, G. M., 1990, A&AS, 85, 1049

[129] Stirpe, G. M., 1991, A&A, 247, 3

[130] Strateva, I. V., Strauss, M. A., Hao, L., Schlegel, D. J., Hall, P. B. et al., 2003, AJ, 126, 1720

[131] Sulentic, J. W., Marziani, P., Dultzin-Hacyan, D., 2000, ARA&A, 38, 521

[132] Sutherland, R., Dopita, M., 1993, ApJS, 88, 253

[133] Ulrich M.-H., 2000, A&AR, 10, 135

[134] Ulrich, M.-H. & Horne, K., 1996, MNRAS, 283, 748

[135] Ulvestad, J. S., Wong, D. S., Taylor, G. B., Gallimore, J. F., Mundell, C. G., 2005, AJ, 130, 936.

[136] Vanden Berk, D. E., Richards, G. T., Bauer, A., Strauss, M. A., Schneider, D. P. et al., 2001, AJ, 122, 549

[137] Vestergaard, M., Peterson, B. M., 2005, ApJ, 625, 688

[138] Viegas, S., Contini M., 1994, ApJ, 428, 113

[139] Vlasyuk ,V. V., 1993, Bull. Spec. Astrophys. Ops., 36, 107

[140] Wandel, A., Peterson, B. M., Malkan, M. A., 1999, ApJ, 526, 579

[141] Zheng, W., Binette, L., Sulentic, J. W., 1990, ApJ, 365, 115

9 Appendix A - *CLOUDY*

The numerical code CLOUDY for spectral simulations make it possible to understand complex physical environments starting from first principles (Ferland et al. 1998). The program iteratively determines the physical conditions (temperature, level of ionization, and chemical state) within a non-equilibrium gas, possibly exposed to an external source of radiation (as is the case for e.g. H II regions or AGN), and predicts the resulting spectrum. One such spectrum is presented in Figure 43, that is calculated for the conditions in the Orion nebulae. The code CLOUDY is open source and is freely available on internet, and team of scientists is constantly work on its improvement and development.

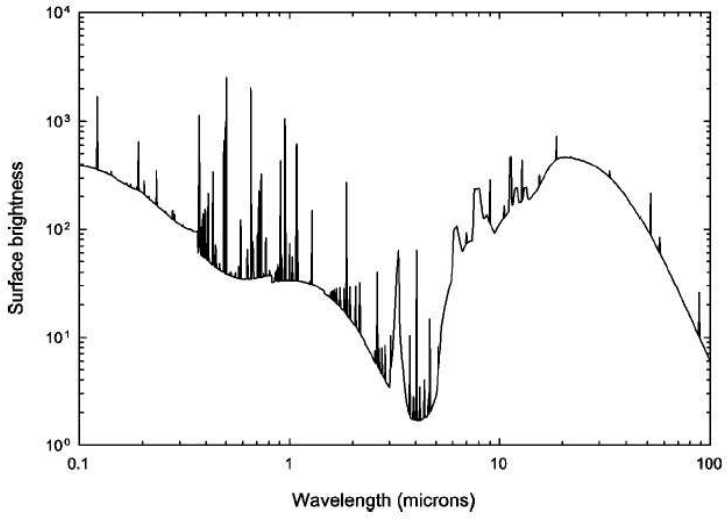

Figure 43: An example of the predicted spectrum of the Orion nebulae obtained with CLOUDY (Ferland 2003).

9.1 Creation and developments of the CLOUDY program

The spectral synthesis CLOUDY code for was designed and developed by Ferland et al. (1998). It was originally written in FORTRAN but latest versions are rewritten for C and C++. The code was born in 1978 and its original purpose was to simulate emission-line regions of Active Nuclei, a major research emphasis at the time, but it has until now significantly developed and expanded in various fields. For example, the size of the code (i.e. the number of lines

in the code) grows roughly 7% per year. The version C07.02.01 was the latest version when this work was done, and was released in July 2007. The code was then completely rewritten in C++, which made it roughly 30% faster. With every new version, the code fidelity improves, new commands are added, and atomic and molecular rate coefficients become better as theory and experiment makes progress. Beside Gary J. Ferland, scientists that contributed the most to the code development are: Peter G. Martin, Hagai Netzer, Peter van Hoof, Peter Martin, and Joe Weingartner.

9.2 Basic assumptions used in the program

The program CLOUDY computes the non-equilibrium ionization, thermal, and chemical state of a cloud that may (or may not) be exposed to an external radiation field. The usual assumption is that atomic processes have had time to reach steady state, so the density of a species or level i is given by a balance equation of the following form:

$$\frac{\partial n_i}{\partial t} = \sum_{(j \neq i)} n_j R_{ji} + S - n_i \left(\sum_{(j \neq i)} R_{ij} + L \right) = 0 \ [\mathrm{cm^{-3}s^{-1}}]. \qquad (9.1.1)$$

Here R_{ji} represents the rate $[\mathrm{s^{-1}}]$ that a species j goes to i, S is the rate per unit volume $[\mathrm{cm^{-3}s^{-1}}]$ that new atoms appear in i, a L is the rate $[\mathrm{s^{-1}}]$ they are lost. This equation, together with equations representing conservation of energy and charge, fully specify the problem, that CLOUDY solves in an iterative process. The code is designed to work in 1D geometry and in most simulations the geometry is assumed to be static. All processes of line transfer are described using the escape probabilities.

One powerful asset of this photoionization code is the large number of observables resulting from only a few input parameters. For some parameters the standard values are given in the code, but often the goal is to determine these free parameters from observations. Starting from the input parameters and solving the equations of statistical equilibrium, charge conservation, and conservation of energy, the code determines the level of ionization, the particle density, the gas kinetic temperature, the chemical state and the populations of levels within atoms in a cloud, and then predicts its spectrum (intensities of many millions of spectral lines are predicted by CLOUDY, practically there is no upper limit). All of this is done self-consistently, with the minimum number of free parameters, that are: a) the shape and intensity of the external radiation field striking a cloud (referred to as the incident continuum), b) the chemical composition and grain content of the gas, and c) the geometry of the gas, including its radial extent and the dependence of density on radius.

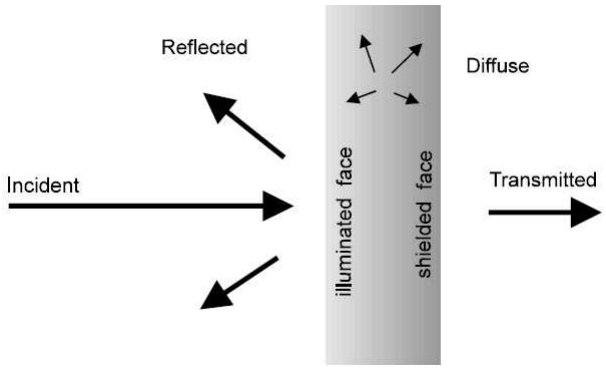

Figure 44: This figure illustrates the possible geometry of the cloud and several of the continua that enter in the calculations.

9.2.1 Continuum

Both the shape and intensity of the external continuum striking the cloud must be specified in the input file. Often this is the region's only source of heat and ionization. Different commands are usually used to specify the continuum shape and intensity, although a few commands specify both. A physically motivated continuum spanning the full energy range should be specified, if possible. The continuum can be specified as a fundamental form (such as blackbody emission, optically thin bremsstrahlung emission, or a power law with optional exponential cutoff), interpolated from tables of points, or as the radiation field transmitted through a cloud, as predicted by previous calculations. Additionally, a set of built-in continua can be specified as look-up tables, e.g. emergent continua from many model atmospheres, the observed Crab Nebula continuum, or several typical AGN continua (e.g. command for the table of the standard AGN continuum is `table AGN`).

The intensity of the external continuum can be given either as a flux (energy or photon) per unit surface area of cloud or as luminosity (energy or photon) radiated by the central object into 4π sr. These can be set by specifying the flux of photons, a flux density, or luminosity, at arbitrary energies, or by giving the absolute visual or bolometric magnitude of the continuum source. The code must be able to derive the flux of photons [cm^{-2} s^{-1}] striking the illuminated face of the cloud, therefore if the continuum is specified as luminosity of the central source then the inner radius of the cloud must be given (if the inner radius is not specified then a plane parallel geometry will be assumed, and it is simulated as a sphere with an inner radius of 10^{30} cm).

9.2.2 Geometry of the gas cloud

The geometry is always 1D spherical, but can be made effectively plane parallel by making the inner radius much larger than the thickness of the cloud. The default is for the gas to have constant density and to fully fill its volume, but other pressure laws and models with only part of the volume filled can be computed as well. The side of the cloud facing the source of ionizing radiation is the *illuminated face* of the cloud. The opposite side, in shadow, is referred to as the *shielded face* of the cloud. The illuminated face is generally hotter and more highly ionized than the shielded face.

CLOUDY normally assumes an open geometry, or one in which the gas has a very small covering factor. This can be changed if setting the covering factor to a large enough value for continuous radiation escaping the cloud in the direction towards the central object to always interact with gas on the other side (a closed geometry).

The code works by dividing a nebula into a set of thin concentric shells, referred to as zones. The zones are chosen to have thicknesses that are small enough for the physical conditions to be nearly constant within. Typically ∼100 to 200 zones are computed in an optically thick model of an H II region. The physical conditions in the first and last zones are always printed and intermediate zones may be printed if needed.

9.2.3 Chemical composition

As for the chemical composition, the program considers the lightest 30 elements in detail. Grains are not part of the default composition. All stages of ionization are treated, and all published charge exchange, radiative recombination, and dielectronic recombination processes are included as recombination mechanisms. Photoionization from valence and inner shells and many excited states, as well as collisional ionization by both thermal and supra-thermal electrons and charge transfer, are included as ionization mechanisms. The chemistry includes many molecules and will go to the fully molecular limit (H in H_2 and C or O in CO). The default composition is solar, several other standard mixtures can easily be specified, and an arbitrary composition can be entered.

9.2.4 Definition of the basic parameters

Here we give some basic definitions of the quantities used by the program, and also used in this work:

◇ **The hydrogen density**, *n(*H*)*, is the total hydrogen density given by

$$n(\mathrm{H}) = n(\mathrm{H}^0) + n(\mathrm{H}^+) + 2n(\mathrm{H}_2) + \sum_{\text{ostali}} n(\mathrm{H}_{\text{ostali}}) \ [\mathrm{cm}^{-3}], \qquad (9.1.2)$$

where $n(\mathrm{H}^0)$, $n(\mathrm{H}^+)$ and $n(\mathrm{H}_2)$ are densities of neutral, ionized and molecular hydrogen, respectively, and $n(\mathrm{H}_{\mathrm{other}})$ represents hydrogen in all other hydrogen-bearing molecules. If not specified differently this quantity is constant throughout the cloud, and is given as e.g. *hden 9.4*, where the number is the logarithm of the hydrogen density.

◇ **The hydrogen column density**, *N(*H*)*, is defined as

$$N(\mathrm{H}) = \int n(\mathrm{H}) f(r) dr \ [\mathrm{cm}^{-2}], \tag{9.1.3}$$

where $f(r)$ is the filling factor, which accounts for clumping of emission-line gas. In practice, this parameter determines the optical thickness of the gas cloud, and it can be given as one of the stopping criterium (the command `stop column density 23` sets that the iteration stops when the hydrogen column density reaches $N(\mathrm{H}) = 10^{23}\mathrm{cm}^{-2}$). The code generally will not converge if it has not done so within ten or so iterations. The most common reason for convergence problems is that the specified column density or thickness causes the simulation to end very near a prominent ionization front. In this case very small changes in the physical conditions result in large changes in the optical depths. This is a physical, not numerical, problem. The code will not have convergence problems if an optical depth is used as a stopping criterion instead.

◇ **The ionization parameter**, U, is the dimensionless ratio of hydrogen-ionizing photon to total-hydrogen densities. It is defined as

$$U \equiv \frac{Q(\mathrm{H})}{4\pi r_{\mathrm{o}}^2 n(\mathrm{H}) c} \equiv \frac{\Phi(\mathrm{H})}{n(\mathrm{H}) c}, \tag{9.1.4}$$

where r_{o} is the separation between the center of the source of ionizing radiation and the illuminated face of the cloud, $n(\mathrm{H})$ is the total hydrogen density (ionized, neutral, and molecular), c is the speed of light, $Q(\mathrm{H})$ is the number of hydrogen-ionizing photons emitted by the central object, and $\Phi(\mathrm{H})$ is the surface flux of ionizing photons. The number is the log of U, and the command is given as e.g. *ionizationparameter* $= -1$.

◇ **The number of ionizing photons**, $Q(\mathrm{H})$, is given with the command $Q(\mathrm{H}) = 57.429$ (this number is randomly given) and represents the log of the total number of ionizing photons emitted by the central object. It is defined as

$$Q(\mathrm{H}) = 4\pi R_\star^2 \int_{\nu_1}^{\nu_2} \frac{\pi F_\nu}{h\nu} d\nu \ [\mathrm{s}^{-1}]. \tag{9.1.5}$$

The default energy range is $(1 - 7.354 \times 10^6$ Ryd[32]), but the range option can be used to change the energy bounds.

[32] 1 Ryd $= 2.18 \times 10^{-11}$erg or 1 Ryd $= 13.6$eV.

◇ **The ionizing photon flux**, $\Phi(\mathrm{H})$, is given with the command $\Phi(\mathrm{H}) = 22.247$ (this number is randomly given). This command specifies the logarithm of the surface flux of hydrogen-ionizing photons striking the illuminated face of the cloud. It is defined as

$$\Phi(\mathrm{H}) \equiv \frac{Q(\mathrm{H})}{4\pi r_{\mathrm{o}}^2} \equiv \frac{R_\star^2}{r_{\mathrm{o}}^2} \int_{\nu_1}^{\nu_2} \frac{\pi F_\nu}{h\nu} d\nu \ [\mathrm{s}^{-1}\mathrm{cm}^{-2}], \tag{9.1.6}$$

and is proportional to the optical depth in excited lines, such as the Balmer lines.

9.3 Installing and starting CLOUDY

The program CLOUDY is open source and is available to all interested scientists. In order to install and prepare the cod for usage, one need to go through some basic and simple steps. The code, atomic database and manual HAZY with detail description of the program and its installation and usage, can be found on the official website *www.nublado.org*. Also, you can find there all previous versions of the code, but the authors recommend to use the latest stable version (when this thesis was written that was version C07.02.01). The program can be installed on any operative system, but further in the text an example for the linux is given.

The CLOUDY package contains the source, a large set of atomic data files, the test suite that is used to validate the code's behavior on your system, the test suite output, and the code's documentation Hazy. Each will be in its own directory and each directory has a *readme.htm* file that describes the contents of that directory in greater detail. If one works with simulations using stellar continuum, then one should download separately grids of stellar spectral energy distributions (SEDs). It is recommended to save all these data into one folder (e.g. */home/user/cloudy/*). The next step is setting the path by editing the file *path.cpp* that is located in the source directory, and which gives the path to the folder with the atomic data, i.e. */data/* folder. Then one should compile the code using a variety of C++ compilers (of course one should use a compiler that corresponds to the operative system - windows, linux or mac). The preferred compiler for linux is *g++* compiler, and the following command should be used for optimized compilation:

```
>g++ -ansi -c -O3 -fno-math-errno -funsafe-math-optimizations -Wall
*.cpp
>g++ -funsafe-math-optimizations -o cloudy.exe *.o
```

Finally, there is a large number of test cases that you should run to confirm that all is well. This is a critical step since it will check for bugs in your

compiler. The first smoke test that checks if anything works, can be executed with the single command "test":

```
>cloudy.exe <enter>
>test <enter>
```

The program is executed with the command *cloudy.exe* that calls the input file (*name_ input_ file.in*) and gives the name to the output file (*name_ output_ file.out*), where both input and output files are ordinary text files. The code is then execute the code by typing:

```
>cloudy.exe <ime_ulazna_datoteka.in> ime_izlazna_datoteka.out
```

It is also recommended to copy the *cloudy.exe* file into */bin/* folder of the local user for linux platform (e.g. */home/user/bin/ cloudy.exe*). In that way the local user can run it from ant folder. The examples of some input files and detail description of the output file are given in the next sections.

9.4 Input file

CLOUDY is driven by a set of command lines. These normally reside in a small input file which the code reads. The code creates an output file as the model is computed. The input file has to include the following quantities: a) the shape and intensity of the external radiation field striking a cloud (referred to as the incident continuum), b) the chemical composition and grain content of the gas, and c) the geometry of the gas, including its radial extent and the dependence of density on radius. Beside these, many other parameters can be set in the input file, the appearance of the output file can be defined, and some specific quantities can be saved in separate files in order to be easily accessible for later analysis (e.g. the shape and intensity of the out continuum can be printed in an additional file).

The commands are four-letter keywords (either upper or lower case) followed by free-format numbers (usually logarithm) that may be mixed with letters. When CLOUDY is executed as a stand-alone program, the usual case, standard input (stdin) is read for input, and standard output (stdout) is used for output. The program begins by echoing the input commands, except for comment lines beginning with a #, %, /, or c_ (a space after the leading c). Comments are ignored. The input stream ends with either a blank line or the end-of-file. The final output files begins with a recapitulation of all entered input commands.

9.5 Some examples of simulations

With CLOUDY program one can simulate physical conditions in many various objects, where photoionization is the main heating source (HII region, planetary nebulae, novae, narrow line region of AGN, etc.), and predict their emission spectra. Also, it is possible to make grids of model, by varying just some parameters, in order to better understand the physical properties inside a photoionized gas. An example of one such grid of simulations is given in Figure 45. In this section we give examples of some input files used for simulating different physical conditions in nebulae, all taken from the manual *Hazy*.

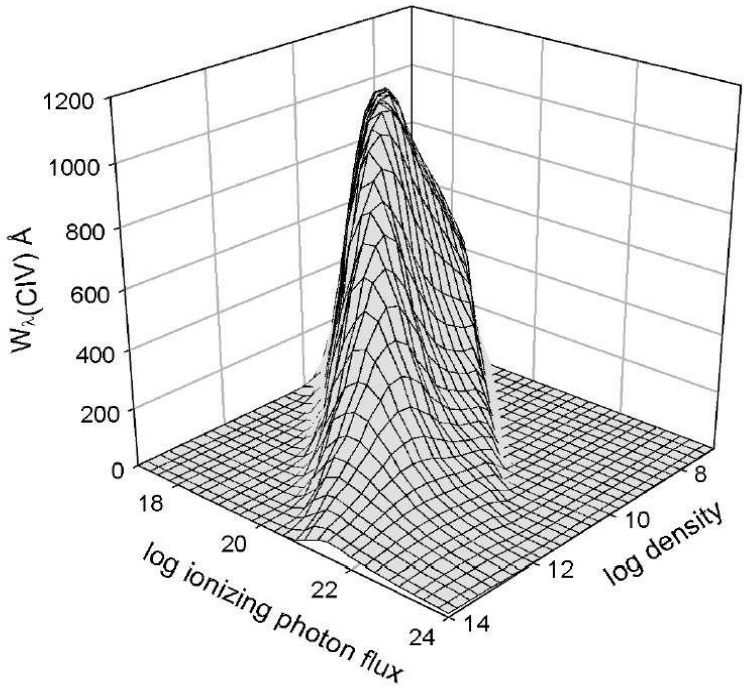

Figure 45: The predicted equivalent width of C IV λ1549 as a function of cloud density and the flux of ionizing photons striking the cloud. The equivalent width of C IV λ1549 line is given on the z-axis, while on x and y, the logarithms of hydrogen density [cm^3] and ionizing photon flux are given [cm^{-2} s^{-1}], respectively (Ferland 2006).

◇ **Eta Car Nova:** This is a model of the envelope of Eta Carinae that is illuminated by a relatively soft radiation field. It is dense and grain-free.

```
title dense nova shell
table star kurucz 35000
absolute bolometric magnitude -8.1
```

```
radius 12
hden 10 sphere
iterate to convergence
print last iteration
punch overview last file='nova.ovr'
punch results last file='nova.rlt'
c nova.in
```

◇ **Orion Nebula:** This is a model of the Orion nebula that is similar to the blister geometry H II region model computed by Baldwin et al. (1991). Orion grains are turned on with the `abundances` command. The constant pressure command does a hydrostatic equilibrium structure. The predicted emission line spectrum is affected by the reddening of the internal grains.

```
title conditions similar to Orion nebula blister
sphere
table star kurucz 39,600K
phi(h) 13.0
turbulence 8 km/sec
hden 4
abundances hii region
constant pressure
iterate
print last iteration
punch overview last file='orion.ovr'
punch results last file='orion.rlt'
c orion.in
```

◇ **Ferland & Persson BLR model:** This model of the BLR of active galactic nuclei was given by Ferland & Persson (1989).

```
title final F+P BLR model table 3
stop column density 25.5
iterate to convergence
print last
ionization parameter -0.5
hden 9.5
table agn
plot continuum
punch overview last file='blr.ovr'
punch results last file='blr.rlt'
c blr.in
```

◇ **Kwan & Krolik BLR model.** This is the "standard" BLR model presented in Kwan & Krolik (1981).

```
title Kwan+Krolik Ap.J. 250, 478 BLR model
init file='c84.ini'
constant gas pressure
f(nu) -7.32148
abundances he-1 c-3.699 n-4 o-3.1549 ne-4 na=-8 mg-4.5229
continue al-10 si-4.4229 s-10 ar-10 ca-10 fe-4.5229 ni=-8
stop column density 23
interpolate (0 -5) (.05 -5) (.1 0) (1 -0.5) (7.353 -2.233)
continue (735 -3.233) (800 -15) (8,000,000 -15)
print last iteration
normalise 1216 100
iterate to convergence
plot continuum range -3
hden 9.60206
punch overview last file='kk.ovr'
punch results last file='kk.rlt'
c kk.in
```

◇ **NLR model:** This model is one of the test cases from the Lexington Meeting suite of nebulae. It is a grain-free NLR model.

```
title Hagai's nlr model for Lexington Meeting
init file='c84.ini'
diel kludge 0
hden 4
stop column 22
abundances -1 c-3.52 n-4 o-3.097 ne-4 na-9
cont mg-4.523 al-8 si-4.523 s-4.824 a-9 ca-8 fe-8 ni-9
interpolate (0 -10) (0.08 -10) (0.1 1) (3676 -4.935) (4700 -11)
continue (4750 -20) (7,400,000 -30)
phi(h) 12.47712
iterate
print faint .01
print last iteration
punch overview last file='nlr.ovr'
punch results last file='nlr.rlt'
c nlr.in
```

◇ **BLR model NGC 5548:** This model is similar to one of the models presented in Ferland et al. (1992) for the well studied Seyfert galaxy NGC 5548.

```
title BLR model from Ferland et al.  1992
hden = 11.0
print last iteration
```

```
ionization parameter -1.0
stop column density 26.0
iterate to convergence
table agn break 100 microns
punch unit 11, overview last file='n5548.ovr'
punch unit 12, results last file='n5548.rlt'
c n5548.in
```

9.6 Output file

The name of the output file is given when executing CLOUDY program. The output file has a standard form, but it can be changed by setting some certain commands in the input file. By default, only results from the last iteration are printed, but the command for printing the previous iterations can be given in the input file. Here we describe how the standard form of the output file looks like.

The final printout begins by reprinting the input commands, as well as the quantities directly calculated from these input parameters. A large block of information that describes the continuum that strikes the illuminated face of the cloud and the chemical composition of the gas come next. Then comes a summary of the conditions in the first and last zone. These results are always printed, but results for intermediate zones can be printed if desired. For every zone, first the number of the zone is written followed by the electron temperature of the zone, the total hydrogen and electron densities, the distance from the center of the central object to the center of the zone, and other related results of the simulation. The next line gives the ratio of different line radiation to gas pressure, P(radiation)/P(gas) if is greater than 5%, and the remaining lines describe the abundances of ionization stages of different elements, and many other details related to the physical conditions in one zone.

A series of messages appear after the printout of the last zone. The first will say why the calculation stopped. In a valid calculation the model will stop because one of the specified stopping criteria specified was met. If no other criteria are specified then the calculation usually stops when the default lowest temperature of 4000 K is reached. If the code stops because of an unintended reason (i.e. internal errors, or reaching the default limit to the number of zones) then a warning is printed saying that the calculation may have halted prematurely. CLOUDY checks that its range of validity was not exceeded in the calculation and does many internal sanity checks, and this is one of its greatest advantages. Warnings are issued to indicate that the program has not treated an important process correctly, which is especially useful when producing grids of models.

The next session print out the calculated emission line spectrum. Two

blocks of output may occur. The block "Emergent line intensities" is the observed intensity as viewed from the illuminated face of a layer that has a large column beyond the shielded face, and the second block "Intrinsic line intensities" is the intrinsic emission from the cloud. The printed list is sorted into four large groups of columns, with each large column sub-divided into four smaller sub-columns. The first sub-column is either the spectroscopic designation of the ion producing the line or an indication of how the line is formed. The second sub-column is the line wavelength, with a 0 to indicate a continuum. The third sub-column is the log of the power in the line, in the units given in the header (luminosity or intensity). The last sub-column is the intensity of the line relative to the reference line, usually Hβ , unless it is set differently in the input file. The third sub-column will be either luminosity or intensity of the line depending on how the ionizing continuum is given in the input file. Only the strongest line will be printed if not requested differently in the input file.

Finally, the last part of the output file contains the series of predicted average values of some quantities e.g. electron densities, ionization parameter, the line and continuum optical depths at various energies, transmitted continuum, and many other properties of the gas cloud.

All mentioned above is printed as default in the output file, but many other additional options exist. More details about these options and all other properties of the CLOUDY program can be found in the help manual *Hazy*.

10 Appendix B - *Atomic processes*

In this appendix we give a selection of the most important atomic processes that contribute to the continuum and line emission of AGN in soft X, UV and optical part of the electromagnetic spectrum. These processes include number of interactions between atoms, ions, electron and photons, such as absorption, emission, ionization, recombination, excitation and deexcitation.

- **Absorption:** An incoming photon of energy $h\nu$ can excite an electron in an atom from energy state m to a higher energy state n:

  $$A^m + h\nu \rightarrow A^n$$

  This process occurs with a probability that is proportional to the occupation number N_m in energy state m and the energy density U_ν of the radiation field, where the transition probabilities are specified by the Einstein coefficient for absorption B_{mn}, giving a transition rate $R = U_\nu B_{mn} N_m$. This process is of the type of discrete bound-bound transitions which produce the absorption lines in the spectrum.

- **Stimulated emission:** An electron in an excited atom at energy state n is stimulated, by a passing photon of energy $h\nu$ from the ambient radiation field, to fall back into a lower state m, emitting during this process a second photon with energy $h\nu = E_n - E_m$:

  $$A^n + h\nu \rightarrow A^m + 2h\nu$$

  The probability of this process is also proportional to the energy density U_ν of the input radiation field, as is the case for absorption, the occupation number N_n of the upper energy state n and Einstein coefficient for stimulated emission B_{nm}, thus the transition rate is $R = U_\nu B_{nm} N_n$. This process is responsible for the laser emission for which the inverse population of energy levels in the transition is needed.

- **Spontaneous emission:** In contrast to stimulated emission, no incoming photon is needed. An electron spontaneously falls from a higher energy state n to a lower state m, which is followed by emission of a photon with energy $h\nu = E_n - E_m$:

  $$A^n \rightarrow A^m + h\nu$$

  The probability is given by the Einstein coefficients for spontaneous emission A_{nm}, so the transition rate is $R = A_{nm} N_n$. This process produce

the emission lines in the spectrum. The quantum mechanics gives the following relations between these three Einstein coefficients

$$A_{nm} = \frac{8\pi h\nu^3}{c^2} B_{nm}$$

$$g_m B_{mn} = g_n B_{nm}$$

where g_m and g_n are the statistical weights of the energy levels m and n.

- **Autoionization:** If an ion is initially in a doubly excited and unstable state A_*^{+i},[33] it can auto-ionize, i.e. it can spontaneously ionize without induced particle or photon, thus leaving an ion and a free electron

$$A_*^{+i} \rightarrow A_*^{+(i+1)} + e^-$$

If an electron from a lower energy state is knocked off, an electron from a higher energy level has to fall back to the emptied lower state to stabilize the ion.

- **Photoionization:** This a bound-free transition, where the incoming photon has a higher energy than the ionization energy (i.e. for the case of hydrogen $>$ 13.6 eV), so that the bound electron becomes free from the atom. The transition from the ionization stage i into the neighboring ionization stage $i+1$ can be schematically described:

$$A^i + h\nu \rightarrow A^{+(i+1)} + e^- + \Delta E$$

where ΔE is the kinetic energy given to the ejected electron, that represents the difference between the energy of the incoming photon and the ionization energy E_i: $\Delta E = h\nu - E_i$. If the incoming photon has a sufficient energy, it may leave the more highly ionized species in an excited state, which subsequently decays by a radiative cascade back to the ground state:

$$A^i + h\nu \rightarrow A_*^{+(i+1)} + e^- + \Delta E$$

and then

$$A_*^{+(i+1)} \rightarrow A^{+(i+1)} + h\nu_1 + h\nu_2 \ ...$$

This kind of photoionization describes the ejection of the outer shell electrons. But, if we increase the energy of the incoming photon still further, it becomes possible to remove one of the inner shell electrons by the process of so-called inner shell photoionization which also results in a change in the electron configuration in the excited species. This may be

[33] The species are denoted with A further in the text, where $+$ stands for a positive ion and $*$ for excited species.

followed by a radiative readjustment back to the ground state. However, in the particular case, another mode of photoionization, so-called *Auger ionization* becomes not only energy possible but indeed more probable process. This is a photoionization from and inner K- or L-shell from a stage i to a stage $i+1$, that is followed by a radiationless autoionization to a stage $i+m+1$, and is completed by a radiative cascade back to the ground state:

$$A^i + h\nu \rightarrow A_{**}^{+(i+1)} + e^- + \Delta E_1$$
$$A_{**}^{(i+1)} \rightarrow A_{*}^{(i+m+1)} + me^- + \Delta E_2$$
$$A_{*}^{(i+m+1)} \rightarrow A^{(i+m+1)} + h\nu_1 + h\nu_2 \ ...$$

Note that radiationless autoionization may produce more than one electron, in general the number m becomes greater than unity above some threshold energy and increases as more channels for the Auger process become energetically accessible. Also, in inner shell ionization followed by Auger ionization, two high energy electrons are produced (energy of several hundred electron volts). Such fast electrons are capable of either heating the gas or of collisionally exciting and/or ionizing ions with excitation or ionization potential less than the energy of the fast electron.

- **Collisional ionization:** This process occurs by collisions of ions with free electrons, when an orbiting electron (generally the outermost) of the ion in the ionization stage i is removed, and the ion is left in the next higher ionization state $i+1$:

$$A^i + e^- \rightarrow A^{+(i+1)} + 2e^- - \Delta E_{A^i}$$

An energy equal to the ionization potential of the atom ΔE_{A^i} is removed from the incoming electron, therefore collisional ionization is a process which effectively cools the electron gas. When the energy of the incoming electron exceeds the sum of the ionization potential and the excitation potential, ionization may proceed directly into an excited state of the more highly ionized atom, followed by a radiative return to the ground state. At sufficiently high electron impact energies, more than one electron of the target specie may be excited, leaving the atom in an unstable state, which is stabilized by the radiationless ejection of an electron, possibly followed by a radiative decay of the ionized atom back to its ground state:

$$A^{+i} + e^- \rightarrow A_{*}^{+i} + e^- - E_1$$

followed by

$$A_{*}^{+i} \rightarrow A_{*}^{+(i+1)} + e^- + E_2$$

then

$$A_{*}^{+(i+1)} \rightarrow A^{+(i+1)} + h\nu$$

This process is know as **ekscitacija-autojonizacija** and is favored in heavy elements which nave a large number of inner shell electrons and only one or two electrons in the outer shell.

- **Radiative recombination (or two-body recombination):** This process is a free-bound transition and it is the inverse process to photoionization. In radiative recombination a free electron is captured by an ion into one of the available energy states, while the excess energy is removed by emission of a photon. In most cases, the electron is captured into an excited state, usually into a stage of large principal quantum number and high angular momentum. The recombined but still excited ion radiates several photons in a radiative cascade, as it returns to the ground state:

$$A^{+i} + e^- \rightarrow A_*^{+(i-1)} + h\nu$$

then

$$A_*^{+(i-1)} \rightarrow A^{+(i-1)} + h\nu_1 + h\nu_2 + h\nu_3 \ ...$$

The photon in the first line represents a recombination continuum photon since the energy of the impacting electron may take any value. However, photons ν_1, ν_2, ν_3 ... represent quantized transitions between bound states, and thus represents the recombination lines.

- **Dielectric recombination:** This process is often more important than radiative recombination. In this case the excitation of the core electron happens by capture of the passing electron:

$$A^{+i} + e^- \rightarrow A^{+(i-1)^*}$$

where $A^{+(i-1)^*}$ is a very unstable ion in a $i-1$ ionization stage, with two excited electrons, i.e. one of the electrons is in an autoionized state and the other is in an excited state. The ion first stabilize itself when one of the valence electrons radiates back to the ground state (with photon emission), and then the ion returns to its ground state by radiative cascade emitting the recombination lines ν_1, ν_2, ν_3 ....

- **Three-body recombination:** This is the inverse process to colissional ionization, where the emitter A is collisionally transferred from an ionization stage i to a stage $i-1$, where no photon is emitted:

$$A^{+i} + 2e^- \rightarrow A^{+(i-1)} + e^-$$

This process is significant only for the high densities as it requires three bodies (two electrons and one ion), but it anyhow occurs in the emission regions of AGN.

- **Charge-exchange reaction:** This process can occur during the collision of two ions by the interaction of the electron clouds surrounding the ions. The charge-exchange reactions occur effectively when there are energy matches between states of systems A_1^{+j}, A_2^{+l} and $A_1^{+j\pm1}, A_2^{+l\pm-1}$. The cross section can be quite large when the resonance is nearly exact, and especially for the case when $j = 1$ and $l = 0$ (or the other way around), there is an attractive polarization that enhances the cross section. Because the energies are almost the same, these reaction can go in both directions and for low temperatures, and the equilibrium can be achieved very fast. The important example of the charge-exchange reaction for the photoionized gas with low temperatures is the reaction between neutral hydrogen and single ionized oxygen, as well as between the neutral nitrogen and ionized hydrogen.

- **Thomson scattering:** This is a process that contributes to the continuum emission (as all following processes) with no wavelength dependence, where the photons are scattered on electrons. The scattering rate is proportional to the electron density.

- **Free-free emission:** This process, also called bremsstrahlung, is the result of the non-elastically scattering of electrons on ions, where emitted photons have energies corresponding to the energy difference of the incoming and outcoming electron $h\nu = E_2 - E_1$.

- **Inverse Compton scattering:** As a result of scattering on high energy electrons, the part of kinetic energy of electrons is moved to the scattered photons. The most important are collisions of relativistic electrons and low energy photons (e.g. photons with radio frequencies).

- **Synchrotron emission:** In this process relativistic electrons emit polarized synchrotron radiation while moving in a helicoid around the magnetic lines.

- **Creation/anhilation of pairs $e^{\pm}$:** This is the process of creation of electron - positron pairs from high energy γ photons.

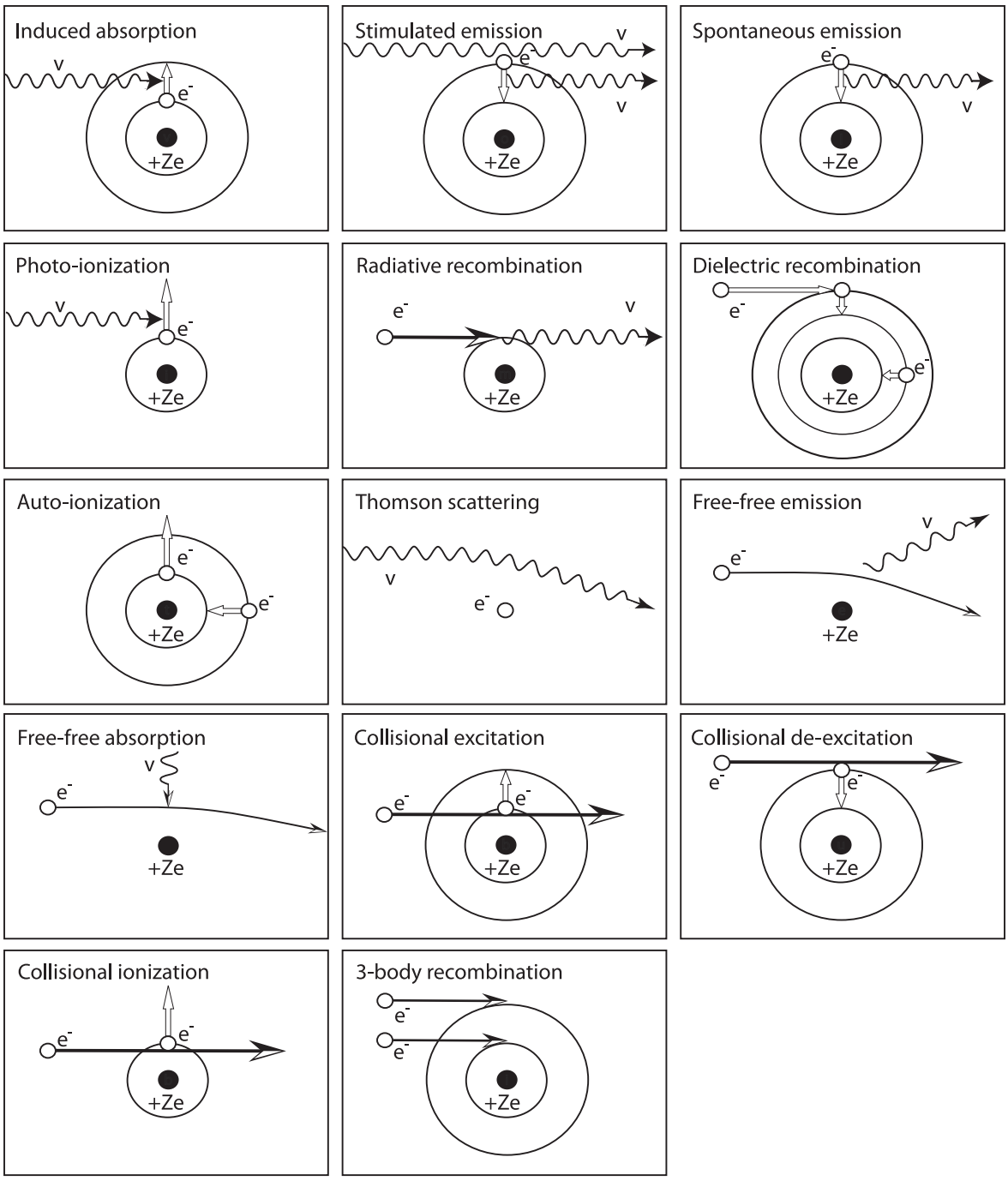

Figure 46: Diagrams that describe the process of absorbtion, emission, ionization, recombination, excitation, and deexcitation. Atoms and ions with the charge $+Ze^-$ are marked with full dots, electrons with open dots, electron orbits with circles, electron transitions with arrows, and photons with wiggly arrows. Time is proceeding from left to right.